Supporting Information for

Stability of metal–metal interactions in dinuclear Pt–Au complexes as a function of bridging Pt–arene ring electronics

Katelynn Farmer-Mason, Jeffrey W. Bacon, Eric S. Cueny*

Department of Chemistry, Boston University, 590 Commonwealth Ave., Boston, Massachusetts 02215, United States

Corresponding Author

*ecueny@bu.edu

Contents

General Experimental Considerations

The solvents and reagents were used as received from commercial sources unless otherwise noted. Dry solvents were obtained from a Pure Process Technology solvent purification system. The compounds **1**,[1] **2**,[2] **1-F**,[3] **2-F**,[4] **3**,[5] and **3-OMe**[6] were synthesized according to literature procedures. All syntheses were carried out under a nitrogen atmosphere using standard Schlenk technique unless otherwise specified. All NMR spectroscopic data were collected using a Bruker Avance Neo 600 MHz NMR spectrometer equipped with a BBFO SmartProbe. All NMR spectra are recorded in ppm and referenced to residual proteo solvent resonances. High resolution mass spectrometry data were collected on a Waters QTof Premier.

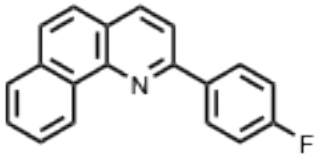

Synthesis of 2-(4-fluorophenyl)benzo[*h*]quinoline (3-F)

An oven-dried Schlenk flask was charged with magnesium turnings (0.0996 g, 4.01 mmol) and heated with a heat gun for 15 minutes under vacuum. Iodine (approx. 10 mg) was added to the flask at room temperature. While stirring, the flask was gently heated with a heat gun until iodine gas was observed, and the flask was allowed to cool to room temperature. Dry THF (5 mL) and 1-bromo-4-fluorobenzene (560 µL, 5.12 mmol) were added to the flask, and the reaction was stirred for 2 hours at 60°C. The reaction solution was reduced to 1 mL *in vacuo* before 3 mL of dry toluene and TMEDA (184 µL, 1.22 mmol) were added to the flask. The solution was stirred for 30 minutes followed by the addition of benzo[*h*]quinoline *N*-oxide (0.2000 g, 1.024 mmol), and then the reaction was left to stir for 24 hours at 50°C. The reaction was cooled to 0°C, quenched with aqueous ammonium chloride, and allowed to stir in air for 12 hours. The product was extracted with dichloromethane, dried with $MgSO_4$, filtered, and solvent removed *in vacuo*. The product was further purified by silica gel column chromatography using a Hex:DCM mixture (0.1848 g, 66%). ^{1}H NMR (600 MHz, $CDCl_3$) δ 9.51 (d, J = 8.2 Hz, 1H), 8.31 (dd, J = 8.4, 5.5 Hz, 2H), 8.07 (d, J = 8.4 Hz, 1H), 7.93 (d, J = 7.9 Hz, 1H), 7.86 – 7.72 (m, 4H), 7.62 (d, J = 8.8 Hz, 1H), 7.27 (t, J = 8.6 Hz, 2H). ^{19}F NMR (565 MHz, $CDCl_3$) δ -112.62 (m). ^{13}C{^{1}H} NMR (151 MHz, $CDCl_3$) δ 163.82 (d, $^{1}J_{C-F}$ = 248.7 Hz), 154.29, 146.17, 136.56, 135.88 (d, $^{4}J_{C-F}$ = 2.9 Hz), 133.96, 131.78, 129.25 (d, $^{3}J_{C-F}$ = 8.2 Hz), 128.26, 127.88, 127.49, 126.95, 125.08, 125.05, 124.74, 118.39, 115.73 (d, $^{2}J_{C-F}$ = 21.6 Hz). HRMS (ESI): *m/z* calc for $[M+H]^+$ $C_{19}H_{12}FN$ 274.1032; found 274.1027.

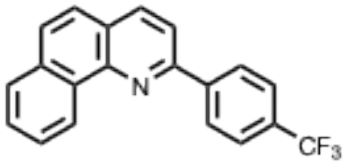

Synthesis of 2-[4-(trifluoromethyl)phenyl]benzo[*h*]quinoline (3-CF_3)

An oven-dried Schlenk flask was charged with 5 mL of anhydrous diethyl ether and 1-bromo-4-(trifluoromethyl)benzene (276 µL, 1.969 mmol). The solution was cooled to 0°C before adding *n*-BuLi (656 µL, 1.641 mmol, 2.5 M in ether) dropwise and stirring for an additional 30 minutes at 0°C. The solution was brought to room temperature, and benzo[*h*]quinoline (0.2500 g, 1.394 mmol) was added to the flask before stirring for 3 hours. The solution was quenched by opening the flask to atmosphere and stirring the solution for 12 hours. The product was extracted with dichloromethane, dried with $MgSO_4$, filtered, and solvent removed *in vacuo*. The product was further purified by silica gel column chromatography using a Hex:DCM mixture (0.3533 g, 78%). ^{1}H NMR (600 MHz, $CDCl_3$) δ 9.45 (d, *J* = 8.1 Hz, 1H), 8.37 (d, *J* = 8.0 Hz, 2H), 8.12 (dd, *J* = 8.2, 2.1 Hz, 1H), 7.93 – 7.85 (m, 2H), 7.80 – 7.76 (m, 4H), 7.75 – 7.70 (m, 1H), 7.62 (dd, *J* = 8.8, 1.9 Hz, 1H). ^{19}F NMR (565 MHz, $CDCl_3$) δ -62.39. ^{13}C{^{1}H} NMR (151 MHz, $CDCl_3$) δ 153.65, 146.28, 142.94, 136.67, 133.93, 131.71, 130.87 (q, $^2J_{C–F}$ = 32.3 Hz), 128.40, 128.07, 127.90, 127.61, 127.09, 125.69 (q, $^3J_{C–F}$ = 3.8 Hz), 125.59, 124.95, 124.68, 124.37 (q, $^1J_{C–F}$ = 272.2 Hz), 118.75. HRMS (ESI): *m/z* calc for $[M+H]^+$ $C_{20}H_{12}F_3N$ 324.1000; found 324.0974.

General Procedure for Pt-Dimer Synthesis

The corresponding 2-arylbenzo[*h*]quinoline derivative was added at room temperature to a suspension of K_2PtCl_4 in N_2 sparged glacial acetic acid (20 mL). The solution was left to stir for the specified time frame (4-6 days) at 126°C under N_2. The precipitate was decanted in air and washed with glacial acetic acid, DI H_2O, and acetone. All Pt-dimers were carried forward to the next step without further purification.

[Pt_2(bhq-Ph)$_2$(μ-Cl)$_2$]

[Pt_2(bhq-Ph)$_2$(μ-Cl)$_2$] was prepared according to the general procedure for Pt-dimer synthesis using K_2PtCl_4 (0.1670 g, 0.4020 mmol), 2-phenylbenzo[*h*]quinoline (0.1283 g, 0.5030 mmol), and was stirred for 4 days. The product was obtained as a light green, air-stable powder (0.1340 g) and was carried forward without further purification.

[Pt_2(bhq-Ph^{OMe})$_2$(μ-Cl)$_2$]

[Pt_2(bhq-Ph^{OMe})$_2$(μ-Cl)$_2$] was prepared according to the general procedure for Pt-dimer synthesis using K_2PtCl_4 (0.3538 g, 0.8523 mmol), 2-(4-methoxyphenyl)benzo[*h*]quinoline (0.2797 g, 0.9801 mmol) , and was stirred for 4 days. The product was obtained as a dark green, air-stable powder (0.4516 g) and was carried forward without further purification.

[Pt_2(bhq-Ph^{F})$_2$(μ-Cl)$_2$]

[Pt_2(bhq-Ph^{F})$_2$(μ-Cl)$_2$] was prepared according to the general procedure for Pt-dimer synthesis using K_2PtCl_4 (0.2590 g, 0.6250 mmol), 2-(4-fluorophenyl)benzo[*h*]quinoline (0.1881 g, 0.6880 mmol) , and was stirred for 5 days. The product was obtained as a green, air-stable powder (0.1699 g) and was carried forward without further purification.

[Pt_2(bhq-Ph^{CF3})$_2$(μ-Cl)$_2$]

[Pt_2(bhq-Ph^{CF3})$_2$(μ-Cl)$_2$] was prepared according to the general procedure for Pt-dimer synthesis using K_2PtCl_4 (0.2910 g, 0.7010 mmol), 2-(4-(trifluoromethyl)phenyl)benzo[*h*]quinoline (0.2605 g, 0.8060 mmol), and was stirred for 6 days. The product was obtained as a green, air-stable powder (0.1260 g) and was carried forward without further purification.

General Procedure for Pt-Dimer Conversion to [(bhq-Ph^R)(PPh$_3$)Pt]

A flask was charged with the corresponding [Pt$_2$(bhq-Ph^R)$_2$(μ-Cl)$_2$] derivative, 2 eq. of triphenylphosphine, excess NaHCO$_3$, and acetonitrile (20 mL). The solution was left to reflux in air for the specified timeframe (24 – 48 hours). The product was extracted with dichloromethane, dried with MgSO$_4$, filtered, and solvent removed *in vacuo*. The resulting product was purified by silica gel column chromatography using a Hex:DCM mixture. Further purification was achieved via recrystallization by slow diffusion of diethyl ether into a dichloromethane solution of product. See X-ray crystallography section for solvent combinations used to form X-ray quality single crystals of each compound.

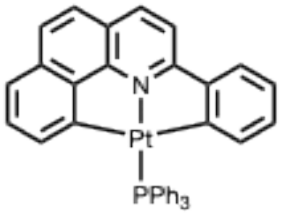

[(bhq-Ph)(PPh$_3$)Pt] (4)

[(bhq-Ph)(PPh$_3$)Pt] was prepared according to the general procedure described above using [Pt$_2$(bhq-Ph)$_2$(μ-Cl)$_2$] (0.0850 g, 0.0877 mmol), and triphenylphosphine (0.0570 g, 0.2191 mmol), and was stirred at reflux for 24 hours. The product was obtained as an orange, air stable powder (0.0930 g, 73%). ^{1}H NMR (600 MHz, CD_2Cl_2) δ 8.11 (d, *J* = 8.5 Hz, 1H), 7.90 (dd, *J* = 11.6, 7.7 Hz, 6H), 7.66 (d, *J* = 8.4 Hz, 1H), 7.61 (d, *J* = 8.7 Hz, 1H), 7.54 (d, *J* = 7.6 Hz, 1H), 7.51 – 7.45 (m, 3H), 7.45 – 7.39 (m, 7H), 7.35 (d, *J* = 7.9 Hz, 1H), 6.98 (t, *J* = 7.5 Hz, 1H), 6.94 (t, *J* = 7.5 Hz, 1H), 6.68 (t, *J* = 7.3 Hz, 1H), 6.31 (d, *J* = 10.5 Hz, $^3J_{Pt-H}$ = 32.9 Hz, 1H), 6.20 (d, *J* = 7.2 Hz, $^3J_{Pt-H}$ = 29.6 Hz, 1H). ^{31}P{^{1}H} NMR (243 MHz, CD_2Cl_2) δ 27.10 (t, *J* = 11.3 Hz, $^1J_{P-Pt}$ = 4020.2 Hz). ^{13}C{^{1}H} NMR (151 MHz, CD_2Cl_2) δ 165.94 (d, *J* = 6.6 Hz, J_{Pt-C} = 702 Hz), 165.48 (s, J_{Pt-C} = 72.6 Hz), 164.63 (d, *J* = 7.9 Hz, J_{Pt-C} = 705 Hz), 155.88 (s, J_{Pt-C} = 67.1 Hz), 151.82 (d, *J* = 2.1 Hz, J_{Pt-C} = 34.1 Hz), 148.14 (d, *J* = 2.1 Hz, J_{Pt-C} = 32.1 Hz), 139.14 (d, *J* = 2.3 Hz, J_{Pt-C} = 54.4 Hz), 139.00, 135.66 (d, *J* = 11.7 Hz, J_{Pt-C} = 41.3 Hz), 135.12 (s, J_{Pt-C} = 21.5 Hz), 135.10 (s, J_{Pt-C} = 57.0 Hz), 132.45 (d, *J* = 57.5 Hz, J_{Pt-C} = 29.0 Hz), 130.98 (d, *J* = 2.3 Hz), 130.45 (s, J_{Pt-C} = 33.2 Hz), 129.87 (s, J_{Pt-C} = 34.7 Hz), 129.28, 128.56 (d, *J* = 10.7 Hz), 124.83 (s, J_{Pt-C} = 27.3 Hz), 124.55 (d, *J* = 3.0 Hz, J_{Pt-C} = 23.1 Hz), 124.00, 122.79, 121.63, 115.26 (d, *J* = 3.9 Hz, J_{Pt-C} = 29.6 Hz). HRMS (ESI): *m/z* calc for [M+H]$^+$ $C_{37}H_{26}NPPt$ 711.1528; found 711.1500.

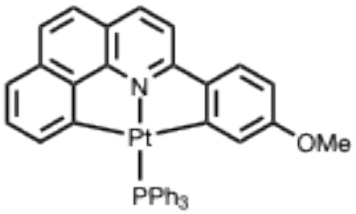

[(bhq-Ph^{OMe})(PPh$_3$)Pt] (4-OMe)

[(bhq-Ph^{OMe})(PPh$_3$)Pt] was prepared according to the general procedure described above using [Pt$_2$(bhq-Ph^{OMe})$_2$(μ-Cl)$_2$] (0.2865 g, 0.2780 mmol), and triphenylphosphine (0.1820 g, 0.6960 mmol), and was stirred at reflux for 24 hours. The product was obtained as an orange, air stable powder (0.3972 g, 96%). ^{1}H NMR (600 MHz, CD_2Cl_2) δ 8.02 (d, J = 8.5 Hz, 1H), 7.96 – 7.87 (m, 6H), 7.56 (d, J = 8.7 Hz, 1H), 7.52 (dd, J = 8.5, 1.7 Hz, 1H), 7.50 – 7.46 (m, 4H), 7.43 (ddd, J = 9.3, 6.8, 2.2 Hz, 6H), 7.38 (d, J = 8.7 Hz, 1H), 7.34 (d, J = 7.8 Hz, 1H), 6.98 (t, J = 7.4 Hz, 1H), 6.46 (dd, J = 8.4, 2.6 Hz, 1H), 6.21 (d, J = 7.1, $^3J_{Pt\text{-}H}$ = 32.2 Hz, 1H), 6.11 (t, J = 2.1, $^3J_{Pt\text{-}H}$ = 33.2, 1H), 3.19 (s, 3H). ^{31}P{^{1}H} NMR (243 MHz, CD_2Cl_2) δ 27.48 (t, J = 8.8 Hz, $^1J_{P\text{-}Pt}$ = 3998.3 Hz). ^{13}C{^{1}H} NMR (151 MHz, CD_2Cl_2) δ 168.74 (d, J = 6.0 Hz, $J_{Pt–C}$ = 705.1 Hz), 165.23 (s, $J_{Pt–C}$ = 75.0 Hz), 164.07 (d, J = 7.5 Hz), 161.74 (s, $J_{Pt–C}$ = 42.3 Hz), 155.76 (s, $J_{Pt–C}$ = 63.4 Hz), 148.05 (d, J = 3.0 Hz, $J_{Pt–C}$ = 33.2 Hz), 144.26 (d, J = 1.5 Hz, $J_{Pt–C}$ = 34.7 Hz), 138.86, 135.62 (d, J = 12.1 Hz, $J_{Pt–C}$ = 40.7 Hz), 135.10 (s, $J_{Pt–C}$ = 24.16), 134.95 (s, $J_{Pt–C}$ = 57.4 Hz), 132.51 (d, J = 57.4 Hz, $J_{Pt–C}$ = 28.7 Hz), 131.00 (d, J = 3.0 Hz), 139.67 (s, $J_{Pt–C}$ = 34.7 Hz), 128.61 (d, J = 10.6 Hz), 128.54, 126.36 (s, $J_{Pt–C}$ = 31.7 Hz), 123.76 (d, J = 3.0 Hz, $J_{Pt–C}$ = 57.4 Hz), 123.72 (d, J = 3.0 Hz), 122.86, 121.70, 115.02 (d, J = 4.5 Hz, $J_{Pt–C}$ = 31.7 Hz), 110.40, 55.00. HRMS (ESI): *m/z* calc for [M–H]$^+$ $C_{38}H_{28}NOPPt$ 739.1478; found 739.1500.

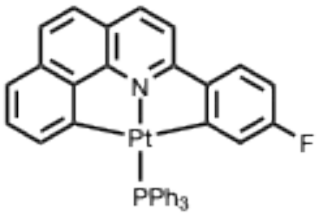

[(bhq-Ph^F)(PPh$_3$)Pt] (4-F)

[(bhq-Ph^F)(PPh$_3$)Pt] was prepared according to the general procedure described above using [Pt$_2$(bhq-Ph^F)$_2$(μ-Cl)$_2$] (0.1699 g, 0.1680 mmol), and triphenylphosphine (0.1100 g, 0.4220 mmol), and was stirred at reflux for 48 hours. The product was obtained as an orange, air stable powder (0.1600 g, 65%). ^{1}H NMR (600 MHz, CD_2Cl_2) δ 8.11 (d, J = 8.5 Hz, 1H), 7.89 (ddd, J = 11.7, 7.1, 1.4 Hz, 6H), 7.63 – 7.58 (m, 2H), 7.56 (dd, J = 8.4, 5.6 Hz, 1H), 7.52 – 7.47 (m, 3H), 7.50 – 7.37 (m, 7H), 7.35 (d, J = 7.8 Hz, 1H), 6.98 (dd, J = 7.9, 7.1 Hz, 1H), 6.59 (td, J = 8.5, 2.6 Hz, 1H), 6.32 (dt, J = 7.1, 1.0 Hz, $^3J_{Pt–H}$ = 32.6 Hz, 1H), 5.75 (ddd, J = 10.5, 2.7, 1.1 Hz, $^3J_{Pt–H}$ = 44.0 Hz, 1H). ^{19}F NMR (565 MHz, CD_2Cl_2) δ -109.98 (m). ^{31}P{^{1}H} NMR (243 MHz, CD_2Cl_2) δ 26.49 (t, J = 8.8 Hz, $^1J_{P–Pt}$ = 3991.9 Hz). ^{13}C{^{1}H} NMR (151 MHz, CD_2Cl_2) δ 170.61 (dd, J = 6.3, 4.1 Hz, $J_{Pt–C}$ = 711 Hz),165.76 (s, $J_{Pt–C}$ = 49.2 Hz), 164.21 (s, $J_{Pt–C}$ = 72.6 Hz), 164.08, 163.22 (d, J = 8.2 Hz, $J_{Pt–C}$ = 714 Hz), 155.83 (s, $J_{Pt–C}$ = 67.4 Hz), 147.99 (d, J = 2.2 Hz, $J_{Pt–C}$ = 31.8 Hz), 147.83 (t, J = 4.7 Hz), 139.03, 135.67 (d, J = 11.7 Hz, $J_{Pt–C}$ = 41.3 Hz), 135.54 (d, J = 0.8 Hz), 135.11 (s, $J_{Pt–C}$ = 23.5 Hz), 132.00 (d, J = 57.7 Hz, $J_{Pt–C}$ = 28.3 Hz),131.15 (d, J = 2.2 Hz), 129.93 (s, $J_{Pt–C}$ = 36.3 Hz), 129.17, 128.65 (d, J = 11.0 Hz), 126.47 (d, J = 8.5 Hz), 124.46 (dd, J = 17.3, 1.5 Hz), 124.35

(d, J = 2.7 Hz), 122.32 (d, $^{1}J_{C\text{-}F}$ = 160.9 Hz), 115.31 (d, J = 4.3 Hz, $J_{Pt\text{–}C}$ = 30.0 Hz), 110.47 (d, $^{2}J_{C\text{-}F}$ = 23.0 Hz). HRMS (ESI): *m/z* calc for $[M]^+$ $C_{37}H_{25}FNPPt$ 728.1356; found 728.1420.

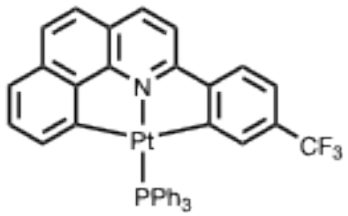

[(bhq-Ph^{CF3})(PPh$_3$)Pt] (4-CF$_3$)

[(bhq-Ph^{CF3})(PPh$_3$)Pt] was prepared according to the general procedure described above using [Pt$_2$(bhq-Ph^{CF3})$_2$(μ-Cl)$_2$] (0.1374 g, 0.1247 mmol), and triphenylphosphine (0.0650 g, 0.2490 mmol), and was stirred at reflux for 48 hours. The product was obtained as an orange, air stable powder (0.1094 g, 56%). ^{1}H NMR (600 MHz, CD_2Cl_2) δ 8.14 (d, J = 8.5 Hz, 1H), 7.94 – 7.83 (m, 6H), 7.68 (dd, J = 8.7, 8.4 Hz, 1H), 7.64 (d, J = 8.7 Hz, 1H), 7.58 (d, J = 7.9 Hz, 1H), 7.49 (td, J = 7.3, 1.7 Hz, 3H), 7.46 – 7.39 (m, 7H), 7.37 (d, J = 7.8 Hz, 1H), 7.17 (d, J = 8.0, Hz, 1H), 7.01 (t, J = 7.5 Hz, 1H), 6.46 (s, 1H), 6.43 (d, J = 7.0 Hz, 1H). ^{19}F NMR (565 MHz, CD_2Cl_2) δ -63.22.^{31}P{^{1}H} NMR (243 MHz, CD_2Cl_2) δ 26.18 (t, J = 10.1 Hz, $J_{P\text{-}Pt}$ = 3993.9).^{13}C{^{1}H} NMR (151 MHz, CD_2Cl_2) δ 166.76 (d, J = 6.6 Hz), 163.67, 163.37 (d, J = 8.5 Hz), 156.02 (s, $J_{Pt\text{–}C}$ = 65.3 Hz), 155.33 (s, $J_{Pt\text{–}C}$ = 37.3 Hz), 148.01 (d, J = 2.3 Hz), 139.22, 135.81 (d, J = 1.4 Hz, $J_{Pt\text{–}C}$ = 59.0 Hz), 135.53 (d, J = 11.6 Hz, $J_{Pt\text{–}C}$ = 40.6 Hz), 135.16, 134.33 (s, $J_{Pt\text{–}C}$ = 57.5 Hz), 131.88 (d, J = 57.9 Hz, $J_{Pt\text{–}C}$ = 27.8 Hz), 131.24 (d, J = 2.2 Hz), 130.82 (q, $^{2}J_{C\text{-}F}$ = 30.3 Hz), 130.18 (s, $J_{Pt\text{–}C}$ = 36.5 Hz), 129.95, 128.68 (d, J = 10.8 Hz), 125.25 (d, J = 3.0 Hz), 124.84 (q, $^{1}J_{C\text{-}F}$ = 273.6 Hz), 124.15 (s, $J_{Pt\text{–}C}$ = 28.0 Hz), 123.93, 122.83, 120.90 (q, $^{3}J_{C\text{-}F}$ = 4.2 Hz), 115.70 (d, J = 3.7 Hz, $J_{Pt\text{–}C}$ = 27.7 Hz). HRMS (ESI): *m/z* calc for $[M–H]^+$ $C_{38}H_{25}F_3NPPt$ 777.1241; found 777.1246.

General Procedure for Dinuclear Complex Formation

A literature method was adapted to synthesize [(bhq-Ph^R)(PPh_3)Pt-Au(PPh_3)][OTf].[2,4] To a solution of Au(PPh_3)Cl in dry THF (1 ml), 1 eq. of AgOTf or $AgPF_6$ was added and the solution left to stir in air for 15 mins in the dark. The resulting solution was filtered through Celite to remove the AgCl salt. One equivalent of the corresponding [(bhq-Ph^R)(PPh_3)Pt] was added to the solution and left to stir for 1 hour in the dark. THF solvent was then removed *in vacuo* to obtain an orange-red solid or oil. Further purification was achieved via recrystallization by slow diffusion of diethyl ether into a dichloromethane solution of product. See X-ray crystallography section for solvent combinations used to form X-ray quality single crystals of each compound.

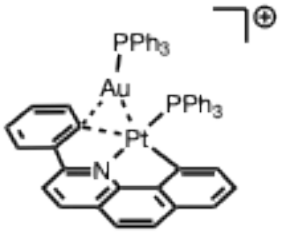

[(bhq-Ph)(PPh_3)Pt–Au(PPh_3)][OTf] (5)

[(bhq-Ph)(PPh_3)Pt–Au(PPh_3)][OTf] was prepared according to the general procedure for dinuclear complex synthesis using Au(PPh_3)Cl (0.0252 g, 0.0509 mmol), AgOTf (0.0130 g, 0.0509 mmol), and[(bhq-Ph)(PPh_3)Pt] (0.0350 g, 0.0509 mmol). The product was obtained as an orange, air stable powder (0.0561 g, 86%). ^{1}H NMR (600 MHz, CD_2Cl_2) δ 8.32 (d, *J* = 8.5 Hz, 1H), 7.86 (dd, *J* = 8.6, 1.7 Hz, 1H), 7.80 – 7.72 (m, 8H), 7.68 (d, *J* = 8.1, 0.9 Hz, 1H), 7.64 (d, *J* = 8.7 Hz, 1H), 7.53 – 7.44 (m, 6H), 7.28 (br. s, 8H), 7.26 (dd, *J* = 7.5, 1.2 Hz, 1H), 7.24 – 7.19 (m, 5H), 7.13 (dd, J = 8.0, 7.2 Hz, 1H), 7.02 (br. s, 5H), 6.85 (td, *J* = 7.5, 1.4 Hz, 1H), 6.18 (d, *J* = 7.5, 1.3 Hz, $^3J_{Pt–H}$ = 32.8 Hz, 1H), 6.01 (d, *J* = 7.2 Hz, $^3J_{Pt–H}$ = 27.8 Hz, 1H). ^{19}F NMR (565 MHz, CD_2Cl_2) δ -78.89. ^{31}P{^{1}H} NMR (243 MHz, CD_2Cl_2) 21.52 (m, $^1J_{P–Pt}$ = 3622.8 Hz), 34.25 (s, $^2J_{P–Pt}$ = 253.3 Hz). ^{13}C{^{1}H} NMR (151 MHz, CD_2Cl_2) δ 164.75 (s, $J_{Pt–C}$ = 66.4 Hz), 154.38, 154.16 (s, $J_{Pt–C}$ = 5.4 Hz), 149.28 (d, *J* = 1.5 Hz, $J_{Pt–C}$ = 43.8 Hz), 148.56, 143.95, 141.79, 141.03, 138.64, 135.77 (d, *J* = 13.6 Hz), 135.47, 134.51 (t, *J* = 15.1 Hz), 133.92 (d, *J* = 13.6 Hz), 133.21, 132.44 (d, *J* = 52.9 Hz), 131.03 (s, $J_{Pt–C}$ = 34.7 Hz), 130.67 (s, $J_{Pt–C}$ = 27.2 Hz), 130.31 (m), 129.79 (d, *J* = 12.0 Hz), 129.54, 129.15 (d, *J* = 11.0 Hz), 128.90, 128.30 (d, *J* = 63.0 Hz), 126.40 (s, $J_{Pt–C}$ = 22.6 Hz), 126.09, 124.44, 121.34 (q, *J* = 320.1 Hz), 117.17 (d, *J* = 3.0 Hz, $J_{Pt–C}$ = 27.2 Hz). HRMS (ESI): *m/z* calc for $[M]^+$ $C_{55}H_{41}AuNP_2Pt$ (i.e. the cationic portion of **5**) 1169.2027; found 1169.2074.

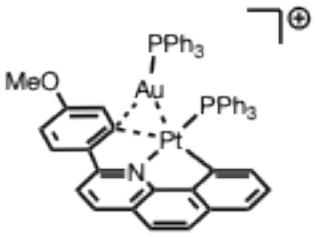

[(bhq-Ph^{OMe})(PPh$_3$)Pt–Au(PPh$_3$)][OTf] (5-OMe)

[(bhq-Ph^{OMe})(PPh$_3$)Pt–Au(PPh$_3$)][OTf] was prepared according to the general procedure for dinuclear complex synthesis using Au(PPh$_3$)Cl (0.0822 g, 0.1663 mmol), AgOTf (0.0427 g, 0.1663 mmol), and[(bhq-Ph^{OMe})(PPh$_3$)Pt] (0.1232 g, 0.1663 mmol). The product was obtained as a red-orange, air stable oil (0.2107 g, 94%). ^{1}H NMR (600 MHz, CD_2Cl_2) δ 8.23 (d, *J* = 8.6 Hz, 1H), 7.77 (ddd, *J* = 12.0, 8.3, 1.4 Hz, 6H), 7.74 – 7.71 (m, 2H), 7.70 (d, *J* = 8.0 Hz, 1H), 7.65 (d, *J* = 8.6 Hz, 1H), 7.61 (d, *J* = 8.7 Hz, 1H), 7.49 (dd, *J* = 8.7, 7.0 Hz, 6H), 7.28 (td, *J* = 7.8, 2.6 Hz, 6H), 7.22 (td, J = 8.0, 1.9 Hz, 6H), 7.15 (dd, *J* = 8.1, 7.1 Hz, 1H), 7.02 (dd, *J* = 13.5, 8.1 Hz, 6H), 6.68 (dd, *J* = 8.5, 2.6 Hz, 1H), 5.98 (t, J = 2.1 Hz, $^3J_{Pt–H}$ = 39.4 Hz, 1H), 5.87 (d, *J* = 7.1 Hz, 1H), 3.14 (s, 3H). ^{19}F NMR (565 MHz, CD_2Cl_2) δ -78.57. ^{31}P{^{1}H} NMR (243 MHz, CD_2Cl_2) δ 34.09 (t, *J* = 13.1 Hz, $^2J_{P–Pt}$ = 250.8 Hz), 21.84 (t, *J* = 9.5 Hz, $^1J_{P–Pt}$ = 3603.5 Hz). ^{13}C{^{1}H} NMR (151 MHz, CD_2Cl_2) δ 165.29 (s, $J_{Pt–C}$ = 69.4 Hz), 161.85 (s, $J_{Pt–C}$ = 54.3 Hz), 153.71 (s, $J_{Pt–C}$ = 51.3 Hz), 153.10, 149.77 (d, *J* = 3.0 Hz, $J_{Pt–C}$ = 30.2 Hz), 145.49 (s, $J_{Pt–C}$ = 37.7 Hz), 140.86, 139.40 (s, $J_{Pt–C}$ = 49.8 Hz), 135.72 (d, *J* = 13.6 Hz), 135.42, 134.51 (t, *J* = 15.1 Hz), 133.98 (d, *J* = 13.6 Hz), 133.20, 132.50 (d, *J* = 52.8 Hz), 130.63, 130.45 – 130.11 (m), 129.74 (d, *J* = 12.0 Hz), 129.43, 129.22 (d, *J* = 11.1 Hz), 128.93, 128.54 (d, *J* = 60.4 Hz), 127.79 (s, $J_{Pt–C}$ = 33.2 Hz), 126.20 (s, $J_{Pt–C}$ = 66.4 Hz), 125.29 (d, *J* = 1.5 Hz, $J_{Pt–C}$ = 19.6 Hz), 124.73, 121.21 (q, *J* = 321.6 Hz), 117.01 (d, *J* = 4.5 Hz, $J_{Pt–C}$ = 27.2 Hz), 114.25, 55.39. HRMS (ESI): *m/z* calc for [M]$^+$ $C_{56}H_{43}AuNOP_2Pt$ (i.e. the cationic portion of **5-OMe**) 1199.2133; found 1199.2173.

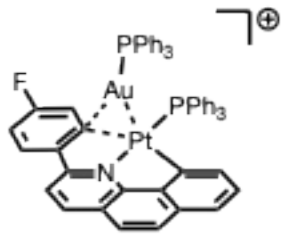

[(bhq-Ph^{F})(PPh$_3$)Pt–Au(PPh$_3$)][OTf] (5-F)

[(bhq-Ph^{F})(PPh$_3$)Pt–Au(PPh$_3$)][OTf] was prepared according to the general procedure for dinuclear complex synthesis using Au(PPh$_3$)Cl (0.0339 g, 0.0686 mmol), AgOTf (0.0176 g, 0.0686 mmol), and [(bhq-Ph^{F})(PPh$_3$)Pt] (0.0500 g, 0.0686 mmol). The product was obtained as an orange, air stable oil (0.0854 g, 92%). ^{1}H NMR (600 MHz, CD_2Cl_2) δ 8.33 (d, *J* = 8.6 Hz, 1H), 7.83 (d, *J* = 8.6 Hz, 1H), 7.80-7.72 (m, 9H), 7.66 (d, *J* = 8.7 Hz, 1H), 7.54 – 7.45 (m, 6H), 7.30 (td, *J* = 7.9, 2.6 Hz, 6H), 7.24 (td, *J* = 7.9, 2.4 Hz, 6H), 7.20 (t, *J* = 1.9 Hz, 1H), 7.00 (dd, *J* = 13.6, 7.6 Hz, 6H), 6.83 (t, *J* = 4.1 Hz, 1H), 6.06 (d, *J* = 9.9 Hz, $J_{Pt–H}$ = 12.4 Hz 1H), 5.78 (d, *J* = 7.1 Hz, $J_{Pt–H}$ = 11.7 Hz, 1H). ^{19}F (565 MHz, CD_2Cl_2) δ -78.88, -107.76 (q, $^3J_{F–H}$ = 5.6 Hz). ^{31}P{^{1}H} NMR (243 MHz, CD_2Cl_2) δ 34.09 (t, *J* = 11.2 Hz, $^2J_{Pt–P}$ = 262.7 Hz), 21.05 (t, *J* = 11.4 Hz, $^1J_{Pt–P}$ = 3594.0 Hz). ^{13}C{^{1}H} NMR (151 MHz, CD_2Cl_2) δ 165.15, 164.95 (s, $J_{Pt–C}$ = 72.5 Hz), 163.45, 158.12 (s, $J_{Pt–C}$ = 826 Hz), 153.50 (s, $J_{Pt–C}$ =51.3 Hz), 150.41 (s, $J_{Pt–C}$ = 28.7 Hz), 148.44 (s, $J_{Pt–C}$ = 36.2 Hz), 141.27, 140.53 (s, $J_{Pt–C}$ = 48.3 Hz), 135.83 (d, *J* = 10.6 Hz), 135.52, 133.93 (d, *J* = 13.6 Hz), 132.50 (d, *J* = 43.8

Hz), 130.27, 130.18, 129.86, 129.75 (d, *J* = 12.0 Hz), 129.51, 129.22 (d, *J* = 10.9 Hz), 128.80, 128.40, 127.76 (d, *J* = 9.0 Hz, J_{Pt-C} = 39.2 Hz), 126.68 (d, *J* = 21.1 Hz, J_{Pt-C} = 71.0 Hz), 125.92, 124.89, 121.47 (q, J_{Pt-C} = 323.1 Hz), 117.47 (s, J_{Pt-C} = 30.2 Hz), 114.1 (d, J_{C-F} = 24.1 Hz) HRMS (ESI): *m/z* calc for $[M]^+$ $C_{55}H_{40}AuFNP_2Pt$ (i.e. the cationic portion of **5-F**) 1187.1933; found 1187.1969

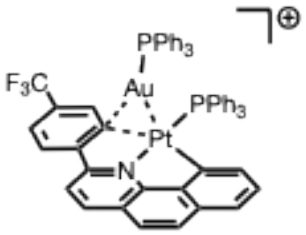

[(bhq-Ph^{CF3})(PPh$_3$)Pt–Au(PPh$_3$)][OTf] (5-CF$_3$)

[(bhq-Ph^{CF3})(PPh$_3$)Pt–Au(PPh$_3$)][OTf] was prepared according to the general procedure for dinuclear complex synthesis using Au(PPh$_3$)Cl (0.0432 g, 0.0873 mmol), AgOTf (0.0224 g, 0.0873 mmol), and [(bhq-Ph^{CF3})(PPh$_3$)Pt] (0.0679 g, 0.0873 mmol). The product was obtained as an orange, air stable powder (0.1114 g, 92%). ^{1}H NMR (600 MHz, CD_2Cl_2) δ 8.40 (d, *J* = 8.5 Hz, 1H), 7.95 (d, *J* = 8.4 Hz, 1H), 7.88 – 7.72 (m, 10H), 7.69 (d, *J* = 8.8 Hz, 1H), 7.58 – 7.46 (m, 6H), 7.39 (d, *J* = 8.0 Hz, 1H), 7.29 (dt, J = 7.8, 3.9 Hz, 6H), 7.27 – 7.20 (m, 7H), 6.98 (dd, *J* = 13.4, 7.6 Hz, 6H), 6.62 (s, $^3J_{Pt-H}$ = 38.3 Hz, 1H), 5.90 (d, *J* = 6.9 Hz, 1H). ^{19}F NMR (565 MHz, CD_2Cl_2) δ -64.08, -78.79. ^{31}P{^{1}H} NMR (243 MHz, CD_2Cl_2) δ 33.96 (s, $^2J_{P-Pt}$ = 257.4 Hz), 20.69 (t, *J* = 10.2 Hz, $^1J_{P-Pt}$ = 3582.6 Hz). ^{13}C{^{1}H} NMR (151 MHz, CD_2Cl_2) δ 164.14 (s, J_{Pt-C} = 71.0 Hz), 155.96 (s, J_{Pt-C} = 31.7 Hz), 154.29 (s, J_{Pt-C} = 792.7 Hz), 153.76 (s, J_{Pt-C} = 45.3 Hz), 150.32 (d, *J* = 3.0 Hz, J_{Pt-C} = 28.7 Hz), 141.59, 140.26 (s, J_{Pt-C} = 49.8 Hz), 139.16, 136.34 (s, J_{Pt-C} = 66.4 Hz), 135.67 (d, *J* = 12.1 Hz), 134.52 (t, *J* = 6.0 Hz), 133.97 (d, *J* = 13.6 Hz), 133.21, 132.60 (d, *J* = 42.3 Hz), 131.68 (q, J_{C-F} = 31.7 Hz), 130.31 (t, *J* = 6.0 Hz), 130.10 (d, *J* = 52.8 Hz), 129.96, 129.78 (d, *J* = 11.9 Hz), 129.56, 129.27 (d, *J* = 11.2 Hz), 128.35 (d, *J* = 61.9 Hz), 126.76 (d, *J* = 1.5 Hz, J_{Pt-C} = 21.1 Hz), 125.63 (s, J_{Pt-C} = 28.7 Hz), 124.86, 124.52, 124.02 (q, J_{C-F} = 273.3 Hz), 121.30 (q, *J* = 320.1 Hz), 117.88 (d, *J* = 4.5 Hz, J_{Pt-C} = 24.1 Hz). HRMS (ESI): *m/z* calc for $[M]^+$ $C_{56}H_{40}AuF_3NP_2Pt$ (i.e. the cationic portion of **5-CF$_3$**) 1237.1901; found 1237.1951.

NMR Spectra of 2-(4-fluorophenyl)benzo[*h*]quinoline (3-F)

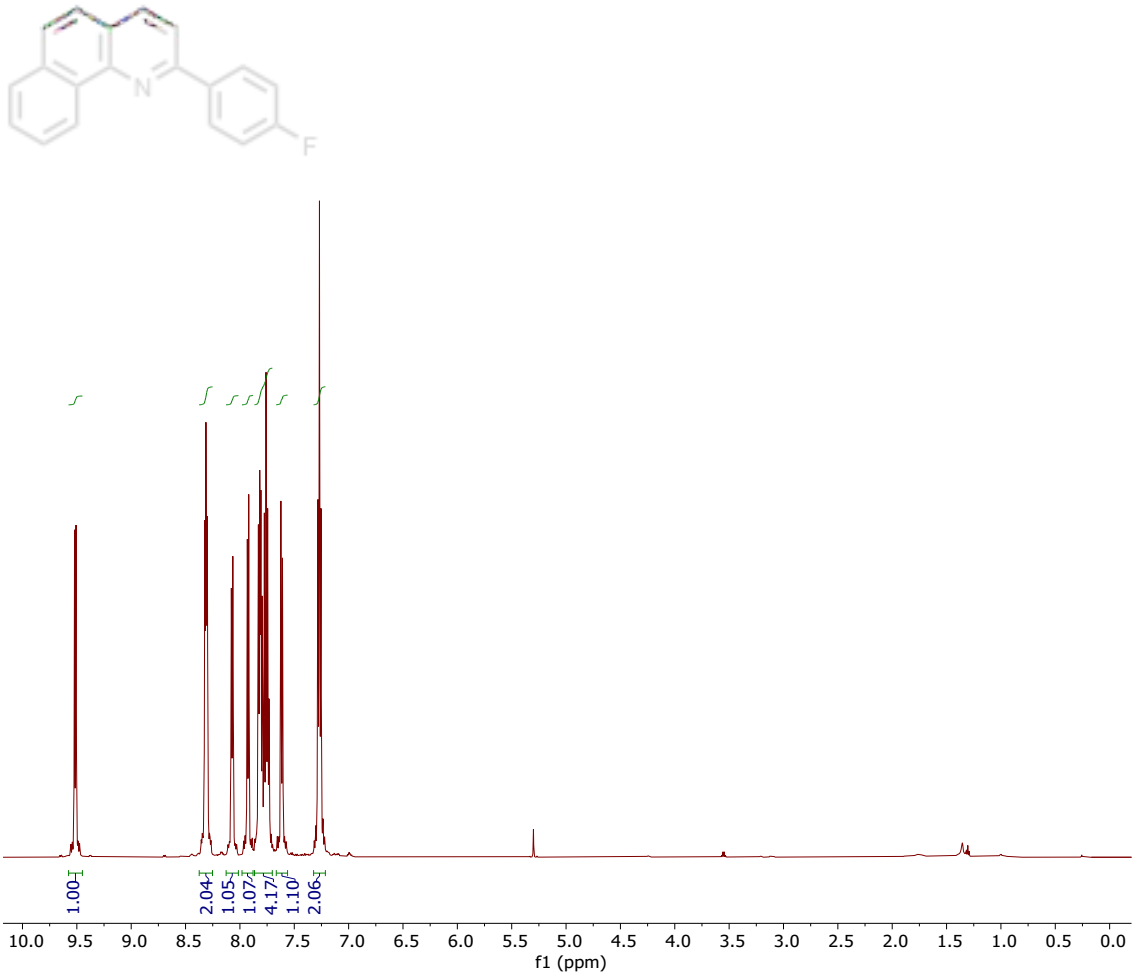

Figure S1. ^{1}H NMR spectrum of 2-(4-fluorophenyl)benzo[*h*]quinoline in $CDCl_3$.

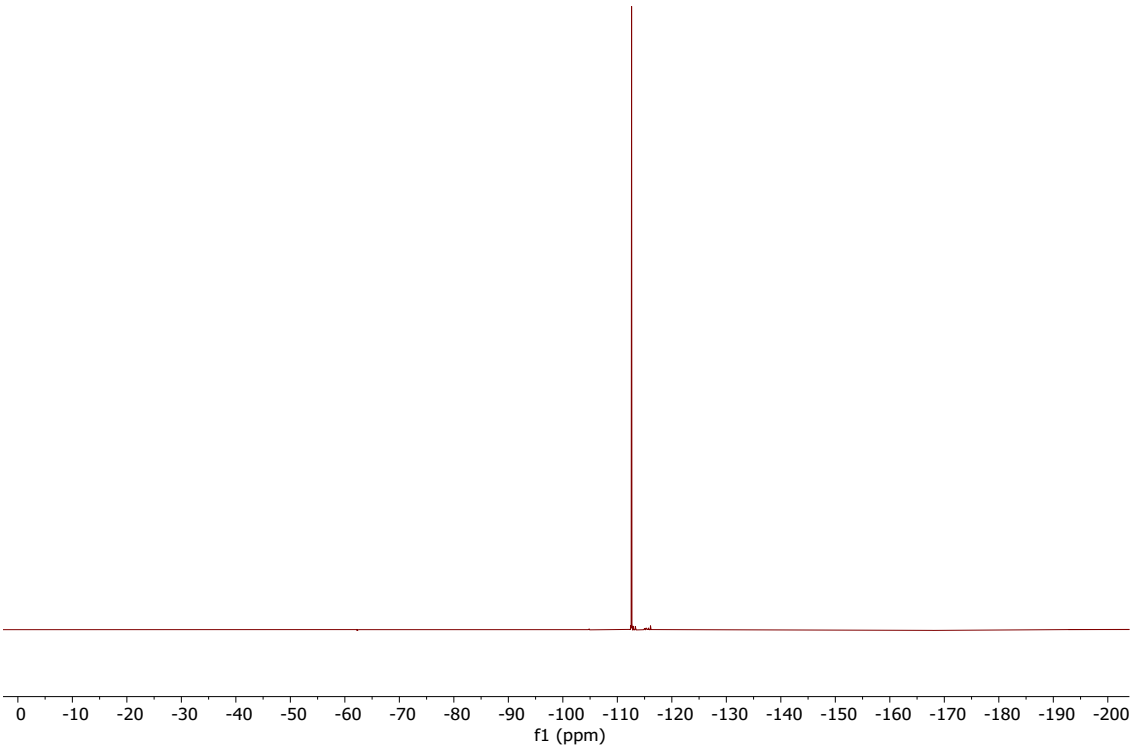

Figure S2. ^{19}F NMR spectrum of 2-(4-fluorophenyl)benzo[*h*]quinoline in $CDCl_3$.

Figure S3. $^{13}C\{^{1}H\}$ NMR spectrum of 2-(4-fluorophenyl)benzo[*h*]quinoline in $CDCl_3$.

NMR Spectra of 2-[4-(trifluoromethyl)phenyl]benzo[*h*]quinoline (3-CF_3)

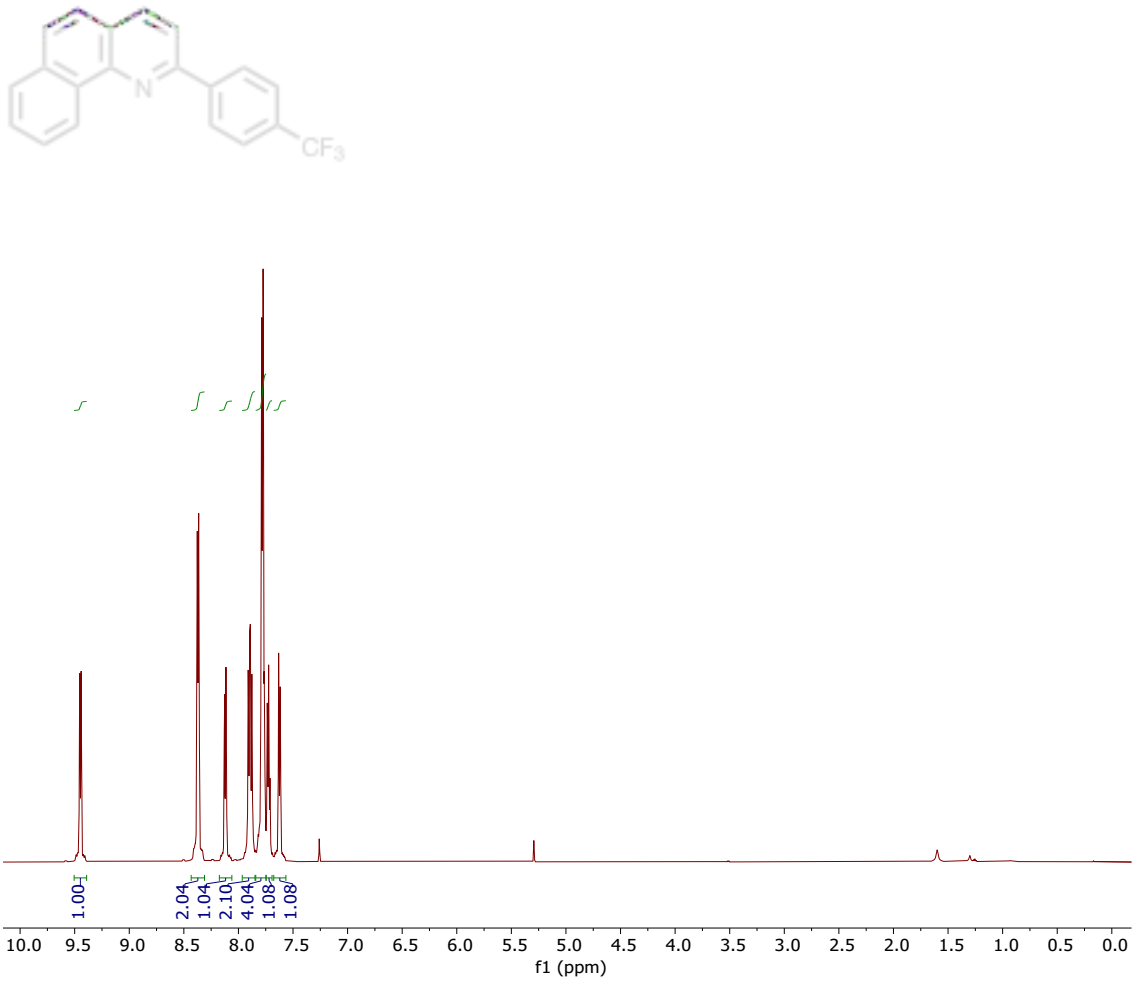

Figure S4. ^{1}H NMR spectrum of 2-[4-(trifluoromethyl)phenyl]benzo[*h*]quinoline in $CDCl_3$.

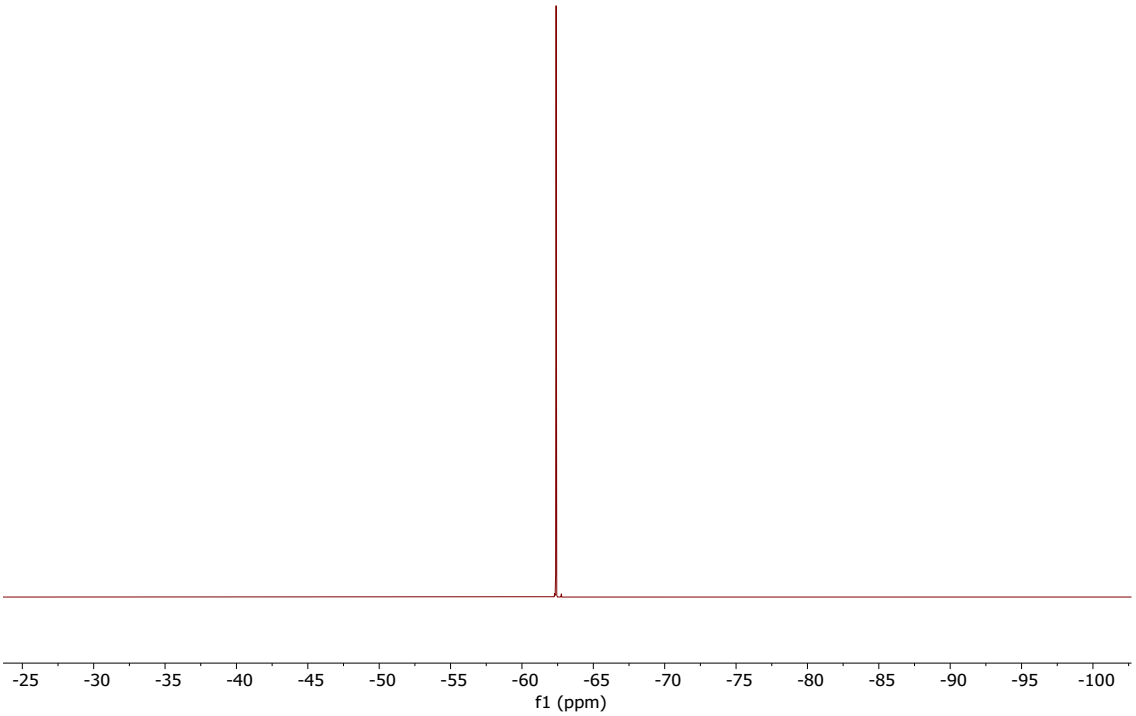

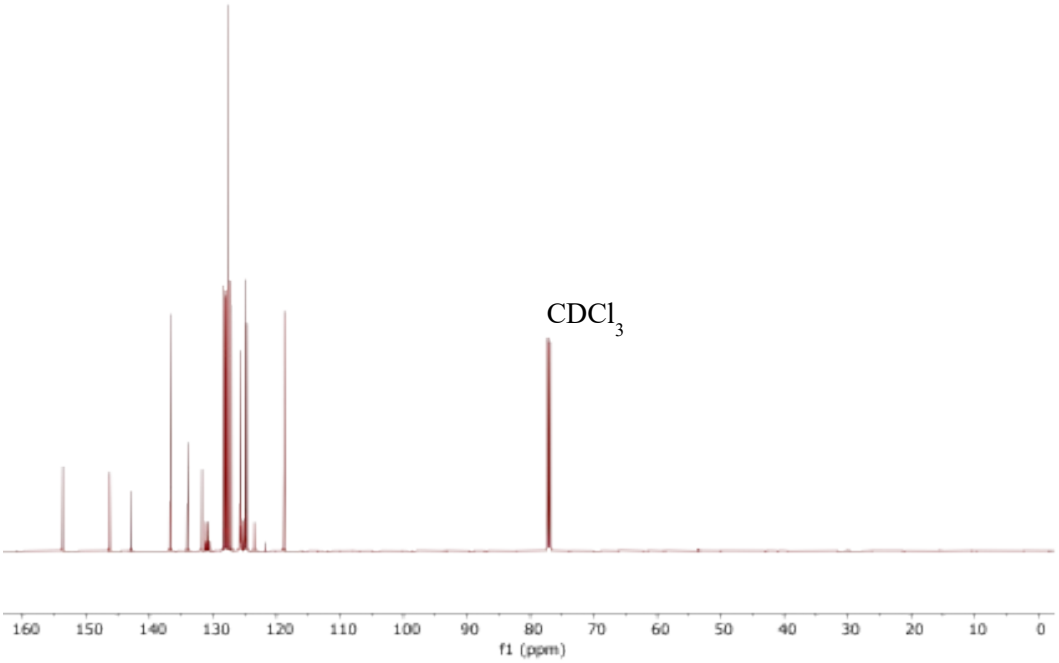

Figure S5. ^{19}F NMR spectrum of 2-[4-(trifluoromethyl)phenyl]benzo[*h*]quinoline in $CDCl_3$.

Figure S6. $^{13}C\{^1H\}$ NMR spectrum 2-[4-(trifluoromethyl)phenyl]benzo[*h*]quinoline in $CDCl_3$.

NMR Spectra of [(bhq-Ph)(PPh_3)Pt] (4)

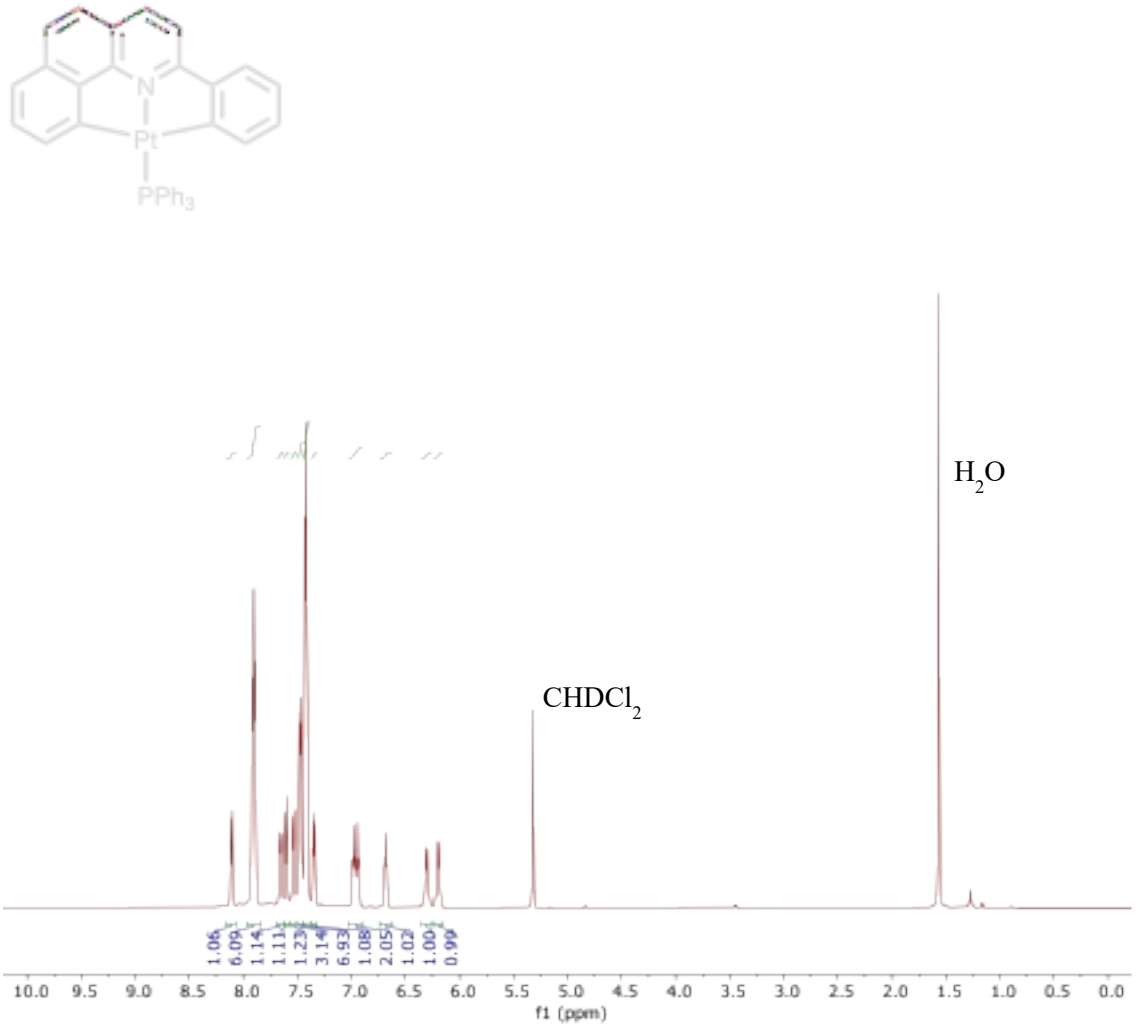

Figure S7. ^{1}H NMR spectrum of **4** in CD_2Cl_2.

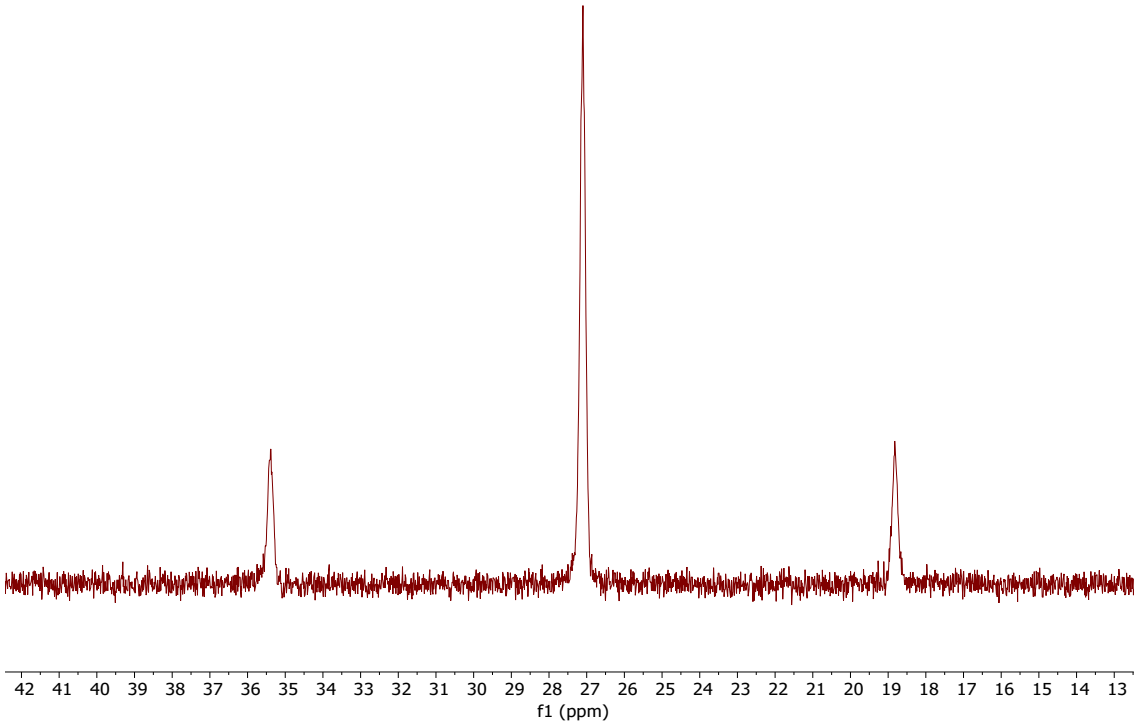

Figure S8. $^{31}P\{^{1}H\}$ NMR spectrum of **4** in CD_2Cl_2.

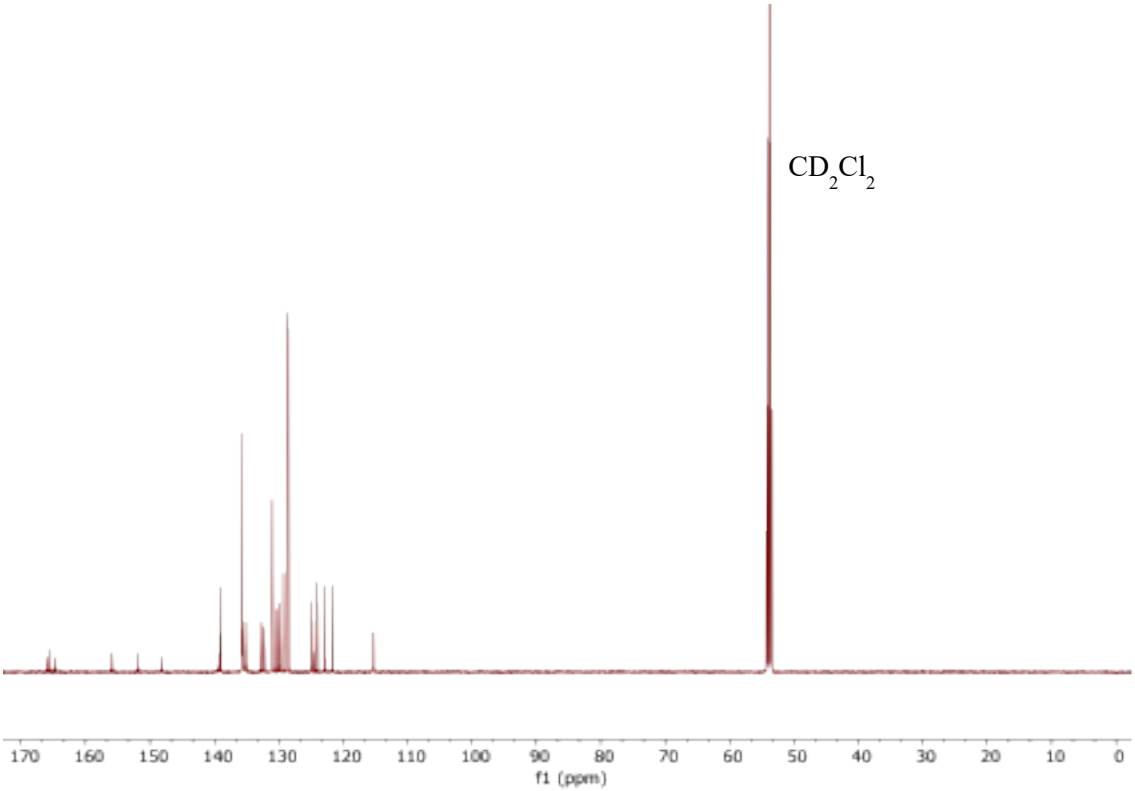

Figure S9. $^{13}C\{^{1}H\}$ NMR spectrum of **4** in CD_2Cl_2.

NMR Spectra of [(bhq-Ph^{OMe})(PPh_3)Pt] (4-OMe)

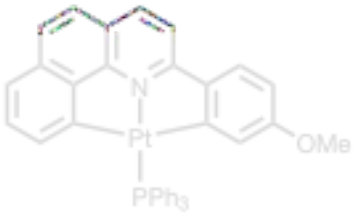

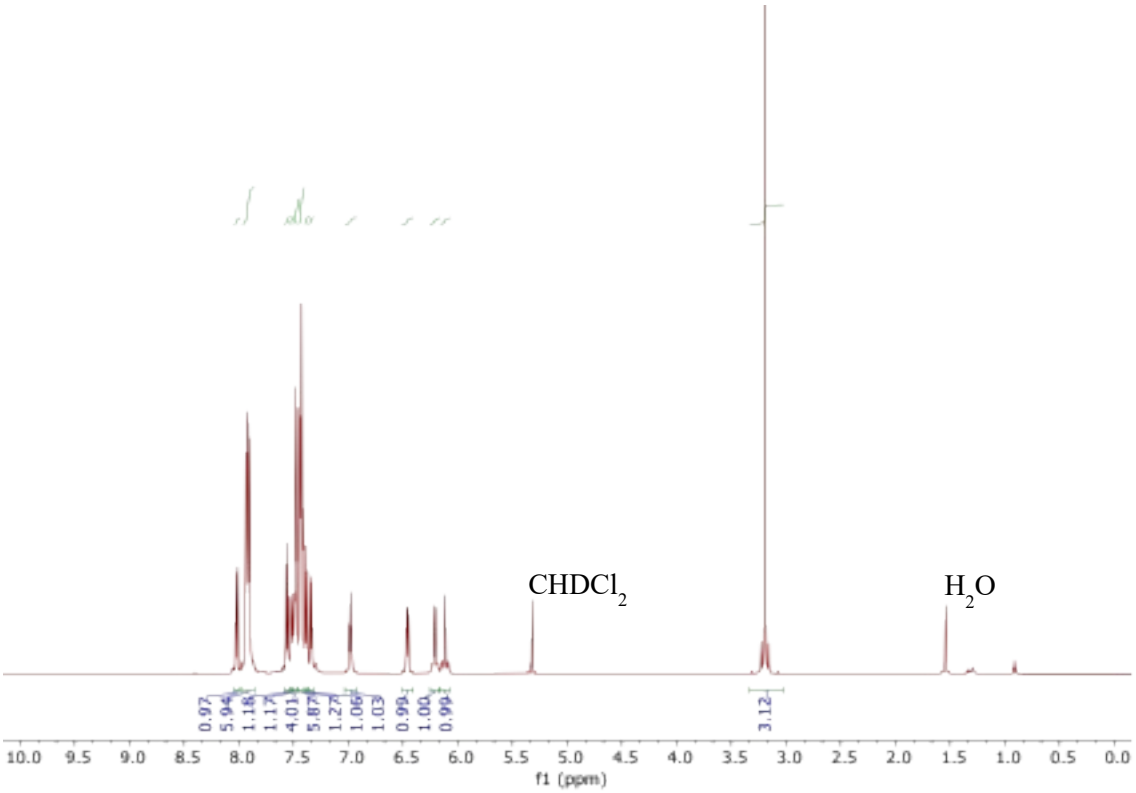

Figure S10. ^{1}H NMR spectrum of **4-OMe** in CD_2Cl_2.

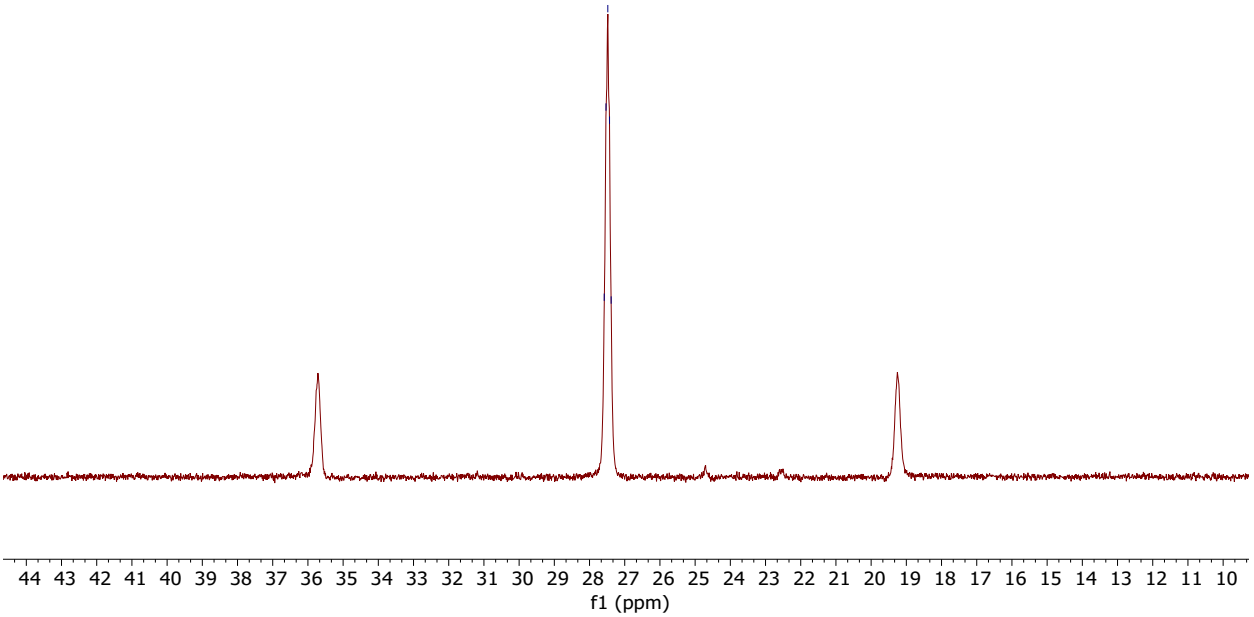

Figure S11. $^{31}P\{^{1}H\}$ NMR spectrum of **4-OMe** in CD_2Cl_2.

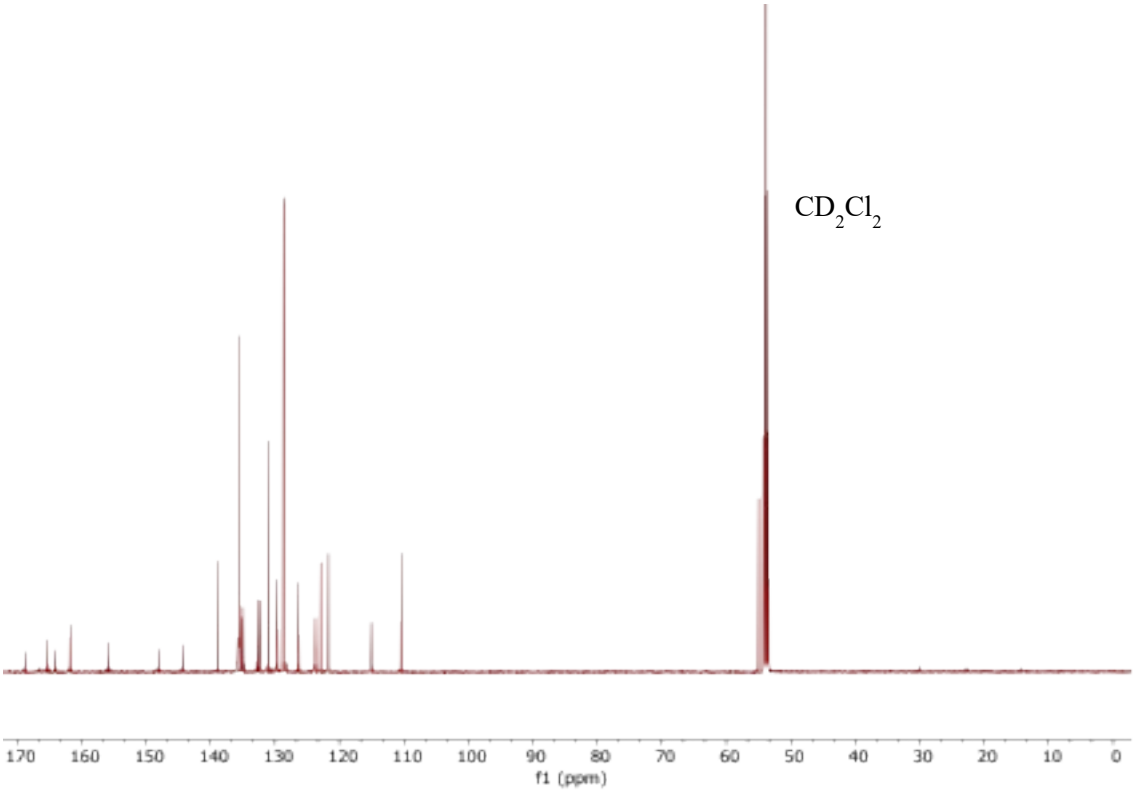

Figure S12. $^{13}C\{^{1}H\}$ NMR spectrum of **4-OMe** in CD_2Cl_2.

NMR Spectra of [(bhq-Ph^{F})(PPh$_3$)Pt] (4-F)

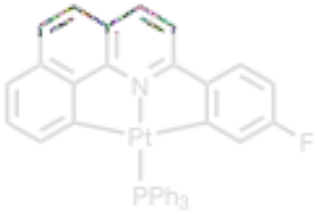

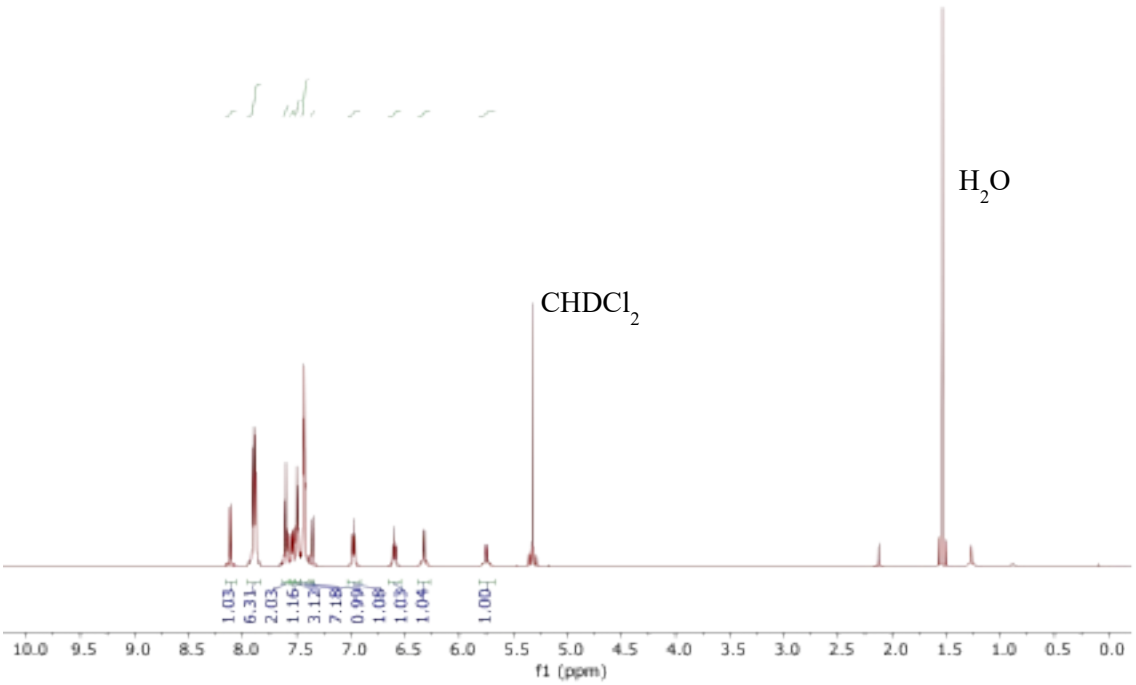

Figure S13. ^{1}H NMR spectrum of **4-F** in CD_2Cl_2.

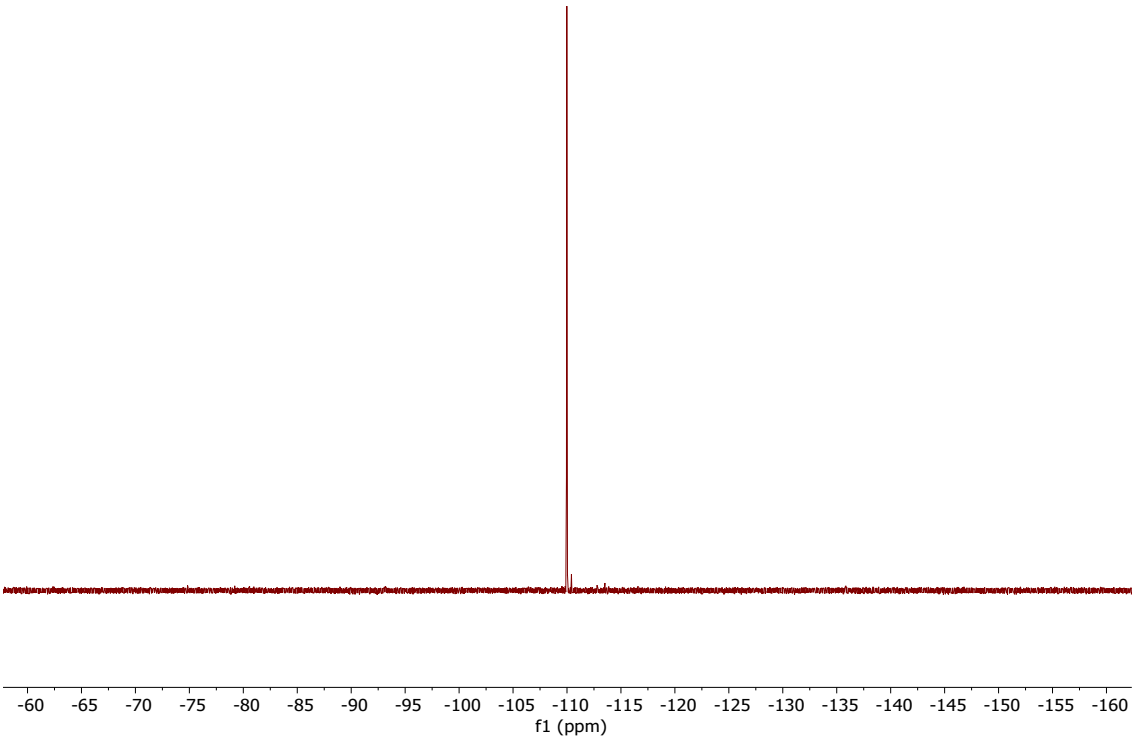

Figure S14. ^{19}F NMR spectrum of **4-F** in CD_2Cl_2.

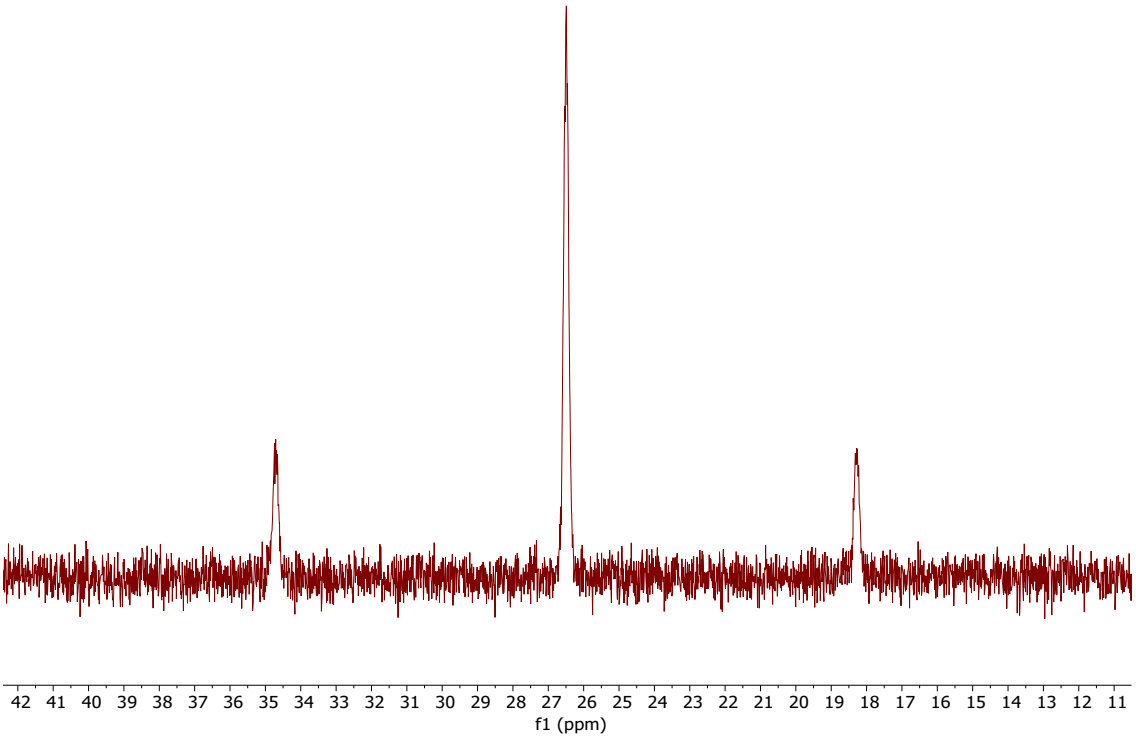

Figure S15. $^{31}P\{^{1}H\}$ NMR spectrum of **4-F** in CD_2Cl_2.

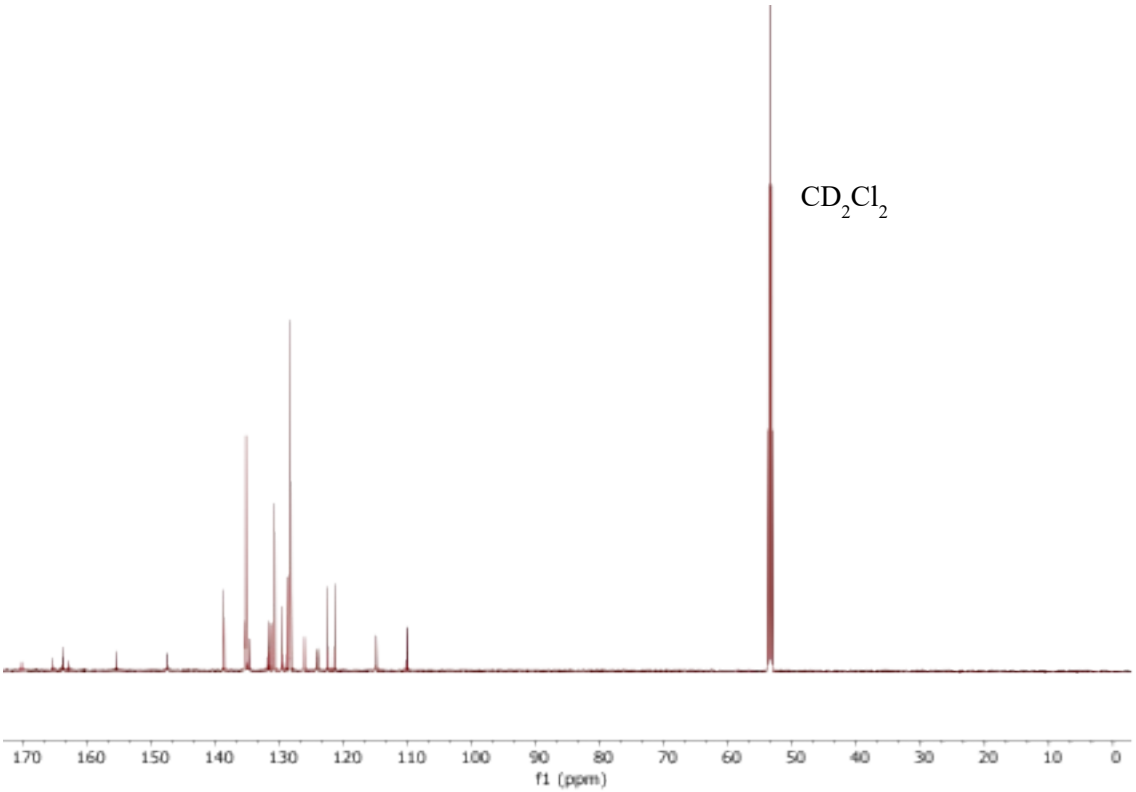

Figure S16. $^{13}C\{^{1}H\}$ NMR spectrum of **4-F** in CD_2Cl_2.

NMR Spectra of [(bhq-Ph^{CF3})(PPh$_3$)Pt] (4-CF$_3$)

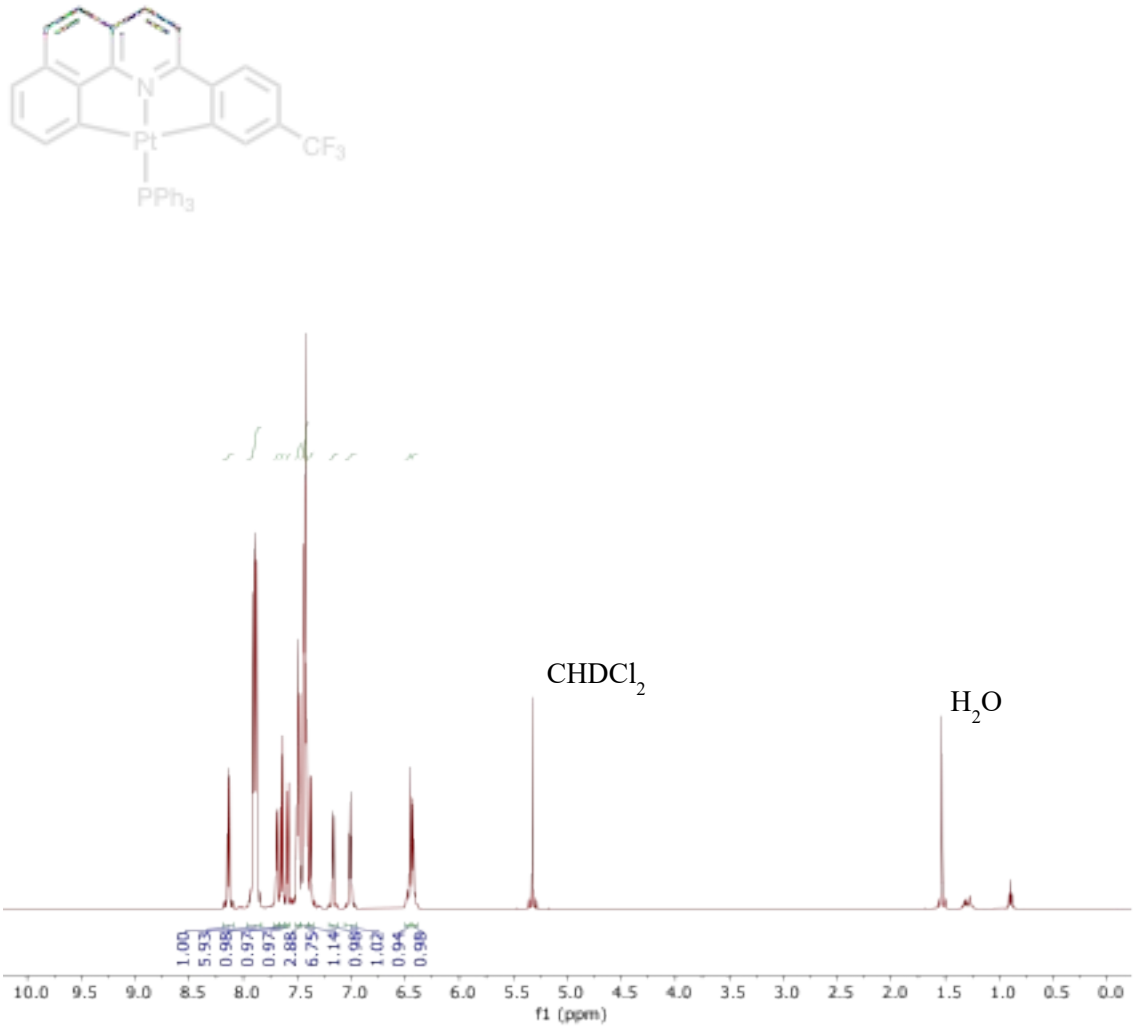

Figure S17. ^{1}H NMR spectrum of **4-CF$_3$** in CD_2Cl_2.

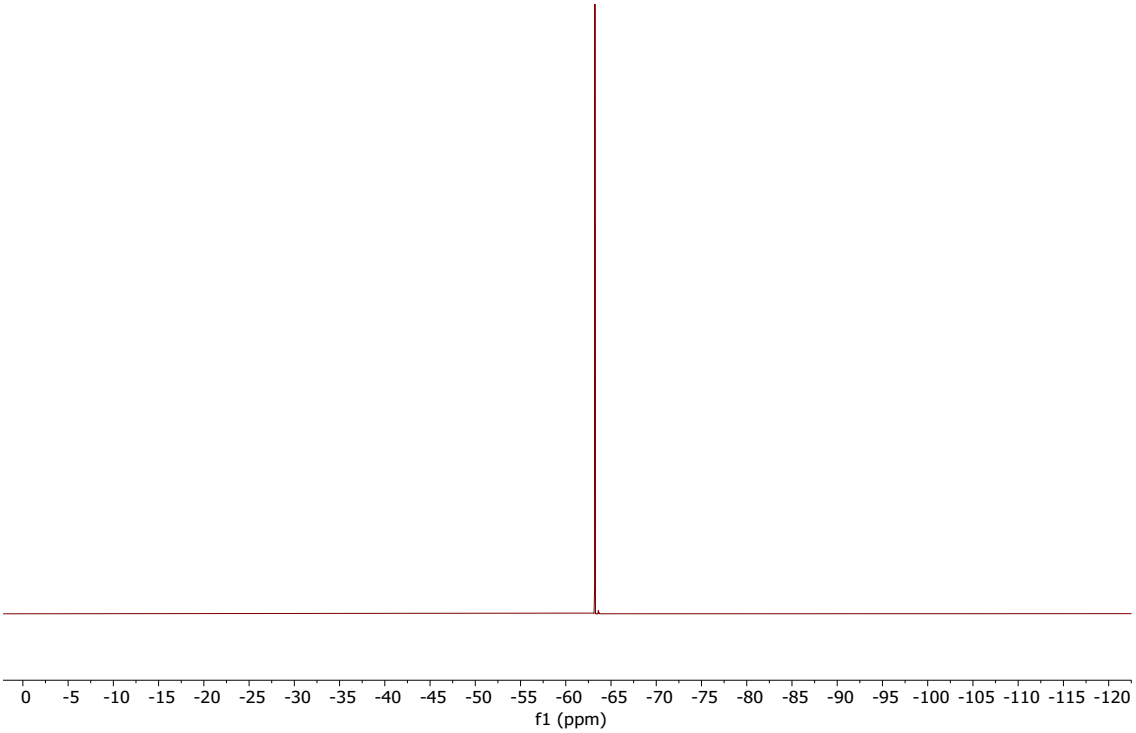

Figure S18. ^{19}F NMR spectrum of **4-CF_3** in CD_2Cl_2.

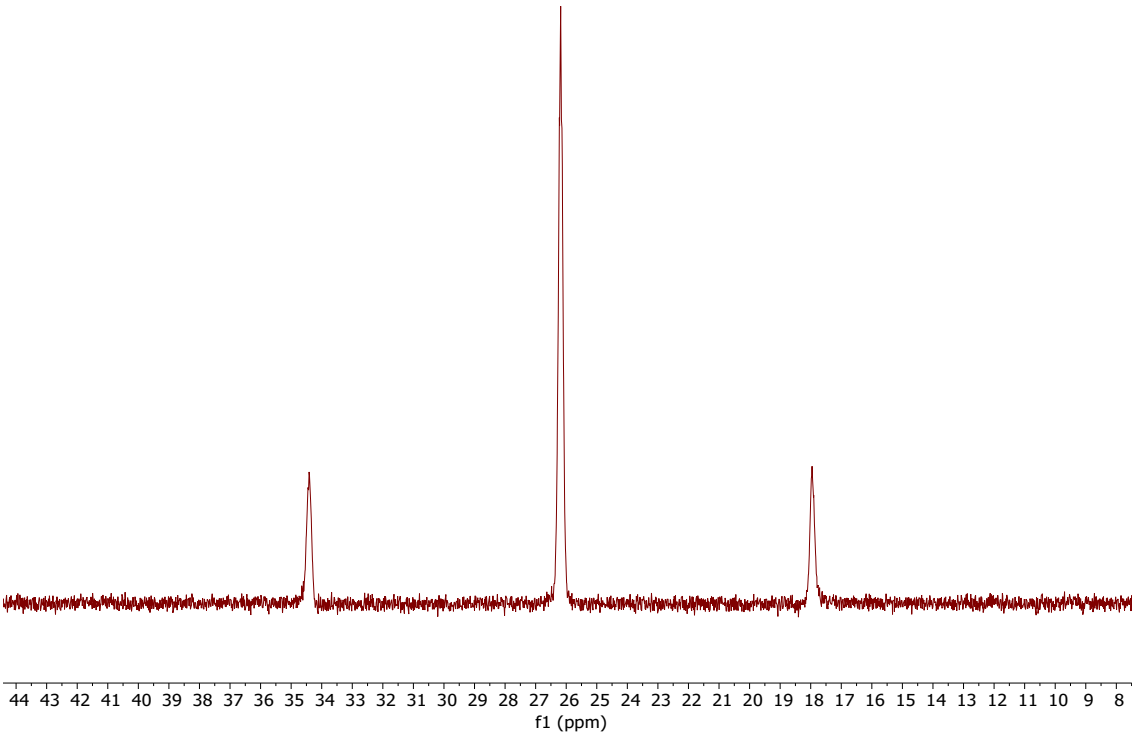

Figure S19. $^{31}P\{^1H\}$ NMR spectrum of **4-CF_3** in CD_2Cl_2.

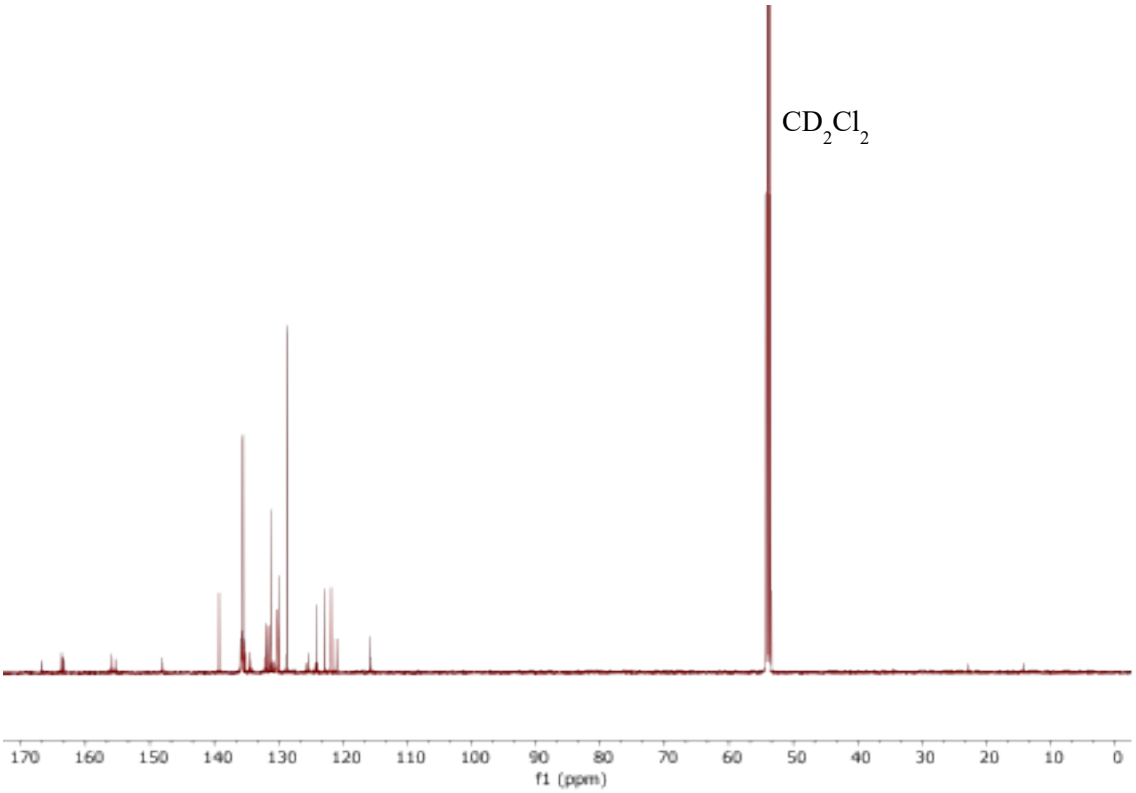

Figure S20. $^{13}C\{^{1}H\}$ NMR spectrum of **4-CF_3** in CD_2Cl_2.

NMR Spectra of [(bhq-Ph)(PPh_3)Pt–Au(PPh_3)][OTf] (5)

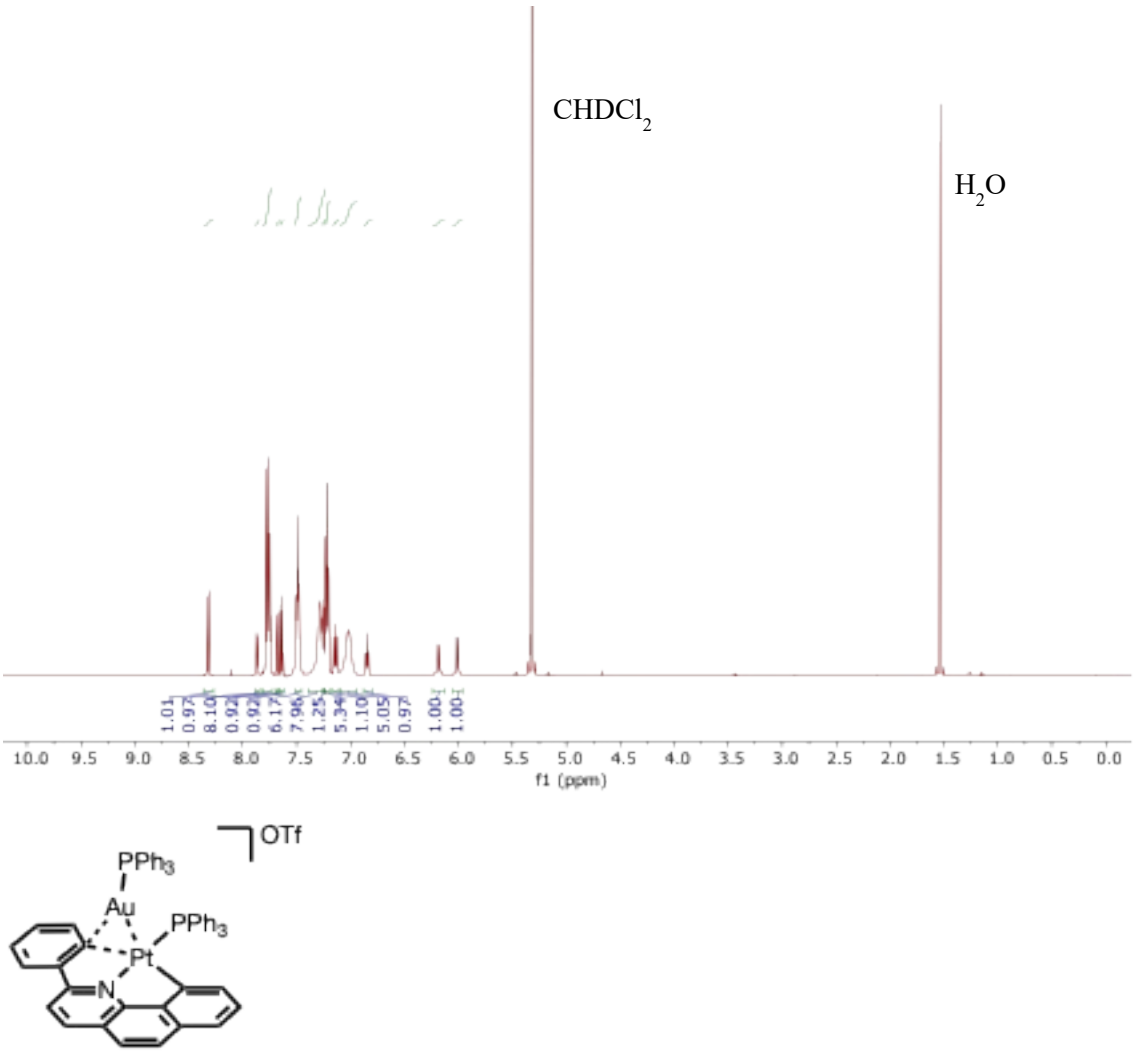

Figure S21. ^{1}H NMR spectrum of **5** in CD_2Cl_2.

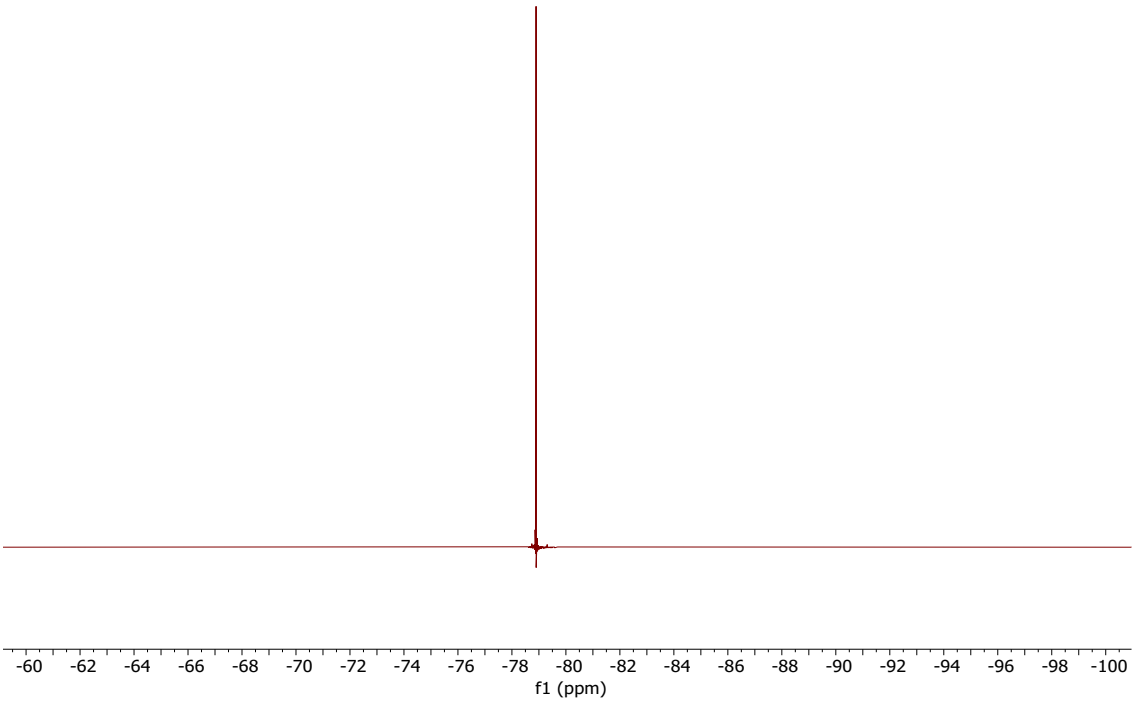

Figure S22. ^{19}F NMR spectrum of **5** in CD_2Cl_2.

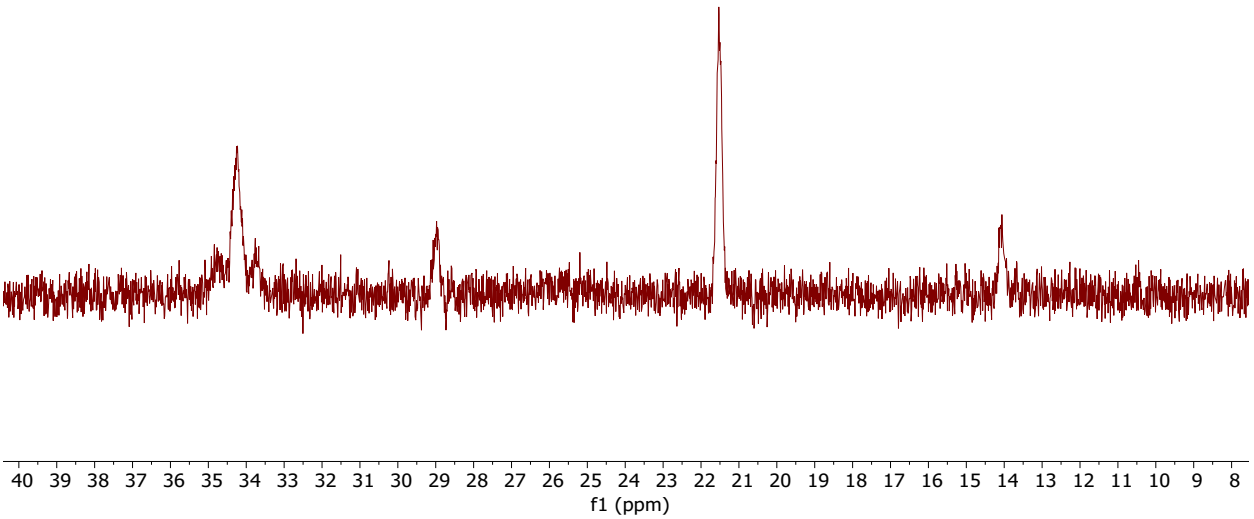

Figure S23. $^{31}P\{^1H\}$ NMR spectrum of **5** in CD_2Cl_2.

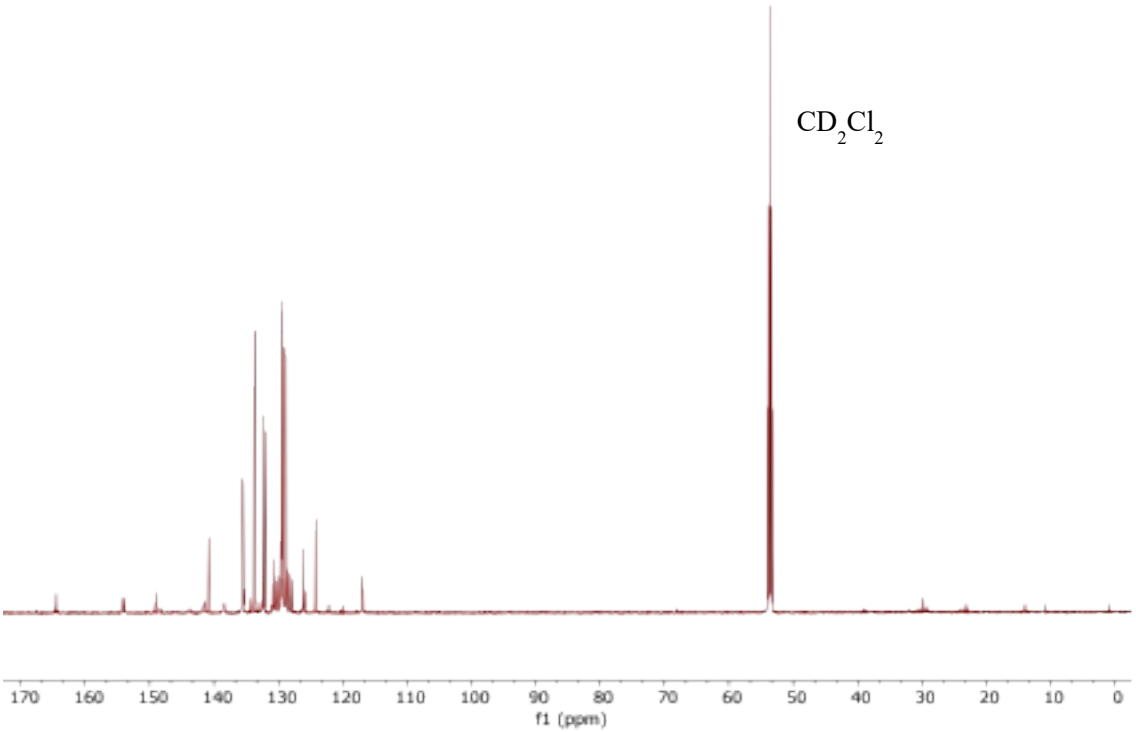

Figure S24. $^{13}C\{^{1}H\}$ NMR spectrum of **5** in CD_2Cl_2.

NMR Spectra of [(bhq-Ph^{OMe})(PPh$_3$)Pt–Au(PPh$_3$)][OTf] (5-OMe)

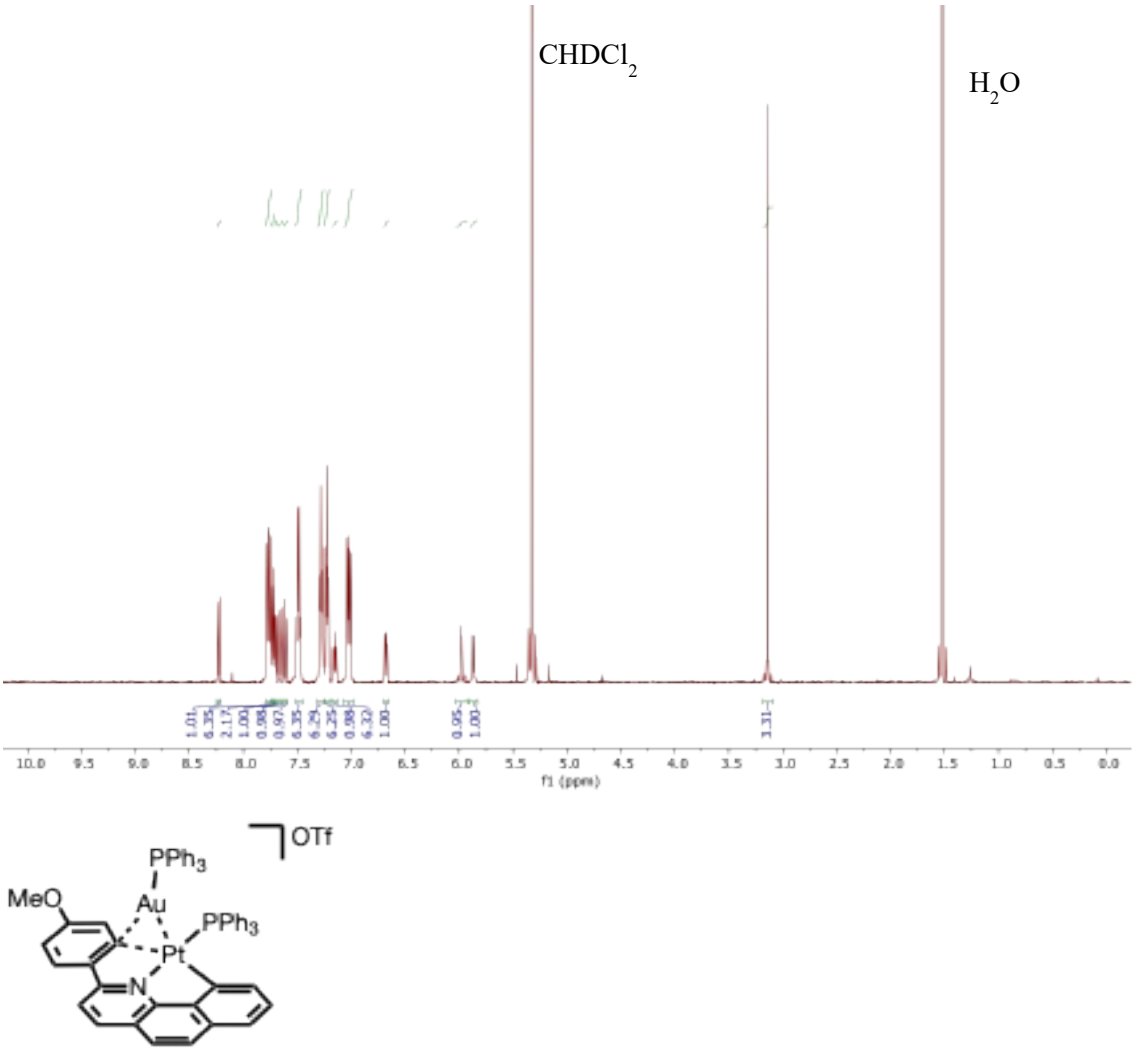

Figure S25. ^{1}H NMR spectrum of **5-OMe** in CD_2Cl_2.

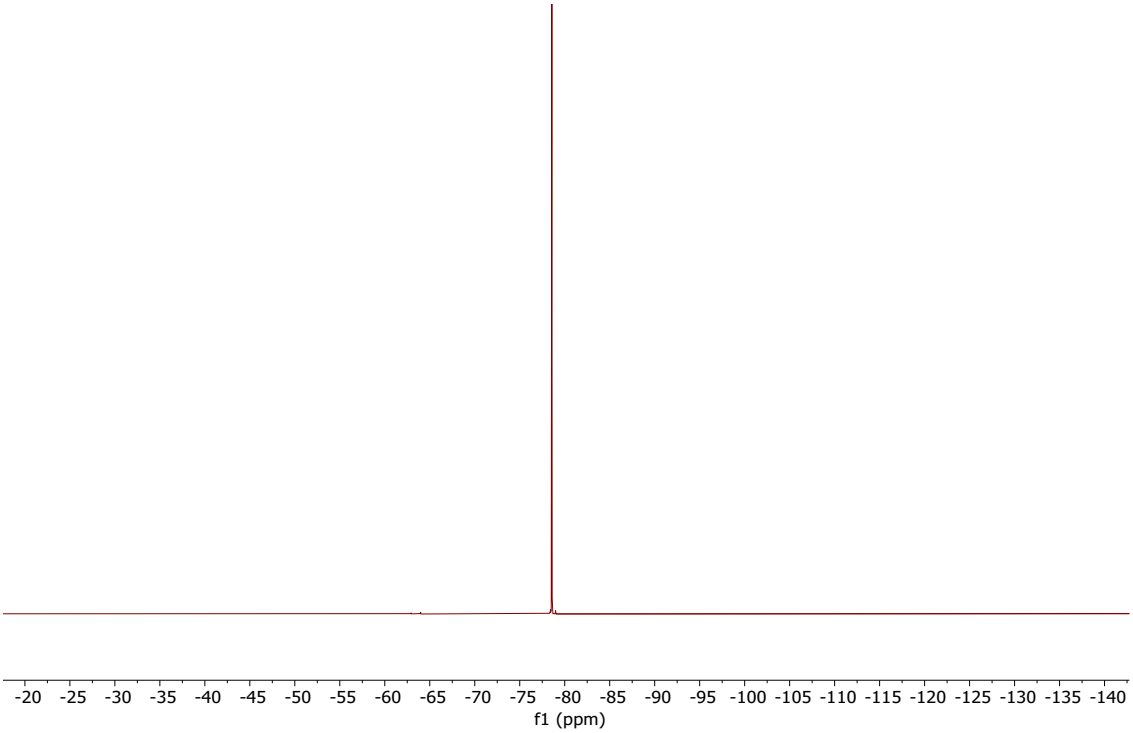

Figure S26. ^{19}F NMR spectrum of **5-OMe** in CD_2Cl_2.

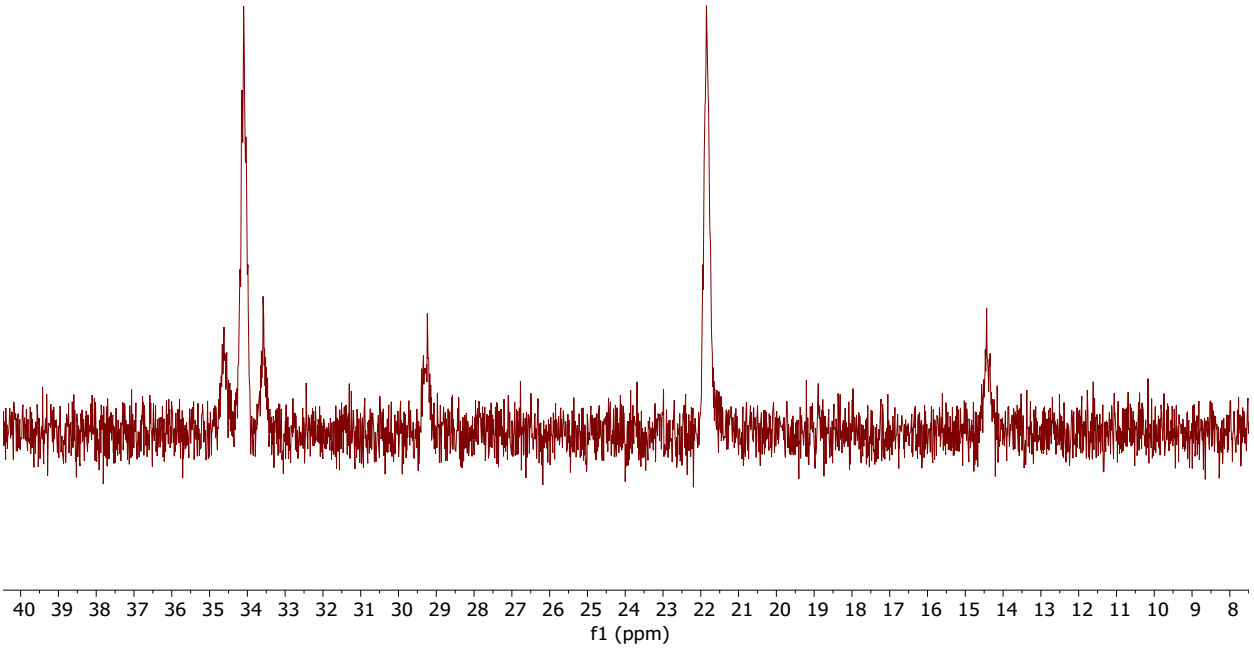

Figure S27. $^{31}P\{^1H\}$ NMR spectrum of **5-OMe** in CD_2Cl_2.

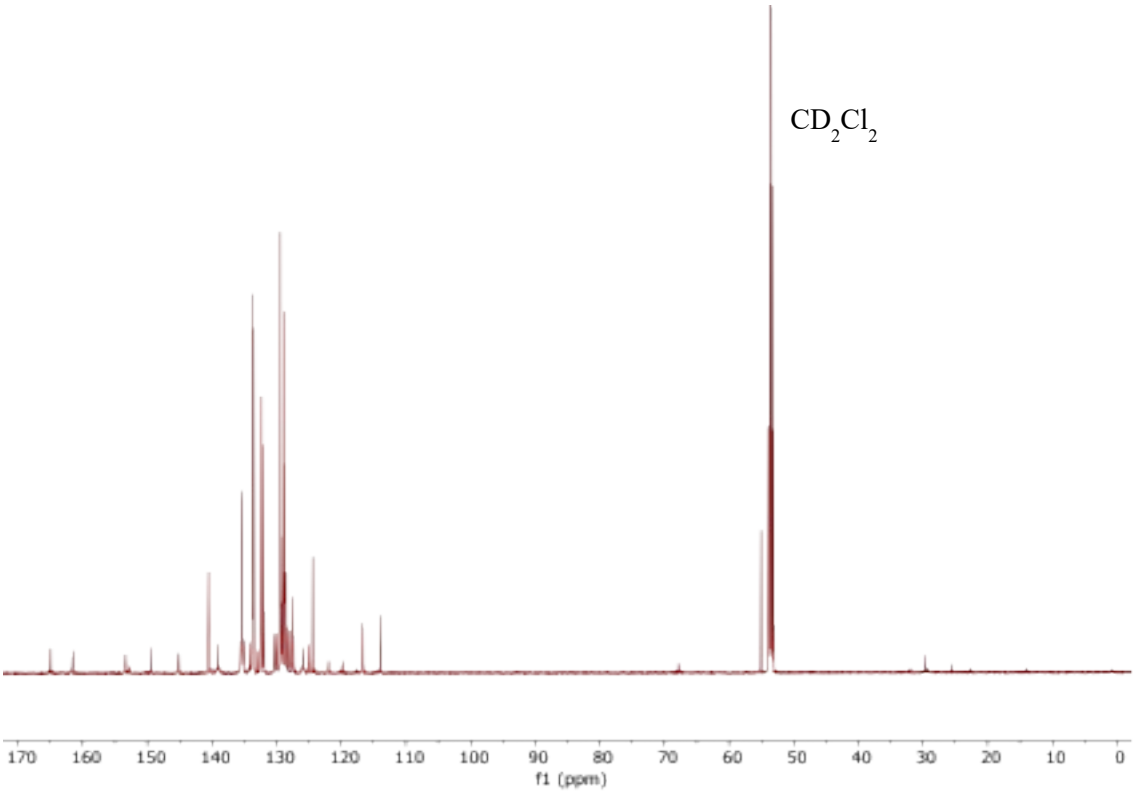

Figure S28. $^{13}C\{^{1}H\}$ NMR spectrum of **5-OMe** in CD_2Cl_2.

NMR Spectra of [(bhq-Ph^F)(PPh$_3$)Pt–Au(PPh$_3$)][OTf] (5-F)

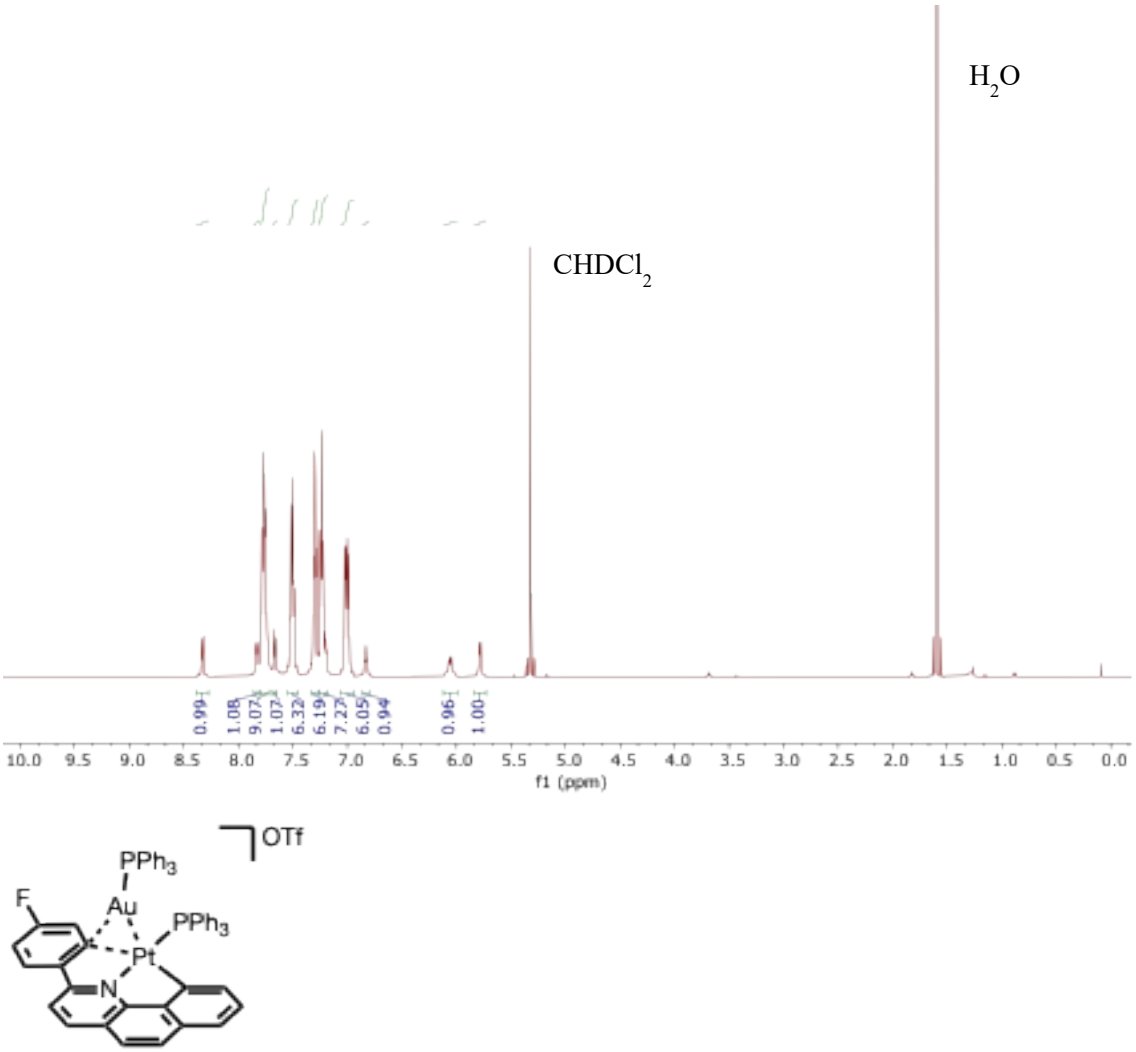

Figure S29. ^{1}H NMR spectrum of **5-F** in CD_2Cl_2.

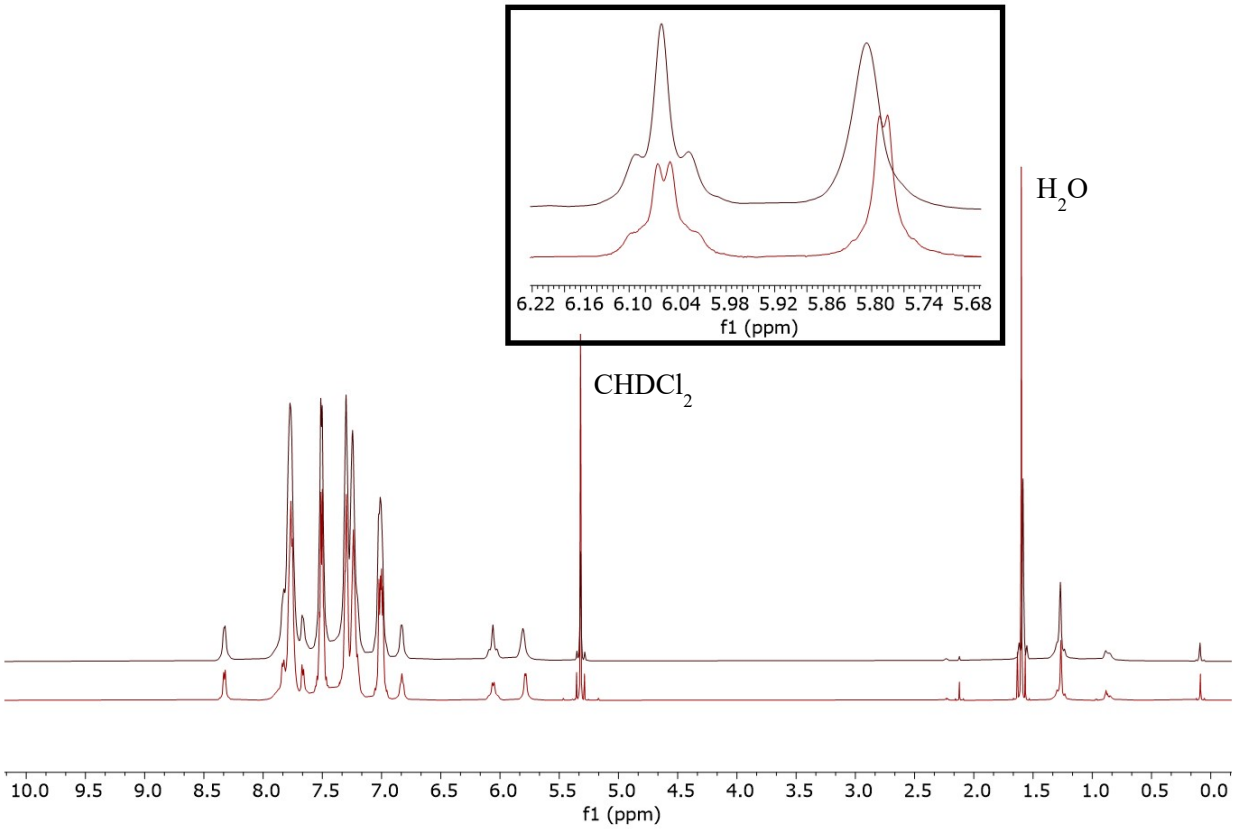

Figure S30. Top spectrum is $^{1}H\{^{19}F\}$ NMR of **5-F** in CD_2Cl_2. Bottom spectrum is ^{1}H NMR of **5-F** in CD_2Cl_2. The box highlights peaks associated with the protons alpha to Pt in complex **5-F**.

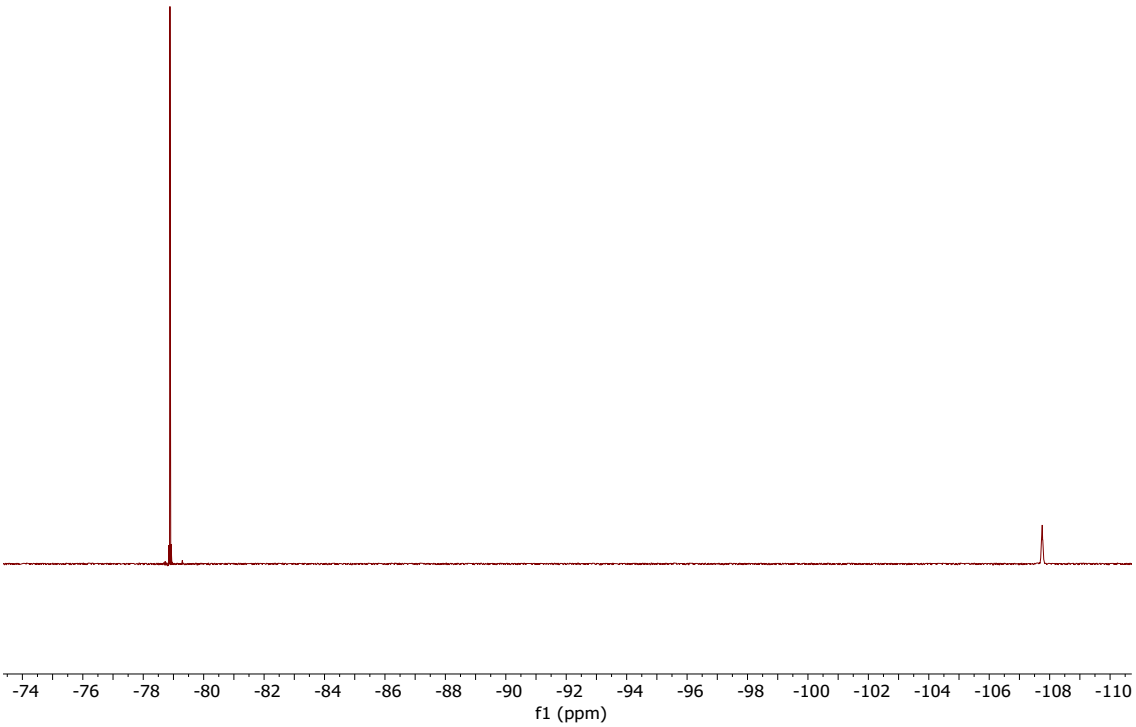

Figure S31. ^{19}F NMR spectrum of **5-F** in CD_2Cl_2.

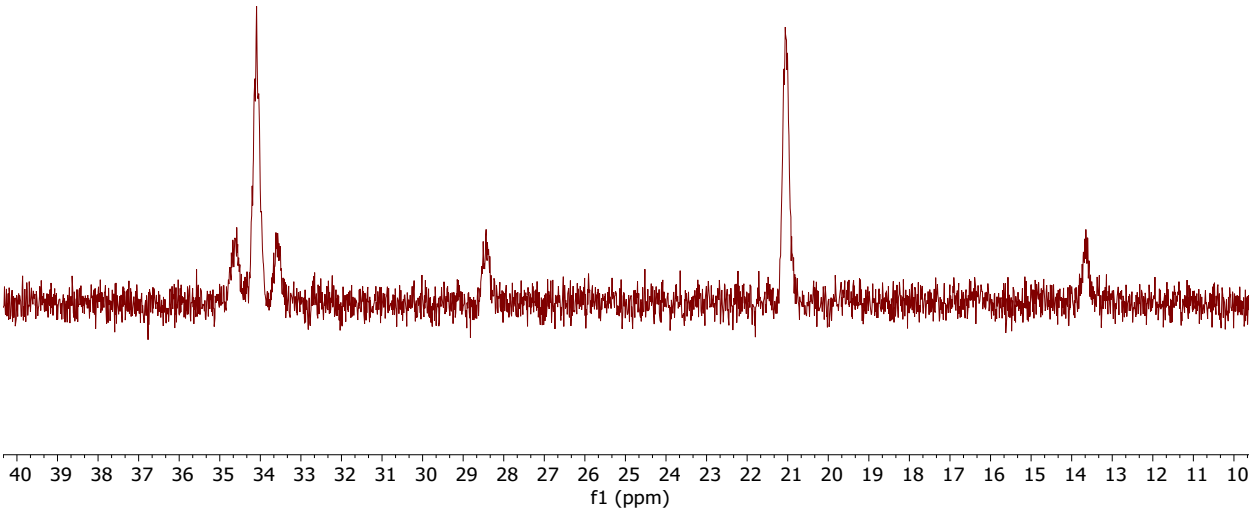

Figure S32. $^{31}P\{^1H\}$ NMR spectrum of **5-F** in CD_2Cl_2.

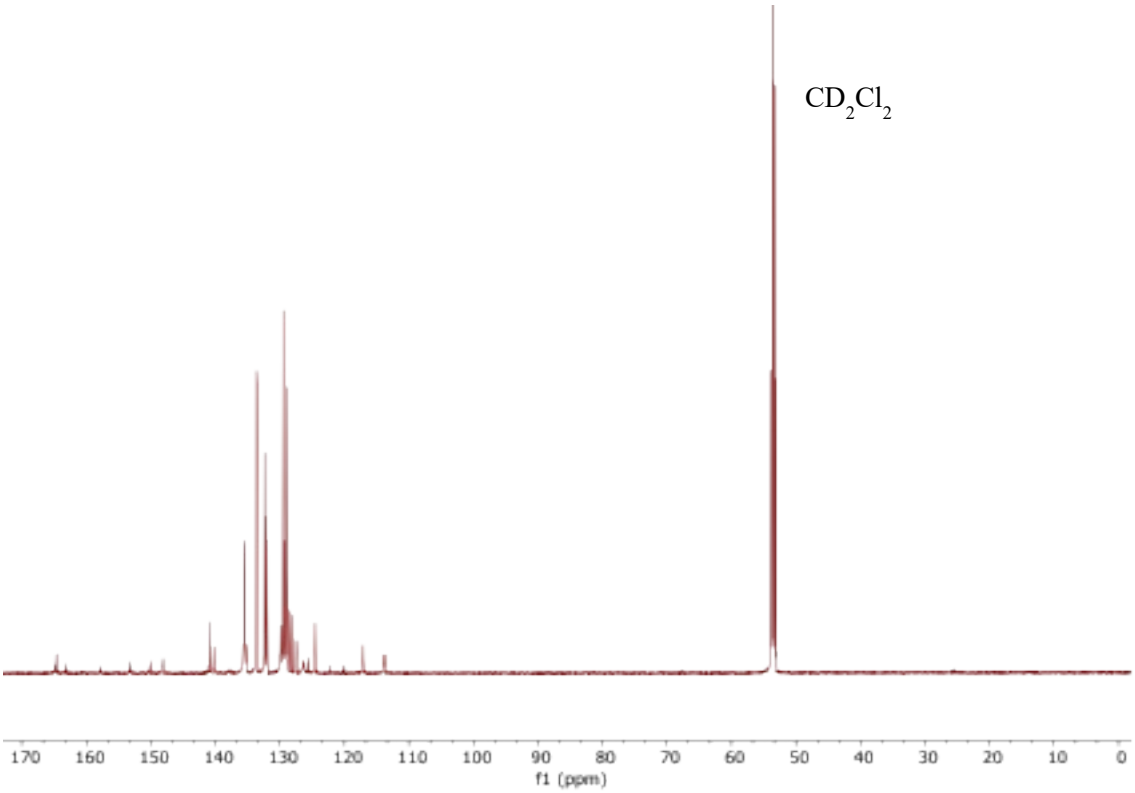

Figure S33. $^{13}C\{^1H\}$ NMR spectrum of **5-F** in CD_2Cl_2.

NMR Spectra of [(bhq-Ph^{CF3})(PPh$_3$)Pt–Au(PPh$_3$)][OTf] (5-CF$_3$)

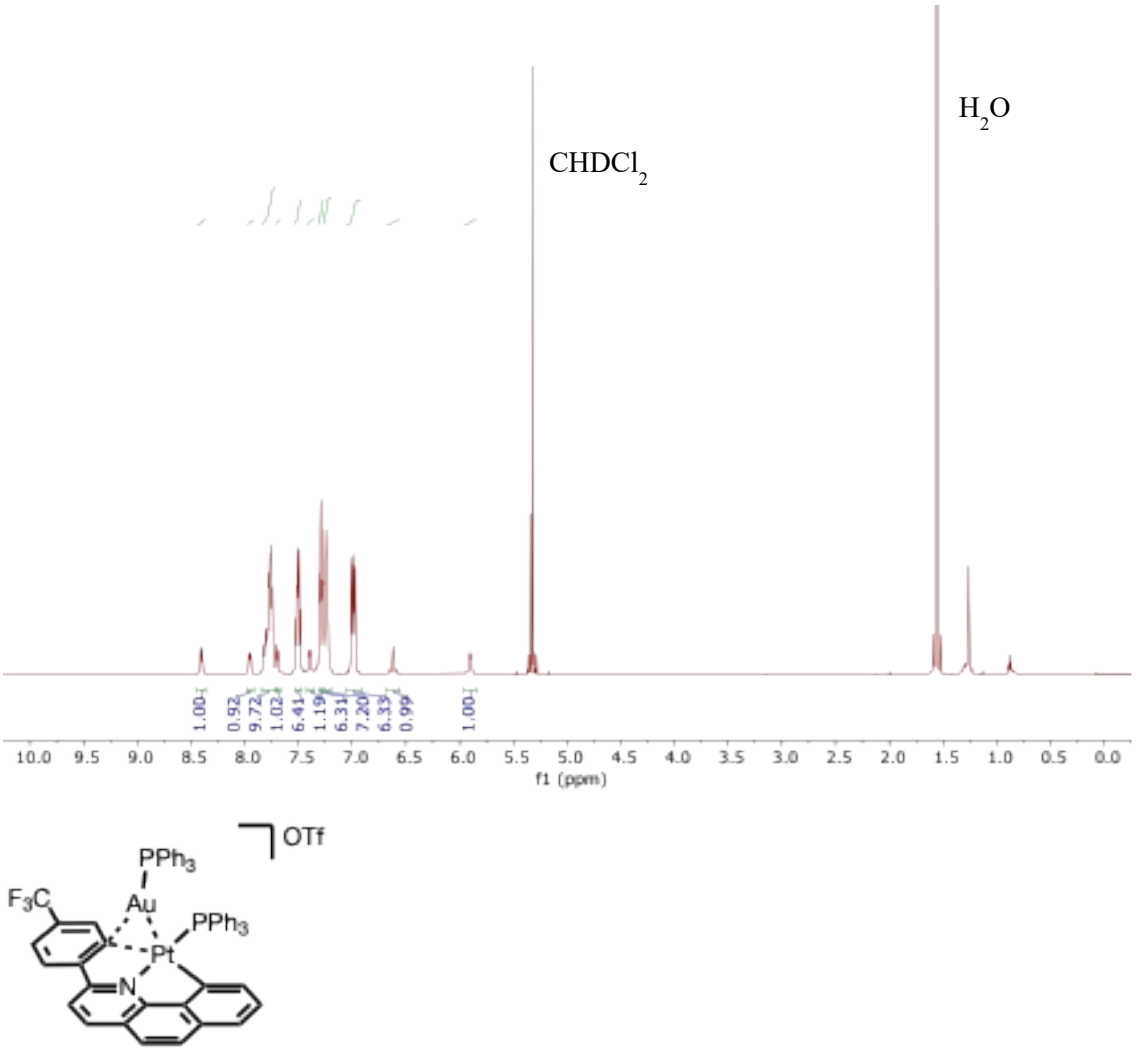

Figure S34. ^{1}H NMR spectrum of **5-CF$_3$** in CD_2Cl_2.

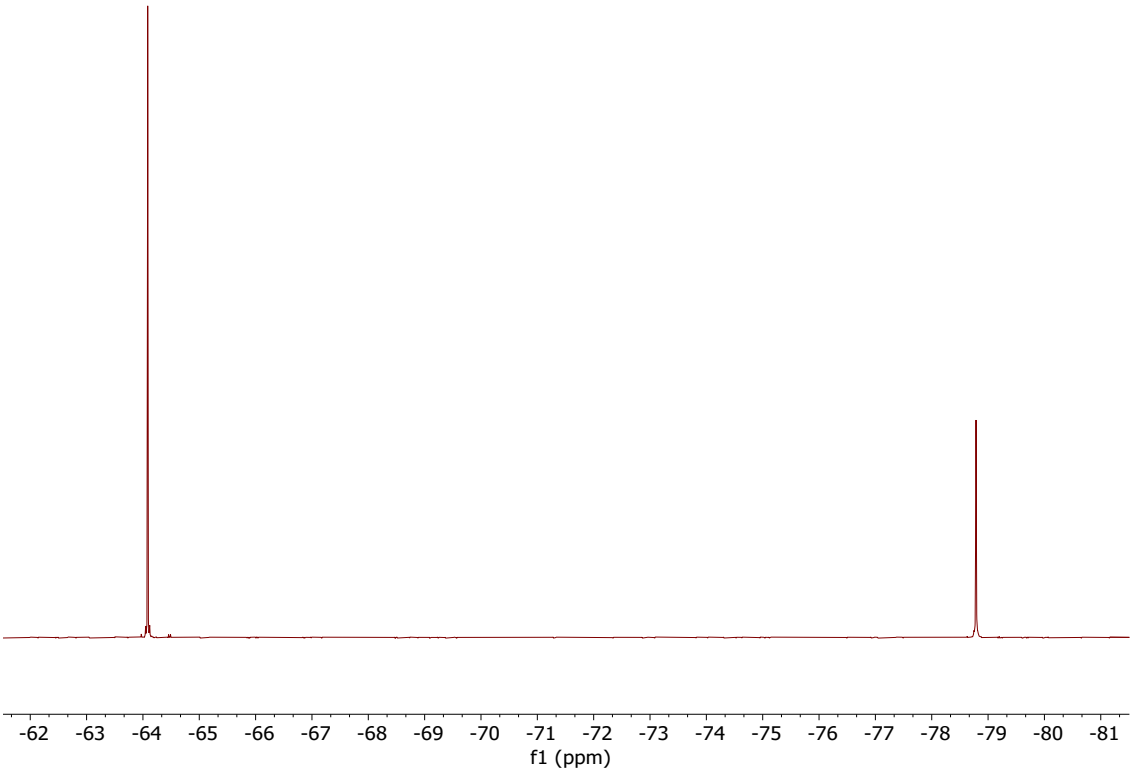

Figure S35. ^{19}F NMR spectrum of **5-CF_3** in CD_2Cl_2.

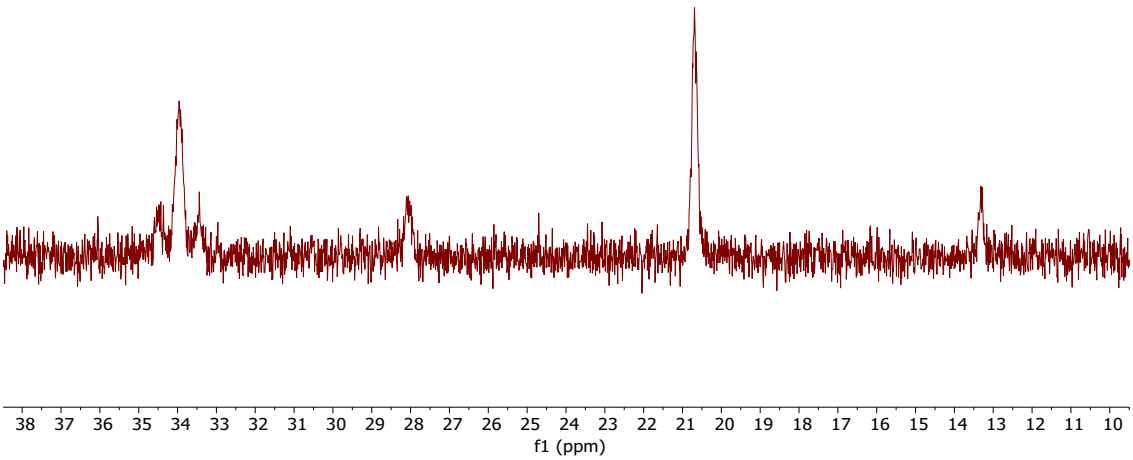

Figure S36. $^{31}P\{^1H\}$ NMR spectrum of **5-CF_3** in CD_2Cl_2.

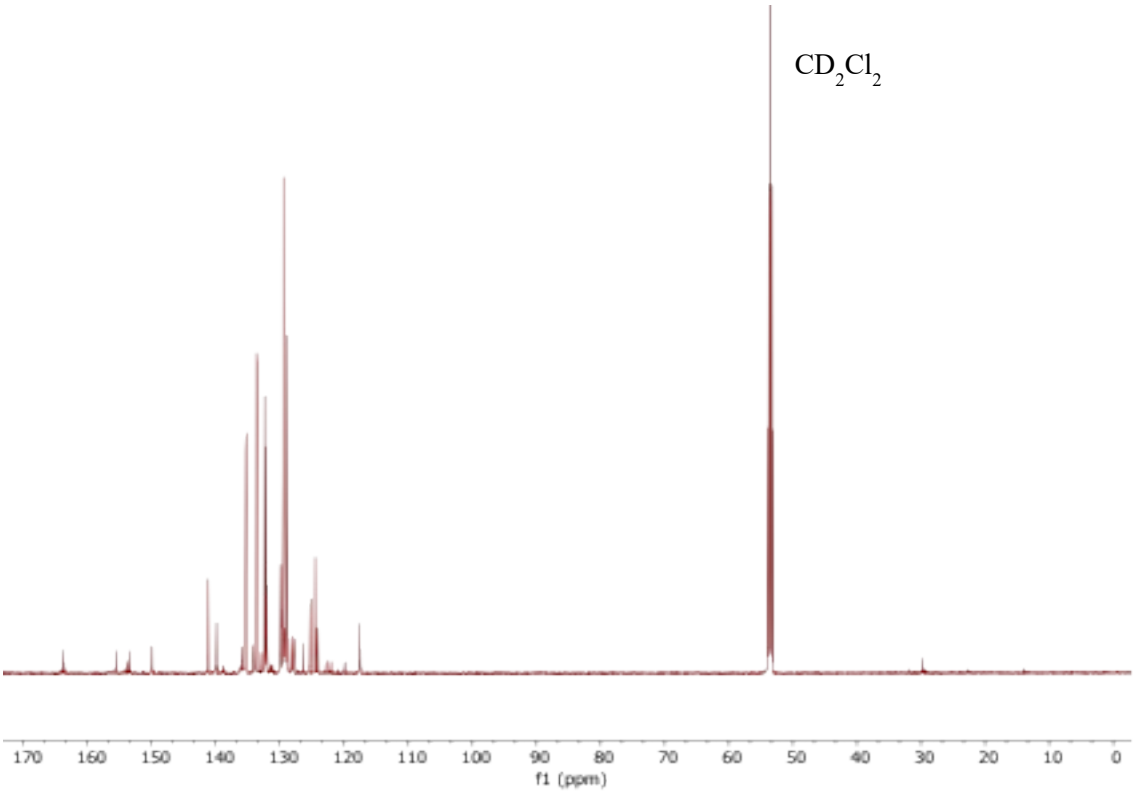

Figure S37. $^{13}C\{^1H\}$ NMR spectrum of **5-CF_3** in CD_2Cl_2.

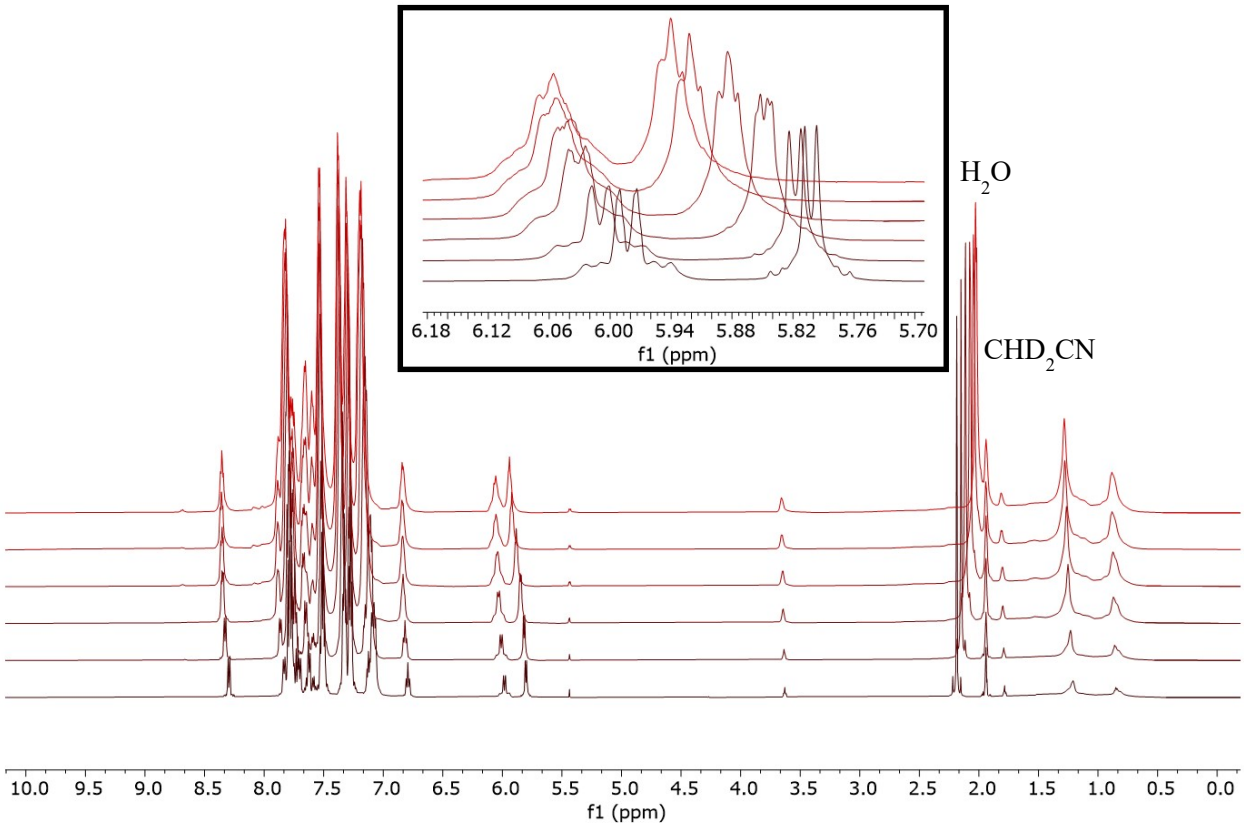

Variable Temperature NMR Spectra of [(bhq-Ph^F)(PPh$_3$)Pt–Au(PPh$_3$)][OTf] (5-F)

Figure S38. ^{1}H NMR spectra of **5-F** in CD_3CN. The bottom ^{1}H NMR spectrum is **5-F** at 25°C. The second spectrum up from the bottom to the top spectrum in ascending order are **5-F** at 35°C, 45°C, 55°C, 65°C, and 70°C. The black box highlights peaks associated with the protons alpha to Pt in complex **5-F**.

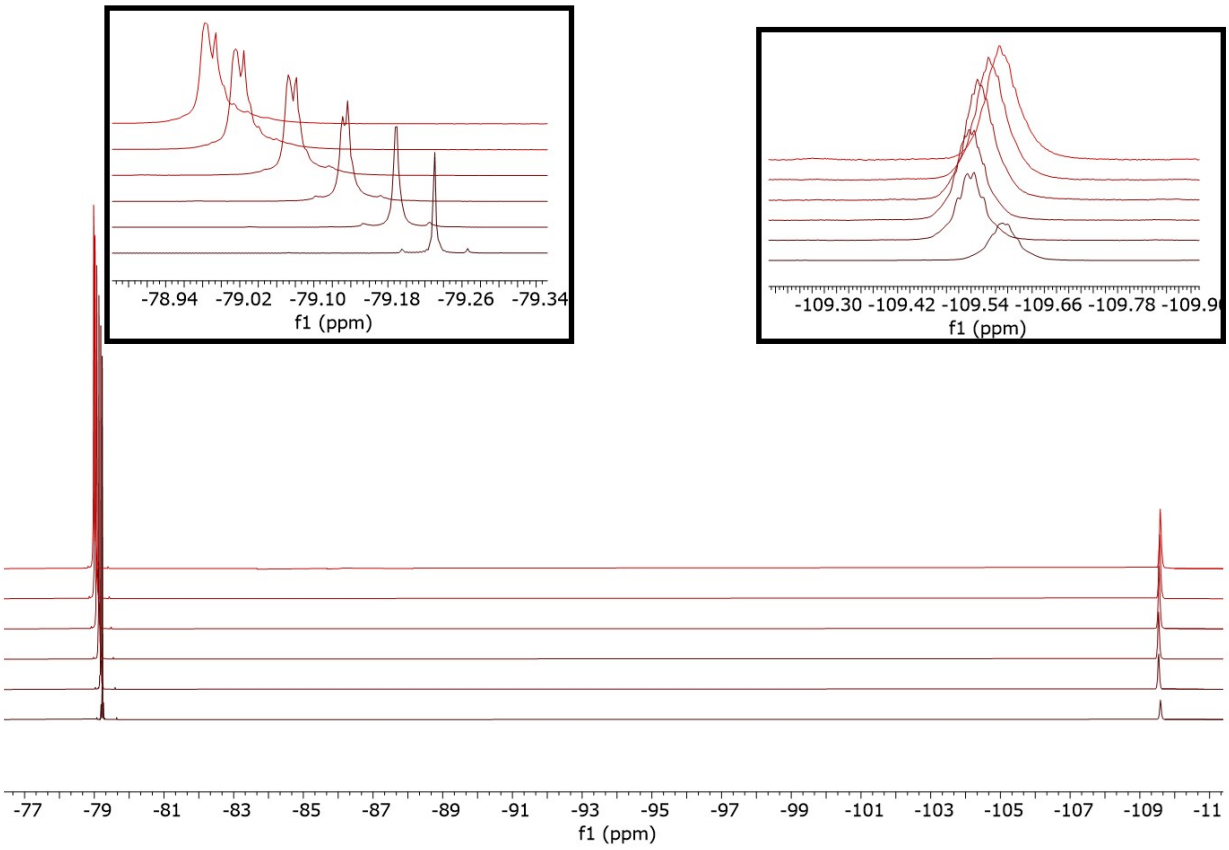

Figure S39. ^{19}F NMR spectra of **5-F** in CD_3CN. The bottom ^{19}F NMR spectrum is **5-F** at 25°C. The second spectrum up from the bottom to the top spectrum in ascending order are **5-F** at 35°C, 45°C, 55°C, 65°C, and 70°C. The box on the top left is the peak associated with the outer sphere triflate ion. The box on the top right is the peak associated with the fluorine substituent on the bhq-Ph^F ligand in **5-F**.

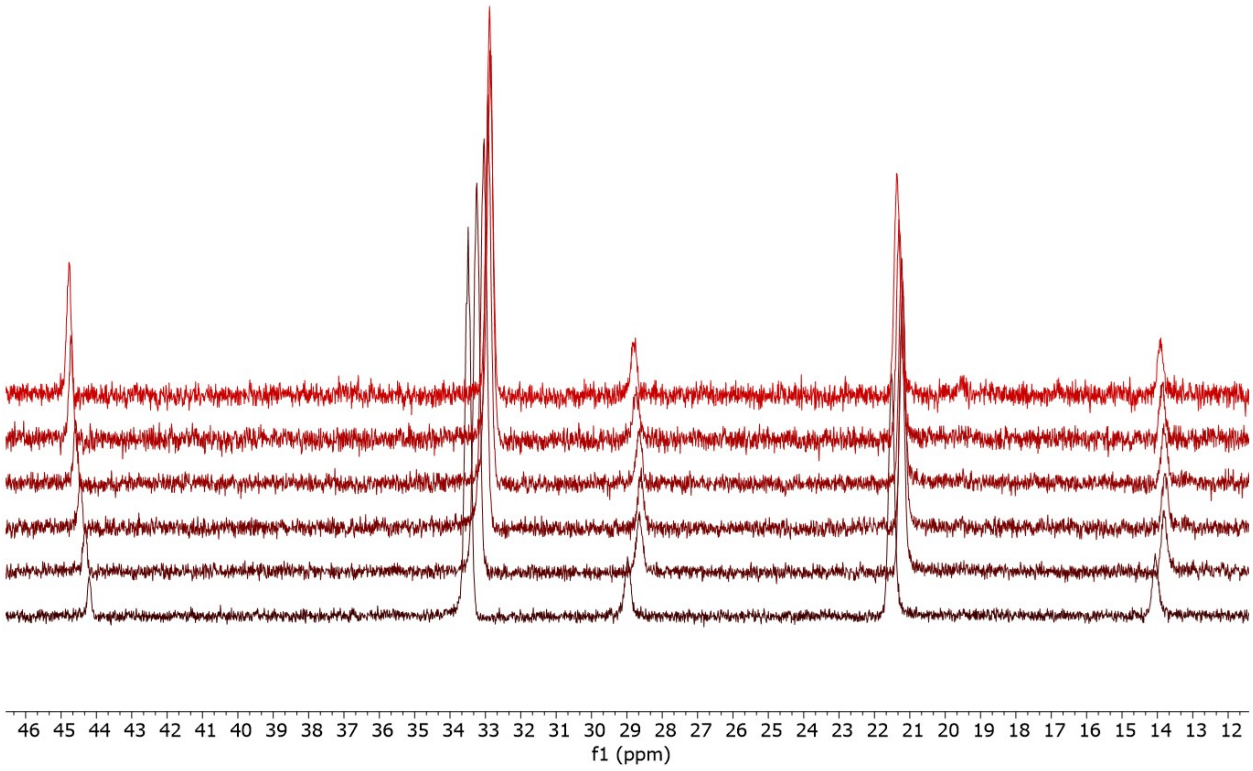

Figure S40. $^{31}P\{^{1}H\}$ NMR spectra of **5-F** in CD_3CN. The bottom $^{31}P\{^{1}H\}$ NMR spectrum is **5-F** at 25°C. The second spectrum up from the bottom to the top spectrum in ascending order are **5-F** at 35°C, 45°C, 55°C, 65°C, and 70°C. The peak observed at ~ 44ppm is associated with $[(PPh_3)_2Au]^+$, a decomposition product.

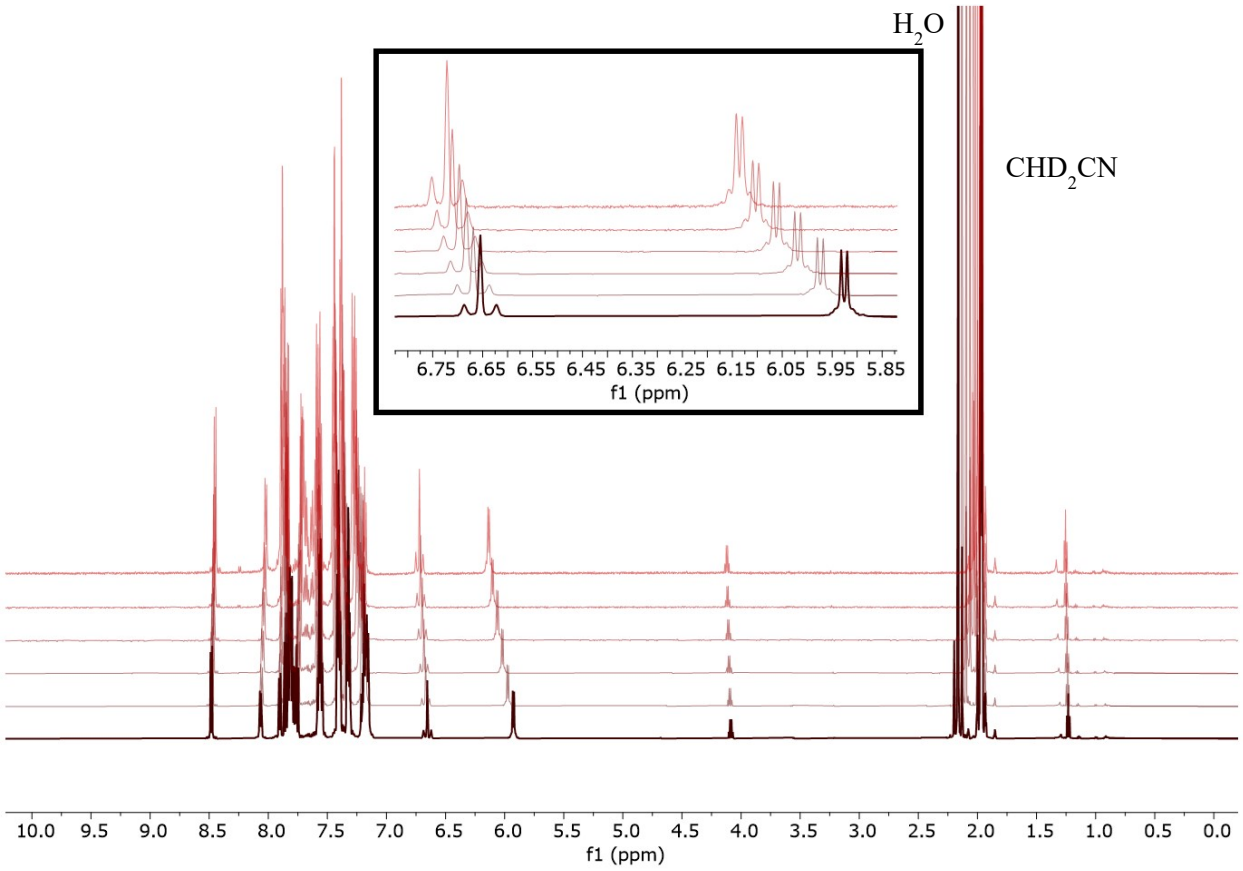

Variable Temperature NMR Spectra of [(bhq-Ph^{CF3})(PPh_3)Pt–Au(PPh_3)][OTf] (5-CF_3)

Figure S41. ^{1}H NMR spectra of **5-CF_3** in CD_3CN. The bottom ^{1}H NMR spectrum is **5-CF_3** at 25°C. The second spectrum up from the bottom to the top spectrum in ascending order are **5-CF_3** at 35°C, 45°C, 55°C, 65°C, and 70°C. The box highlights peaks associated with the protons alpha to Pt in complex **5-CF_3**.

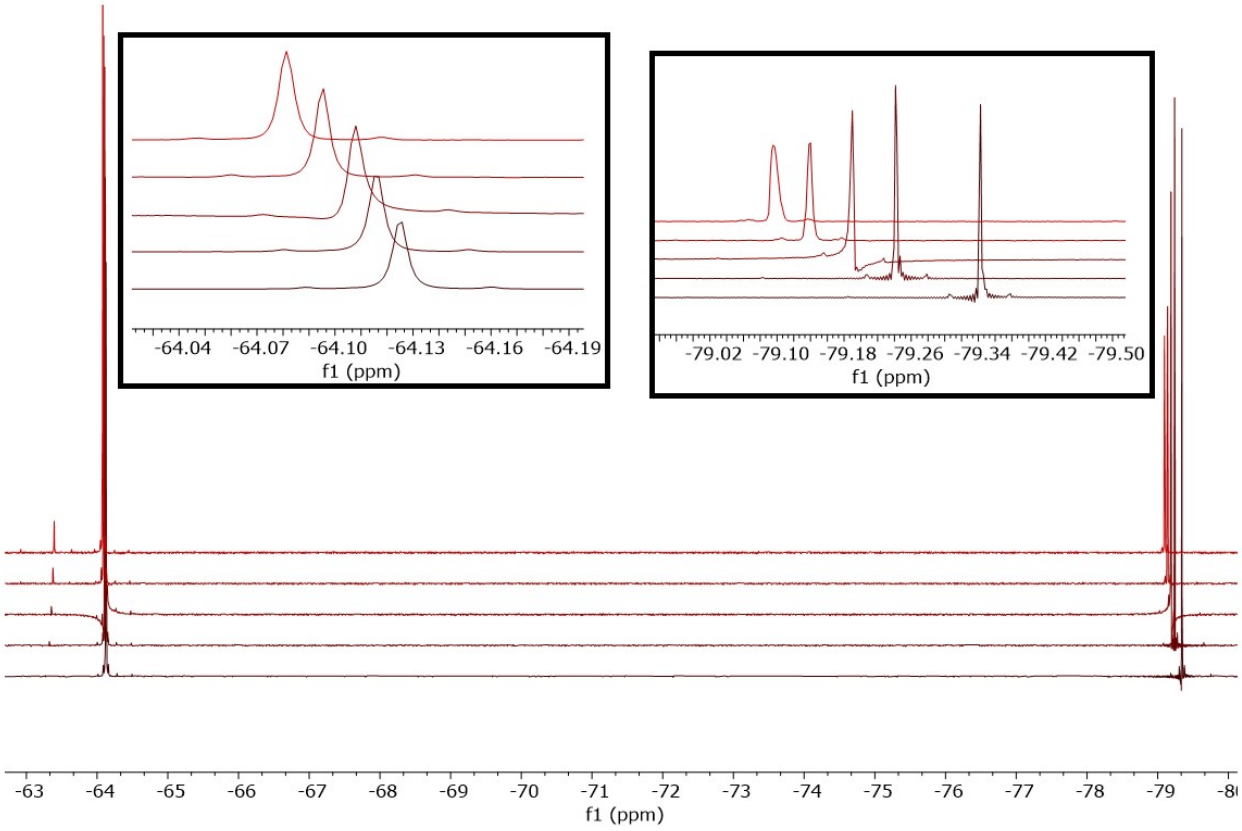

Figure S42. ^{19}F NMR spectra of **5-CF_3** in CD_3CN. The bottom ^{19}F NMR spectrum is **5-CF_3** at 25°C. The second spectrum up from the bottom to the top spectrum in ascending order are **5-CF_3** at 35°C, 45°C, 55°C, 65°C, and 70°C. The box on the top left is the peak associated with the trifluomethyl substituent on the bhq-Ph^{CF3} ligand in **5-CF_3**. The box on the top right is the peak associated with the outer sphere triflate ion.

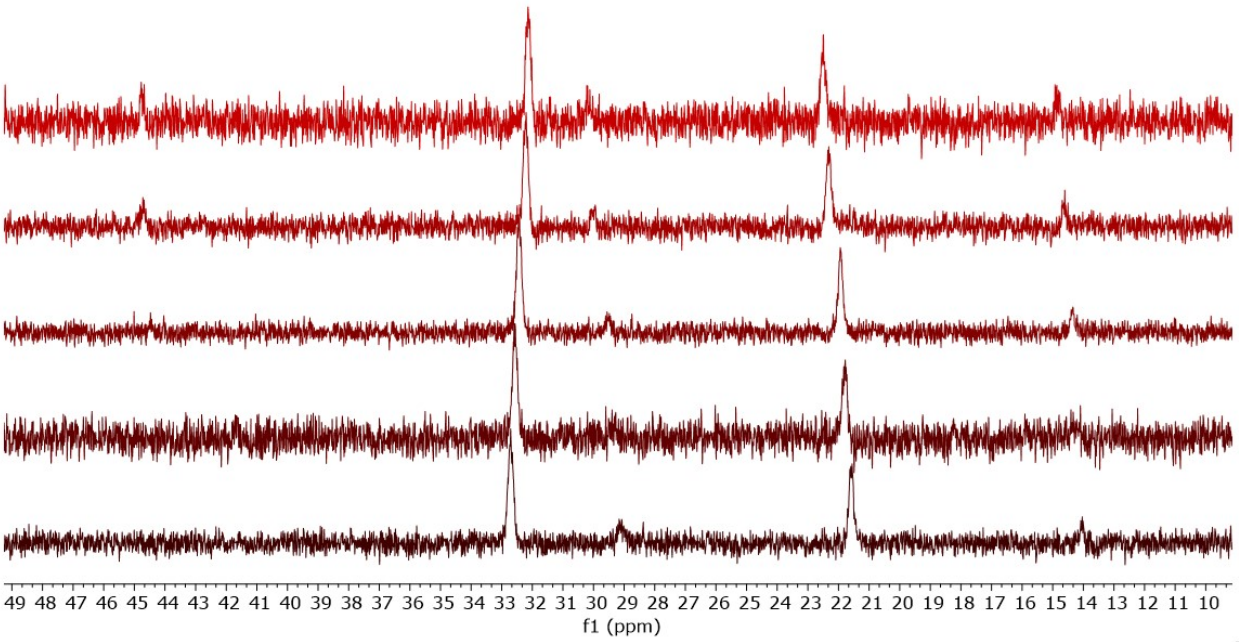

Figure S43. $^{31}P\{^{1}H\}$ NMR spectra of **5-CF_3** in CD_3CN. The bottom $^{31}P\{^{1}H\}$ NMR spectrum is **5-CF_3** at 25°C. The second spectrum up from the bottom to the top spectrum in ascending order are **5-CF_3** at 35°C, 45°C, 65°C, and 70°C.

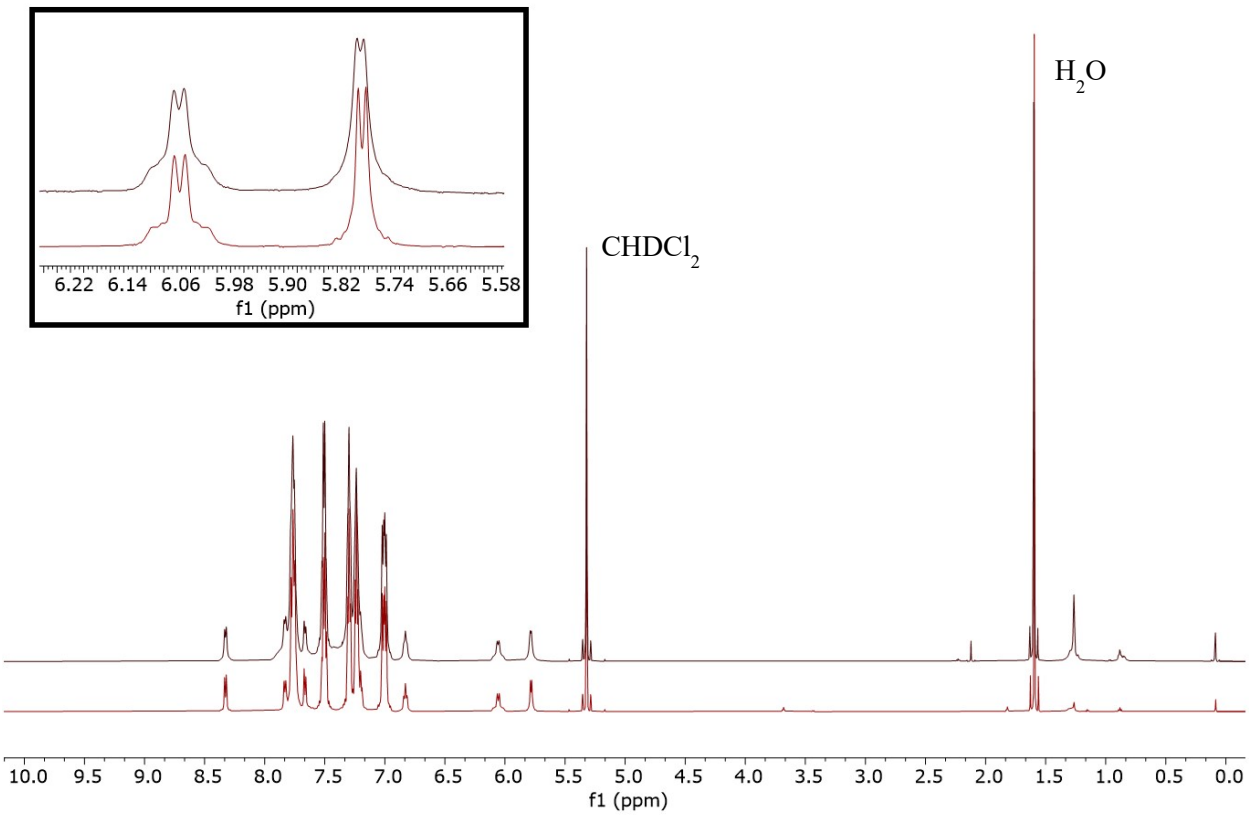

Time Dependent NMR Spectra of [(bhq-Ph^F)(PPh$_3$)Pt–Au(PPh$_3$)][OTf] (5-F)

Figure S44. Top spectrum is ^{1}H NMR of **5-F** synthesized at 25°C in CD_2Cl_2. Bottom spectrum is ^{1}H NMR of **5-F** in CD_2Cl_2; complex was synthesized in THF according to procedure and heated to 45°C for 1 hour. The box highlights peaks associated with the protons alpha to Pt in complex **5-F**.

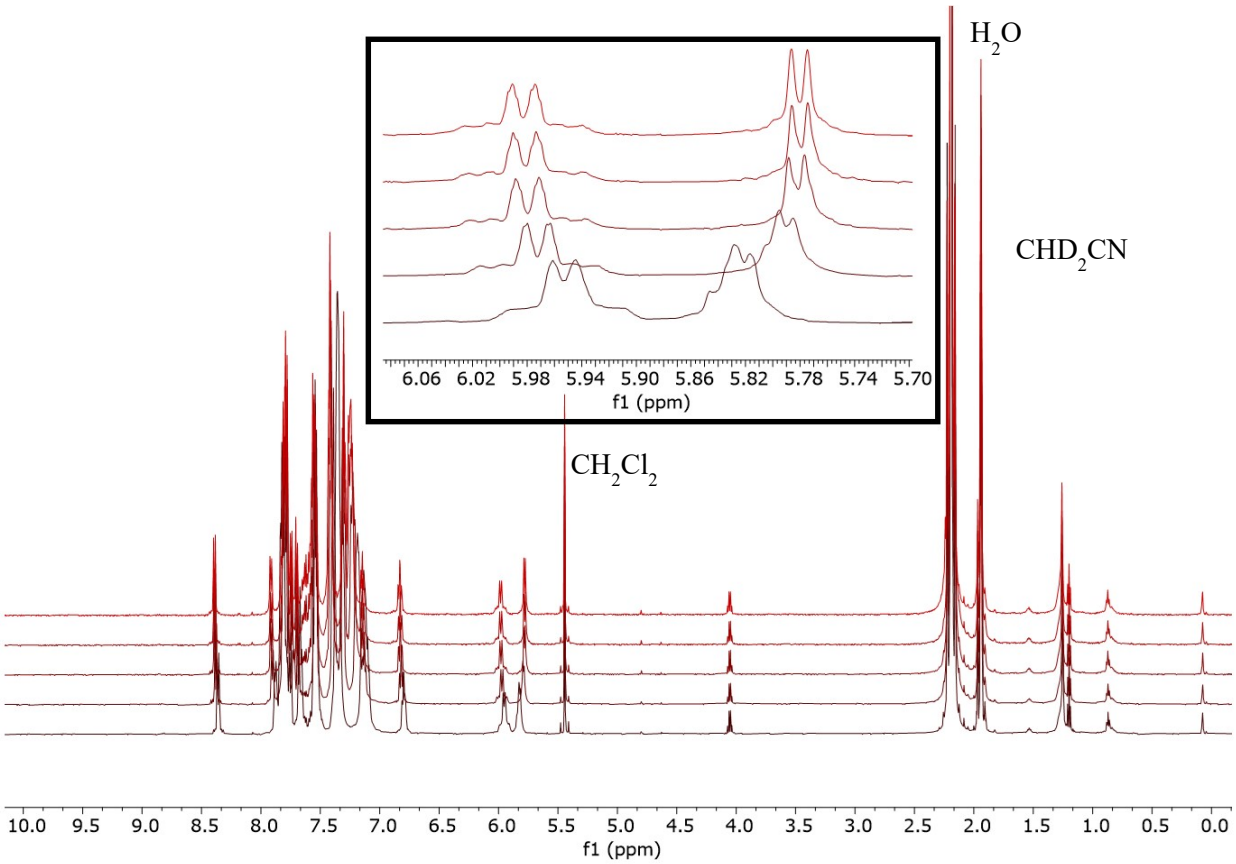

Figure S45. ^{1}H NMR spectra of **5-F** in CD_3CN. Sample was synthesized and maintained at 25°C. The bottom ^{1}H NMR spectrum is **5-F** at 0 hours. The second spectrum up from the bottom to the top spectrum in ascending order are **5-F** after 1 hour, 4 hour, 20 hour, and 28 hour time points. The black box highlights peaks associated with the protons alpha to Pt in complex **5-F**.

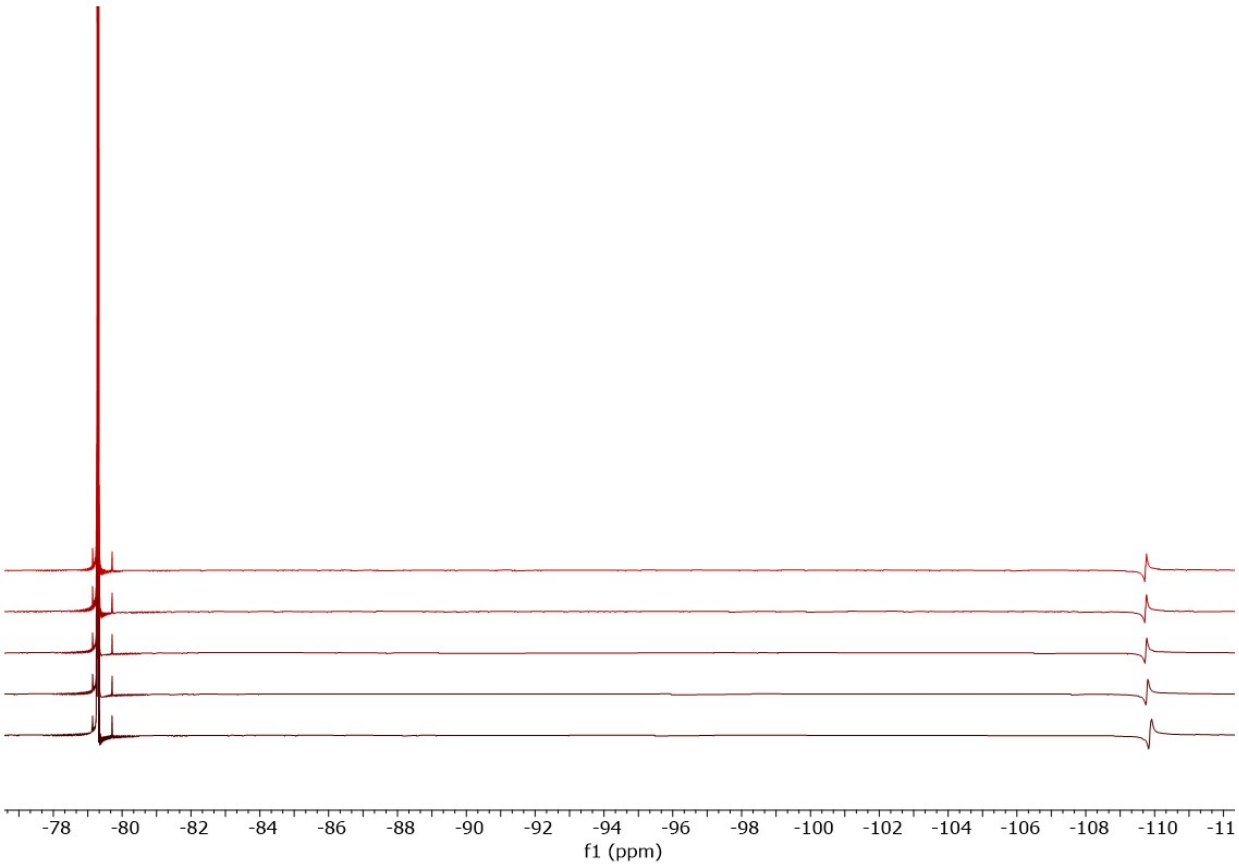

Figure S46. ^{19}F NMR spectra of **5-F** in CD_3CN. Sample was synthesized and maintained at 25°C. The bottom ^{19}F NMR spectrum is **5-F** at 0 hours. The second spectrum up from the bottom to the top spectrum in ascending order are **5-F** after 1 hour, 4 hour, 20 hour, and 28 hour time points.

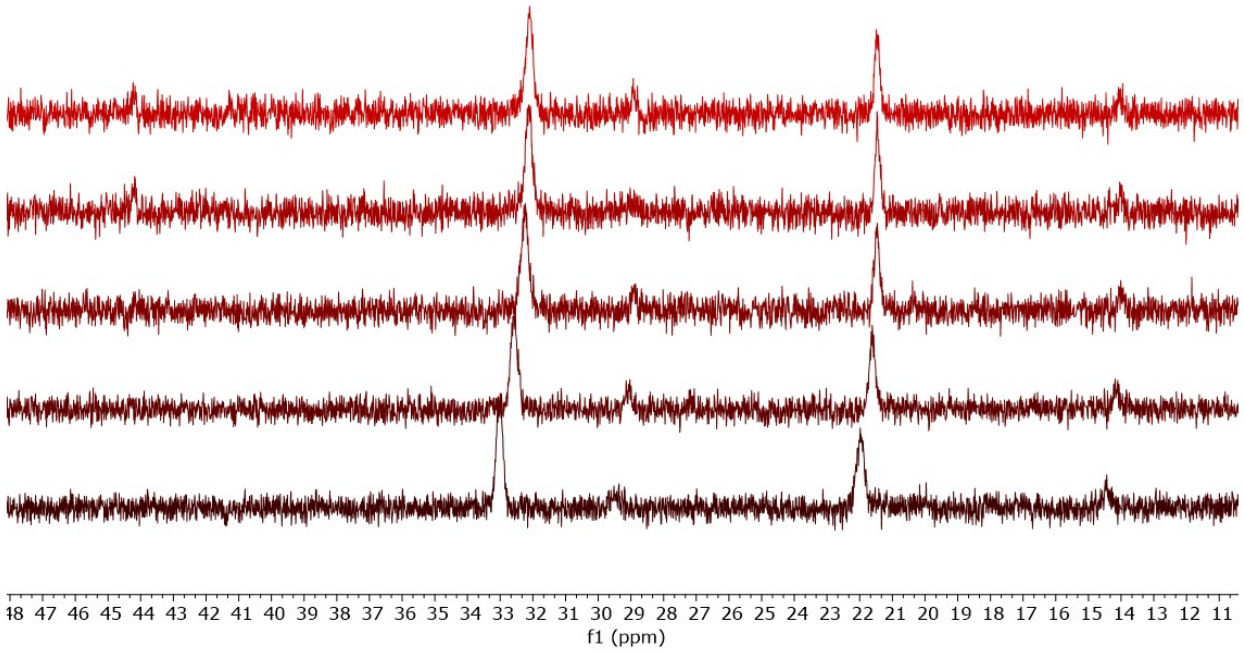

Figure S47. $^{31}P\{^{1}H\}$ NMR spectra of **5-F** in CD_3CN. Sample was synthesized and maintained at 25°C. The bottom $^{31}P\{^{1}H\}$ NMR spectrum is **5-F** at 0 hours. The second spectrum up from the bottom to the top spectrum in ascending order are **5-F** after 1 hour, 4 hour, 20 hour, and 28 hour time points.

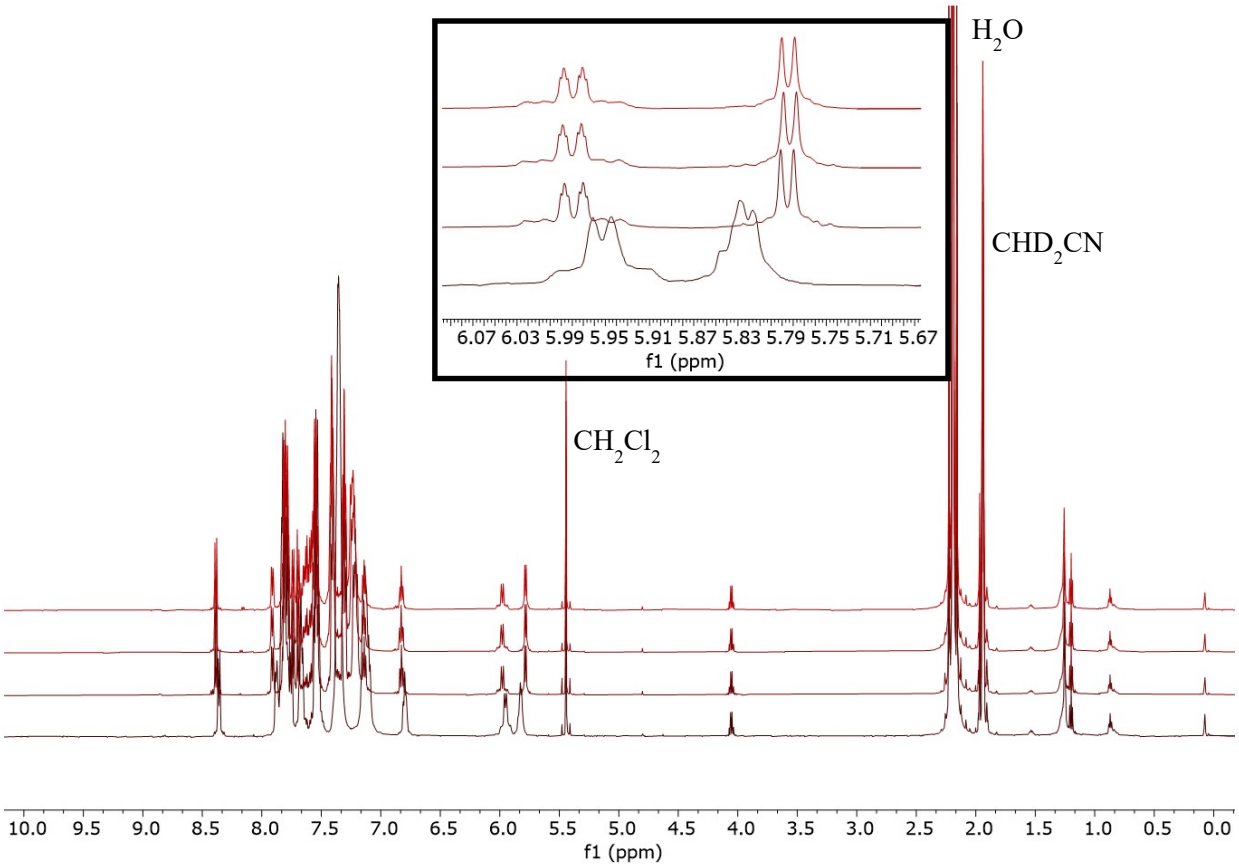

Figure S48. ^{1}H NMR spectra of **5-F** in CD_3CN. Sample was synthesized at 25°C and heated to 35°C. The bottom ^{1}H NMR spectrum is **5-F** at 0 hours at 25°C. The second spectrum up from the bottom to the top spectrum in ascending order are **5-F** after 1 hour, 4 hour, and 20 hour time points heating at 35°C. The black box highlights peaks associated with the protons alpha to Pt in complex **5-F**.

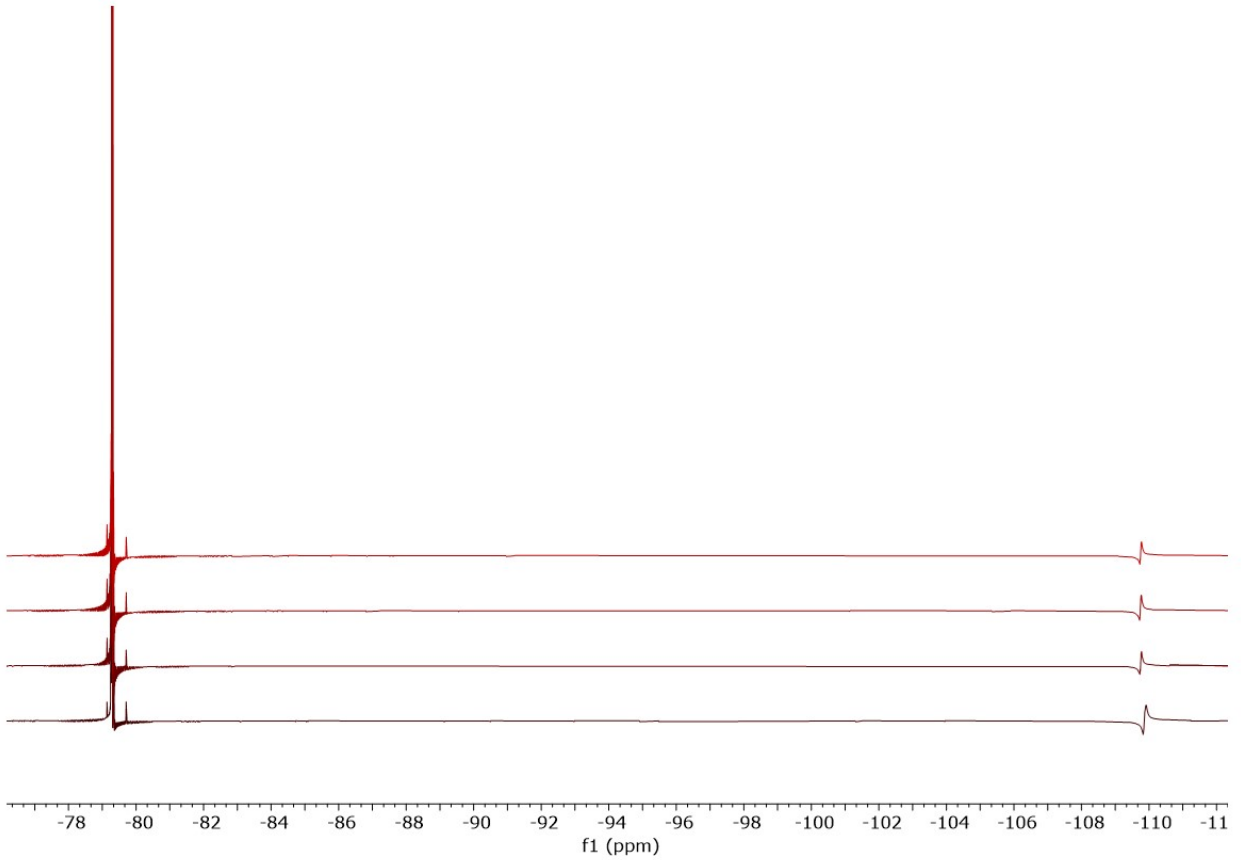

Figure S49. ^{19}F NMR spectra of **5-F** in CD_3CN. Sample was synthesized at 25°C and heated to 35°C. The bottom ^{19}F NMR spectrum is **5-F** at 0 hours at 25°C. The second spectrum up from the bottom to the top spectrum in ascending order are **5-F** after 1 hour, 4 hour, and 20 hour time points heating at 35°C.

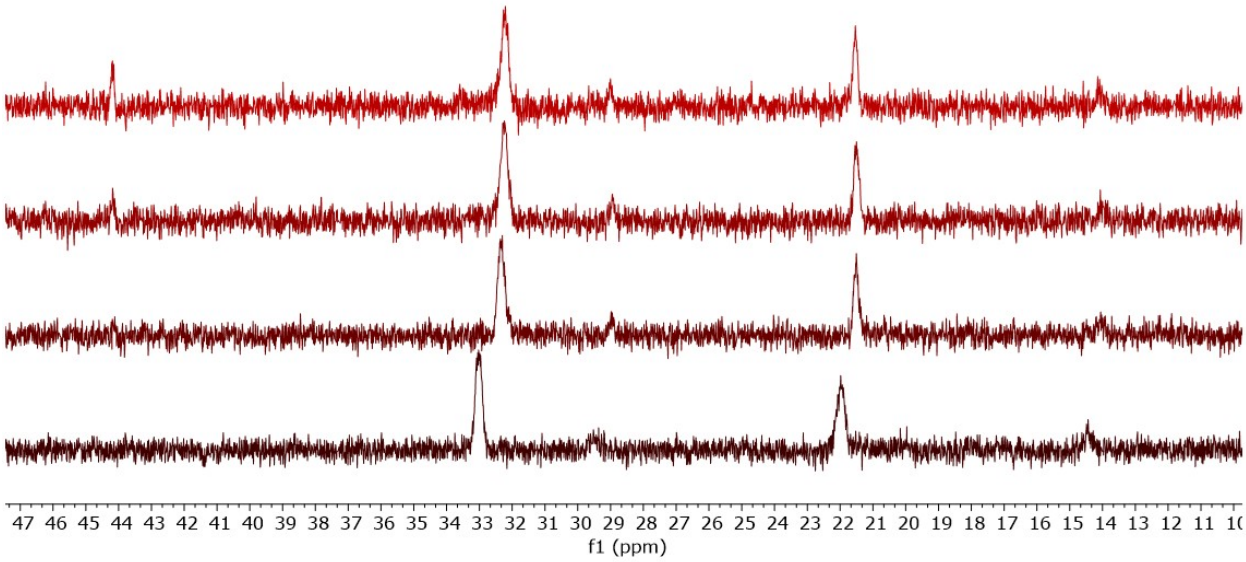

Figure S50. $^{31}P\{^{1}H\}$ NMR spectra of **5-F** in CD_3CN. Sample was synthesized at 25°C and heated to 35°C. The bottom $^{31}P\{^{1}H\}$ NMR spectrum is **5-F** at 0 hours at 25°C. The second spectrum up from the bottom to the top spectrum in ascending order are **5-F** after 1 hour, 4 hour, and 20 hour time points heating at 35°C.

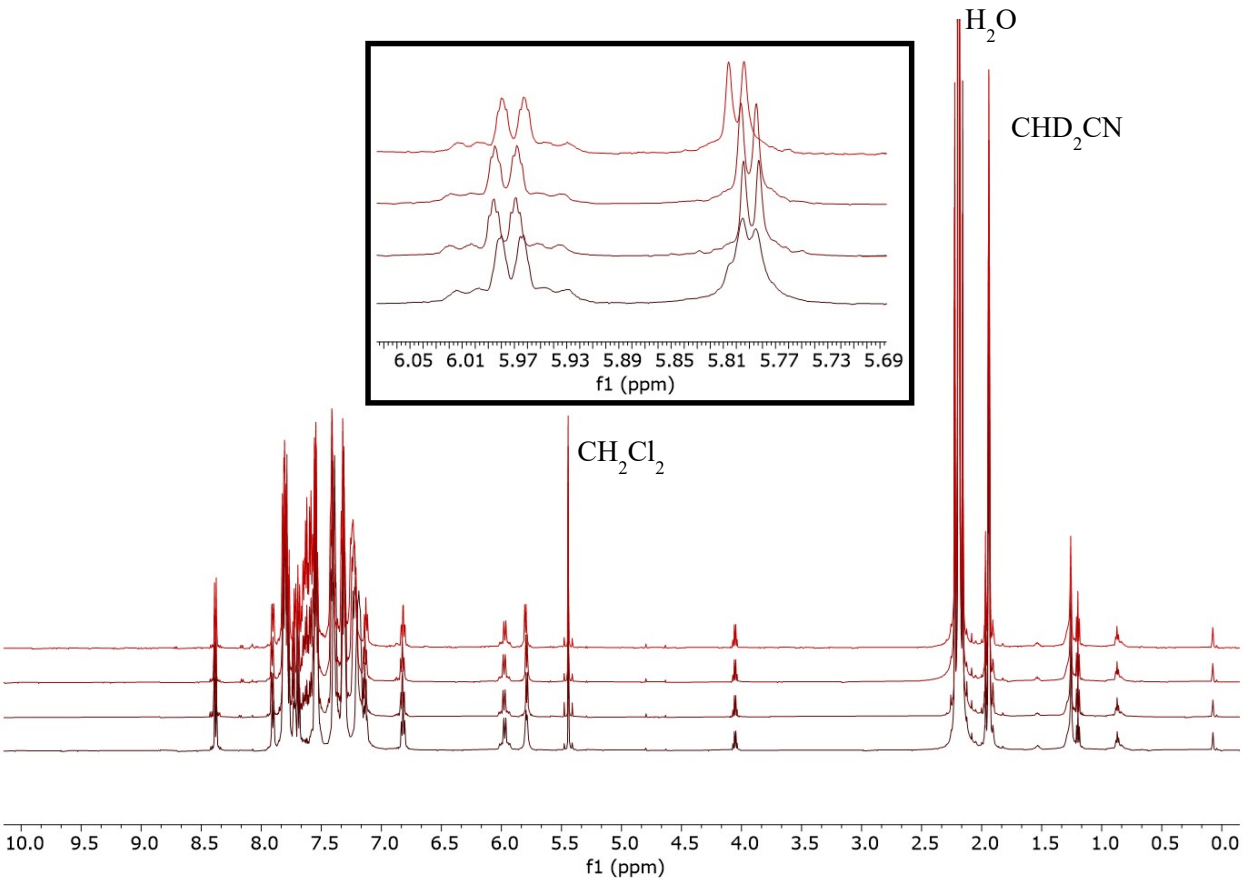

Figure S51. ^{1}H NMR spectra of **5-F** in CD_3CN. Sample was synthesized at 25°C and heated to 50°C. The bottom ^{1}H NMR spectrum is **5-F** at 0 hours at 25°C. The second spectrum up from the bottom to the top spectrum in ascending order are **5-F** after 1 hour, 4 hours, and 20 hours of heating at 50°C. The black box highlights peaks associated with the protons alpha to Pt in complex **5-F**.

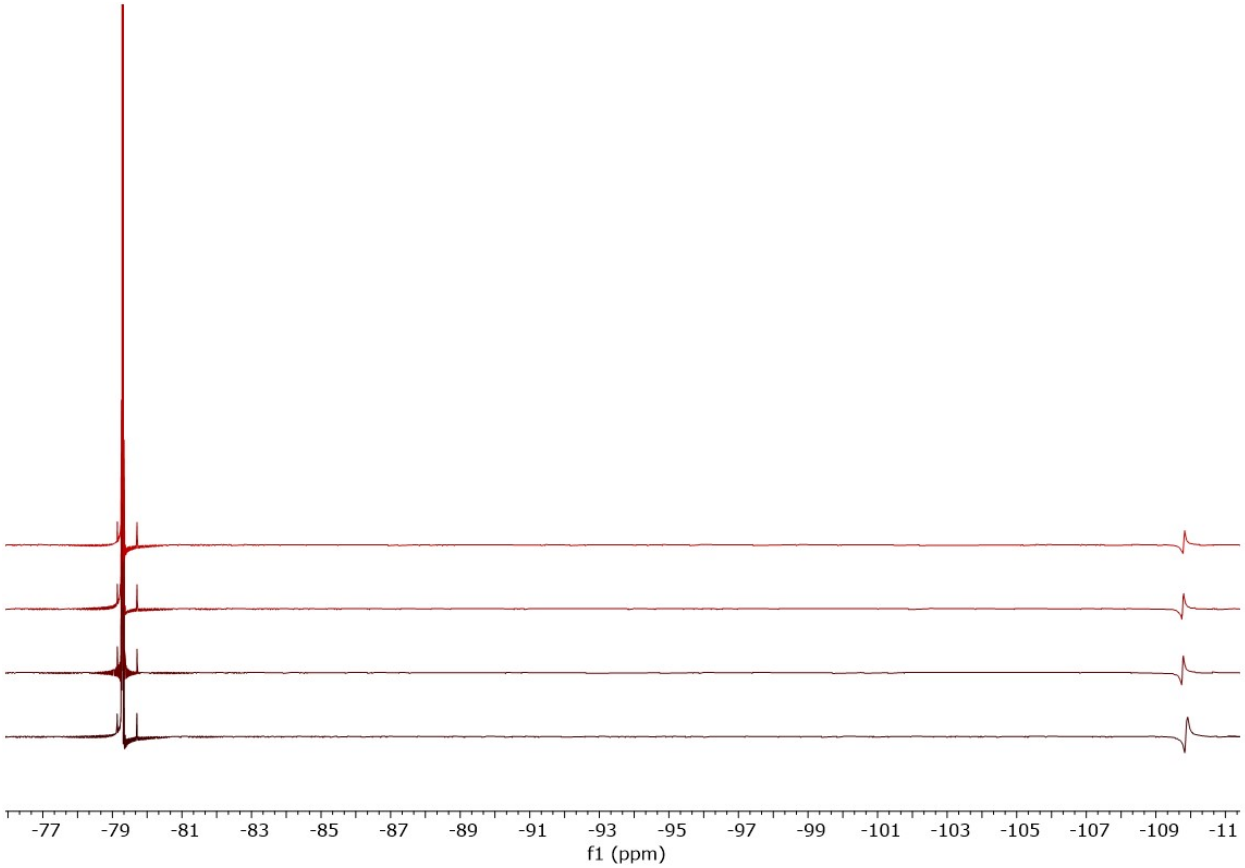

Figure S52. ^{19}F NMR spectra of **5-F** in CD_3CN. Sample was synthesized at 25°C and heated to 50°C. The bottom ^{19}F NMR spectrum is **5-F** at 0 hours at 25°C. The second spectrum up from the bottom to the top spectrum in ascending order are **5-F** after 1 hour, 4 hours, and 20 hours of heating at 50°C.

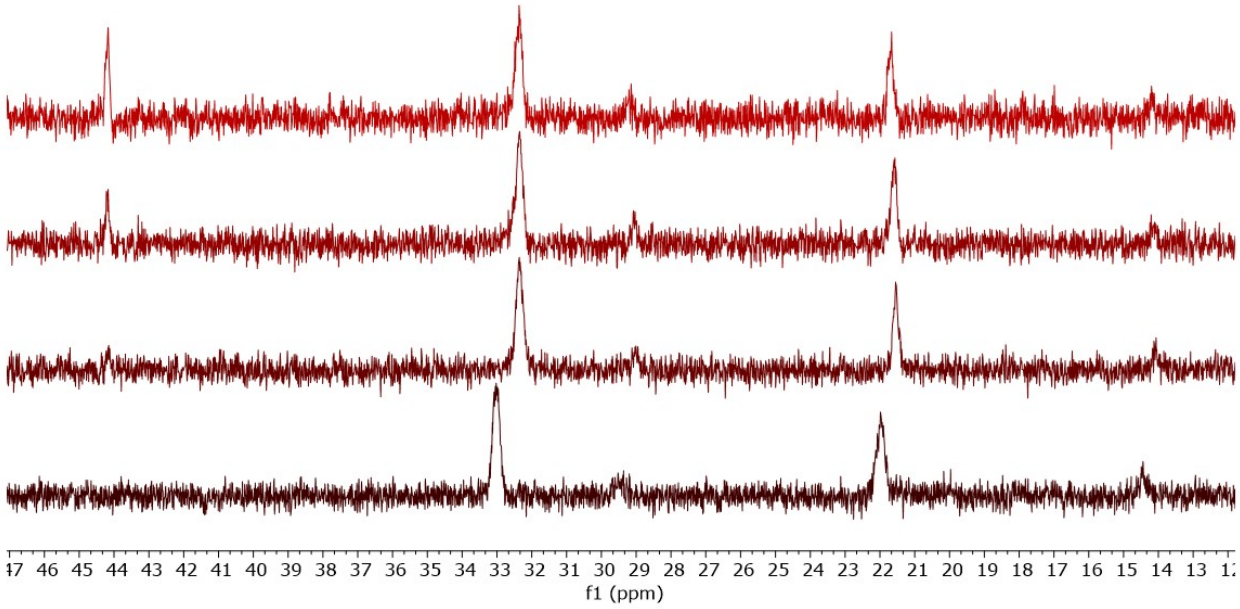

Figure S53. $^{31}P\{^{1}H\}$ NMR spectra of **5-F** in CD_3CN. Sample was synthesized at 25°C and heated to 50°C. The bottom $^{31}P\{^{1}H\}$ NMR spectrum is **5-F** at 0 hours at 25°C. The second spectrum up from the bottom to the top spectrum in ascending order are **5-F** after 1 hour, 4 hours, and 20 hours of heating at 50°C.

General Procedure for Pyridine Titration Experiments

The specified dinuclear complex [(bhq-Ph^R)(PPh$_3$)Pt–Au(PPh$_3$)][OTf] (~ 0.0067 mmol) was dissolved in 0.5 mL CD_2Cl_2, then, ^{1}H, ^{19}F, and ^{31}P{^{1}H} NMR spectra were collected. Pyridine (~0.1 µL, 0.2 eq) was added to the NMR sample using a 5 µL Hamilton syringe, then, ^{1}H, ^{19}F, and ^{31}P{^{1}H} NMR spectra were collected. Additional equivalents of pyridine are added until (bhq-Ph^R)(PPh$_3$)Pt was clearly observed by NMR rather than [(bhq-Ph^R)(PPh$_3$)Pt–Au(PPh$_3$)][OTf]. Due to the small quantities of titrant (0.1 µL) added in these experiments, the actual ratio of pyridine to [(bhq-Ph^R)(PPh$_3$)Pt–Au(PPh$_3$)][OTf] was determined by comparing the integration of [(bhq-Ph^R)(PPh$_3$)Pt–Au(PPh$_3$)][OTf] vs pyridine in the ^{1}H NMR spectrum.

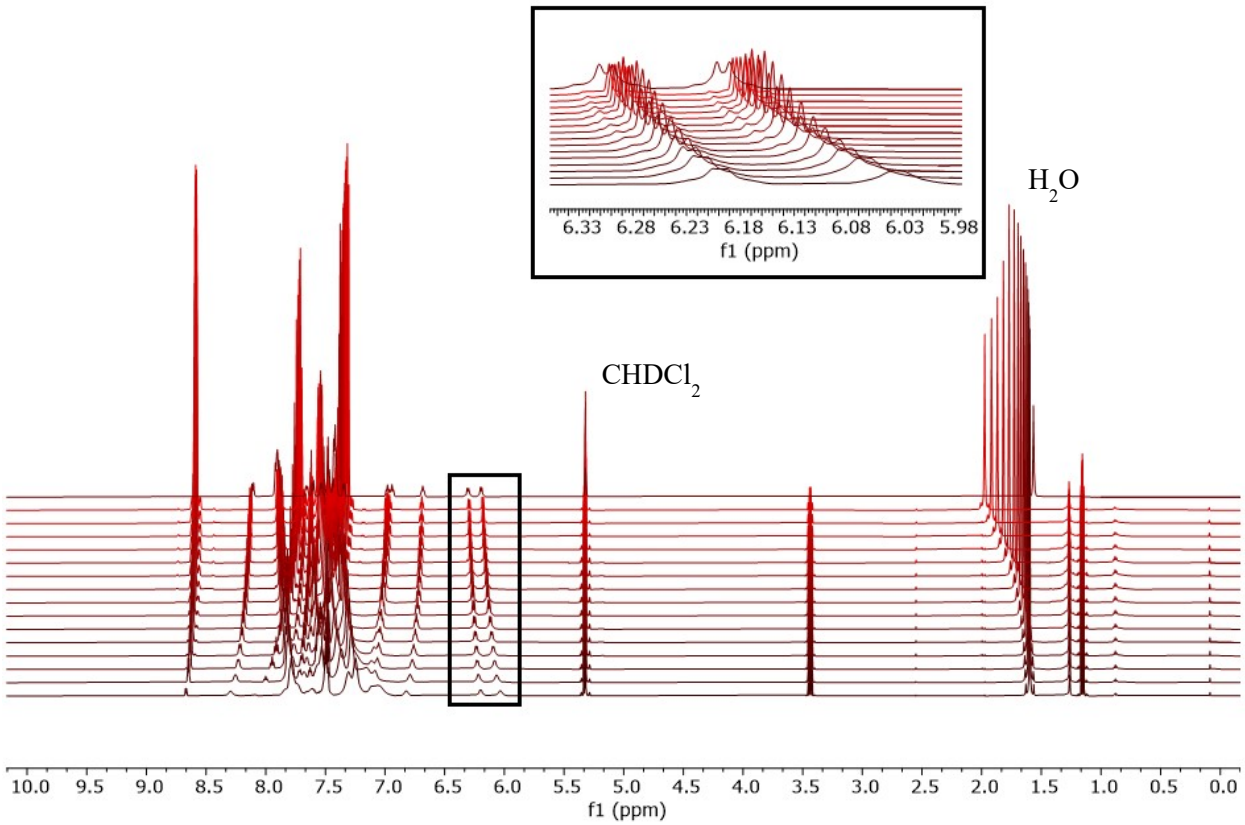

NMR Spectra of Pyridine Titrations of Complex 5

Figure S54. ^{1}H NMR spectra of titration experiments with pyridine and **5** (0.0089g, 0.00678 mmol) in CD_2Cl_2. Bottom ^{1}H NMR spectrum is **5** in the absence of pyridine. Top ^{1}H NMR spectrum is **4** in the absence of pyridine. The second spectrum up from the bottom to the second to last spectrum from the top in ascending order are the titrations of pyridine with 0.18 eq, 0.44 eq, 0.70 eq, 0.96 eq, 1.28 eq, 1.61 eq, 2.13 eq, 2.79 eq, 3.36 eq, 4.31 eq, 5.56 eq, 7.07, 8.59 eq, 10.07 eq, 12.02 eq relative to **5**. The box highlights peaks associated with the protons alpha to Pt in complex **5** and **4**.

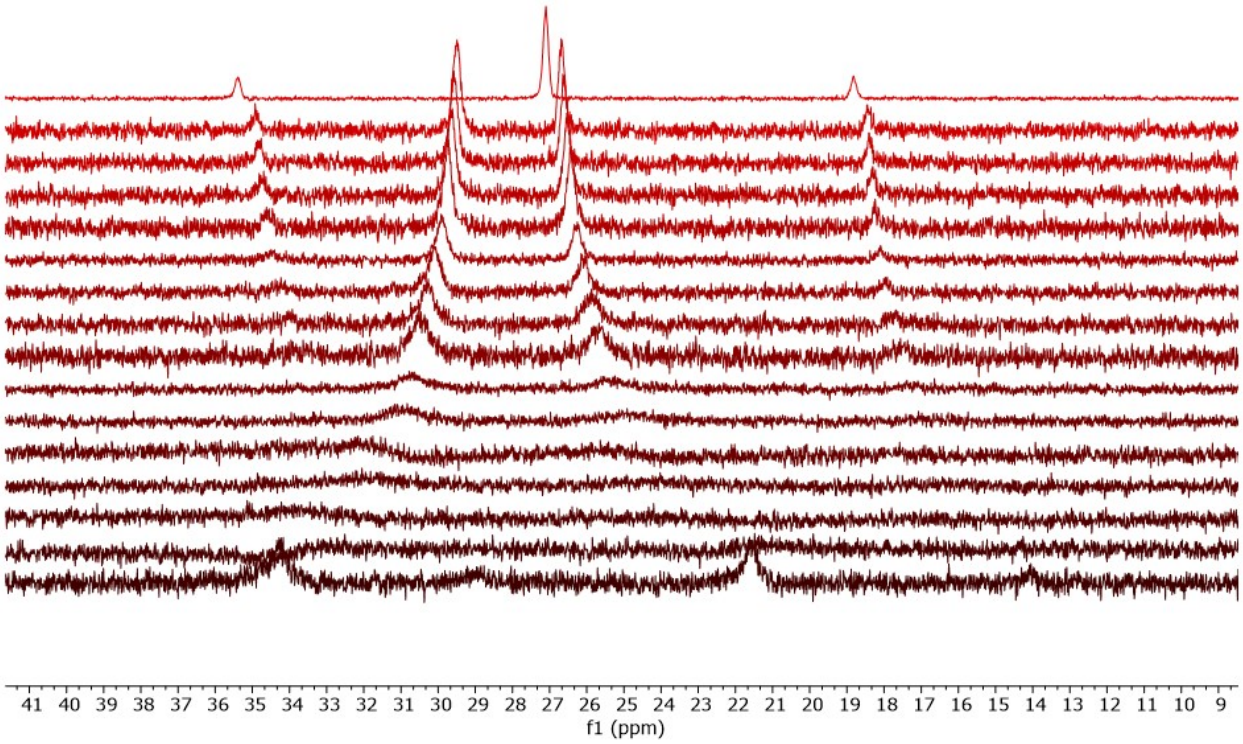

Figure S55. $^{31}P\{^{1}H\}$ NMR spectra of titration experiments with pyridine and **5** (0.0089g, 0.00678 mmol) in CD_2Cl_2. Bottom $^{31}P\{^{1}H\}$ NMR spectrum is **5** in the absence of pyridine. Top $^{31}P\{^{1}H\}$ NMR spectrum is **4** in the absence of pyridine. The second spectrum up from the bottom to the second to last spectrum from the top in ascending order are the titrations of pyridine with 0.18 eq, 0.44 eq, 0.70 eq, 0.96 eq, 1.28 eq, 1.61 eq, 2.13 eq, 2.79 eq, 3.36 eq, 4.31 eq, 5.56 eq, 7.07, 8.59 eq, 10.07 eq, 12.02 eq relative to **5**.

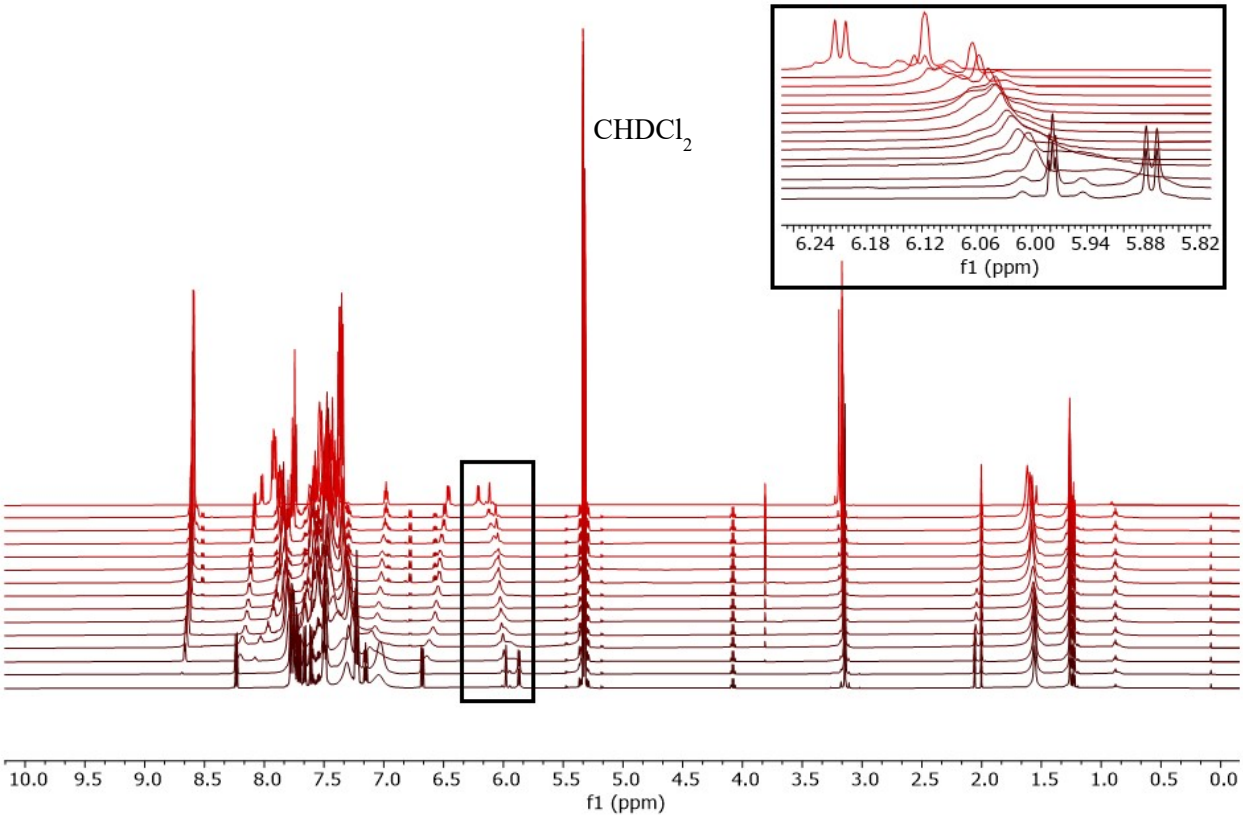

NMR Spectra of Pyridine Titrations with Complex 5-OMe

Figure S56. ^{1}H NMR spectra of titration experiments with pyridine and **5-OMe** (0.0052g, 0.00385 mmol) in CD_2Cl_2. Bottom ^{1}H NMR spectrum is **5-OMe** in the absence of pyridine. Top ^{1}H NMR spectrum is **4-OMe** in the absence of pyridine. The second spectrum up from the bottom to the second to last spectrum from the top in ascending order are the titrations of pyridine with 0.06 eq, 0.442 eq, 0.57 eq, 0.84 eq, 1.19 eq, 1.34 eq, 1.70 eq, 2.15 eq, 2.21 eq, 2.35 eq, 2.94 eq, 4.40, 5.78 eq relative to **5-OMe**. The box highlights peaks associated with the protons alpha to Pt in complex **5-OMe** and **4-OMe**.

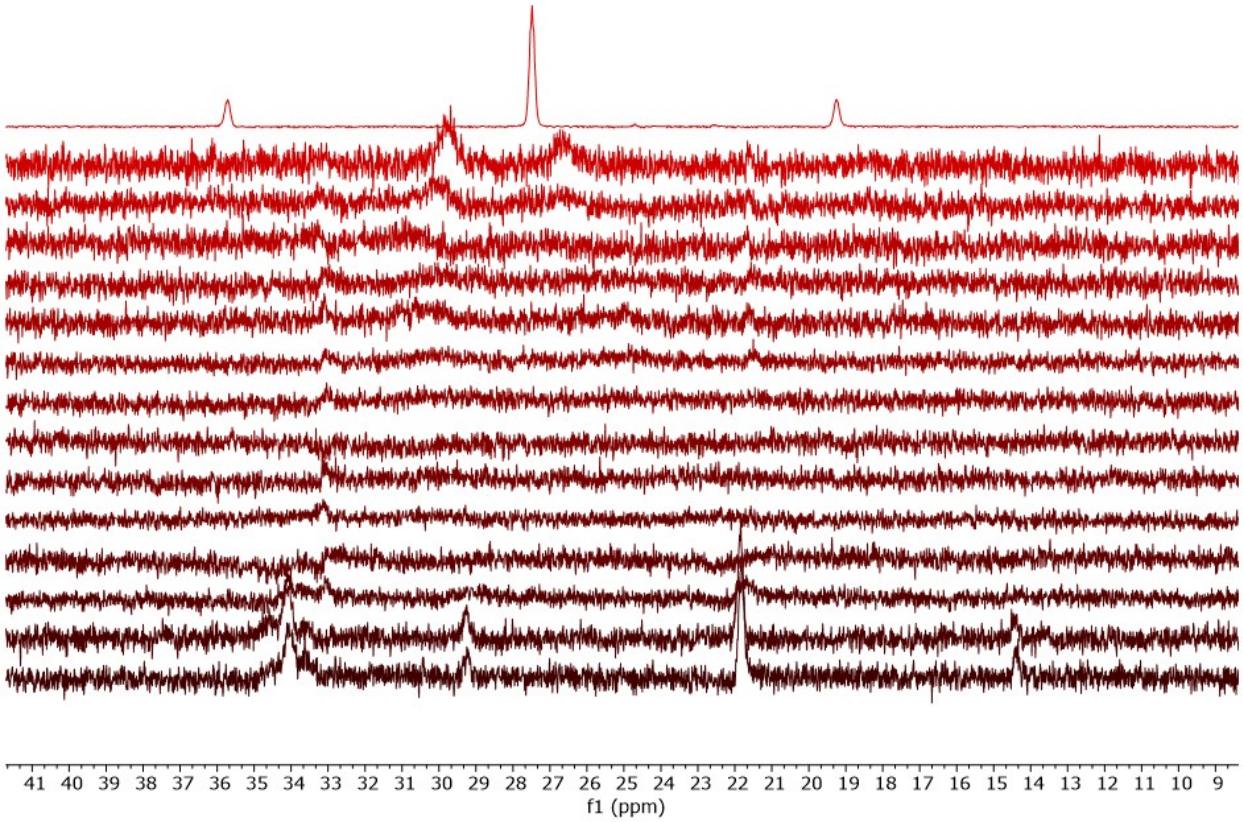

Figure S57. $^{31}P\{^{1}H\}$ NMR spectra of titration experiments with pyridine and **5-OMe** (0.0052g, 0.00385 mmol) in CD_2Cl_2. Bottom $^{31}P\{^{1}H\}$ NMR spectrum is **5-OMe** in the absence of pyridine. Top $^{31}P\{^{1}H\}$ NMR spectrum is **4-OMe** in the absence of pyridine. The second spectrum up from the bottom to the second to last spectrum from the top in ascending order are the titrations of pyridine with 0.06 eq, 0.442 eq, 0.57 eq, 0.84 eq, 1.19 eq, 1.34 eq, 1.70 eq, 2.15 eq, 2.21 eq, 2.35 eq, 2.94 eq, 4.40, 5.78 eq relative to **5-OMe**.

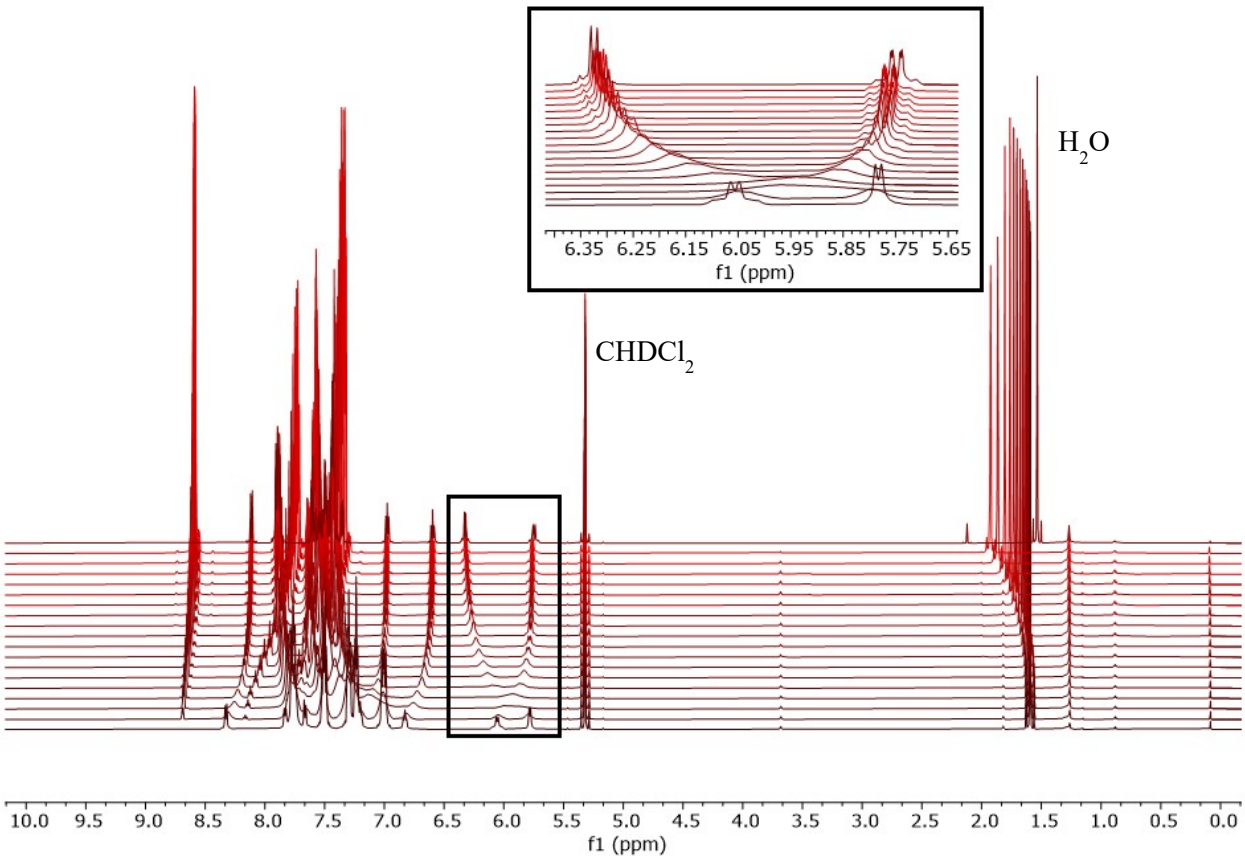

NMR Spectra of Pyridine Titrations with Complex 5-F

Figure S58. ^{1}H NMR spectra of titration experiments with pyridine and **5-F** (0.0095g, 0.00710 mmol) in CD_2Cl_2. Bottom ^{1}H NMR spectrum is **5-F** in the absence of pyridine. Top ^{1}H NMR spectrum is **4-F** in the absence of pyridine. The second spectrum up from the bottom to the second to last spectrum from the top in ascending order are the titrations of pyridine with 0.19 eq, 0.36 eq, 0.51 eq, 0.74 eq, 1.00 eq, 1.10 eq, 1.42 eq, 1.72 eq, 1.99 eq, 2.45 eq, 2.88 eq, 3.52 eq, 4.15 eq, 4.91 eq, 6.05 eq, 7.50 eq, 9.22 eq relative to **5-F**. The box highlights peaks associated with the protons alpha to Pt in complex **5-F** and **4-F**.

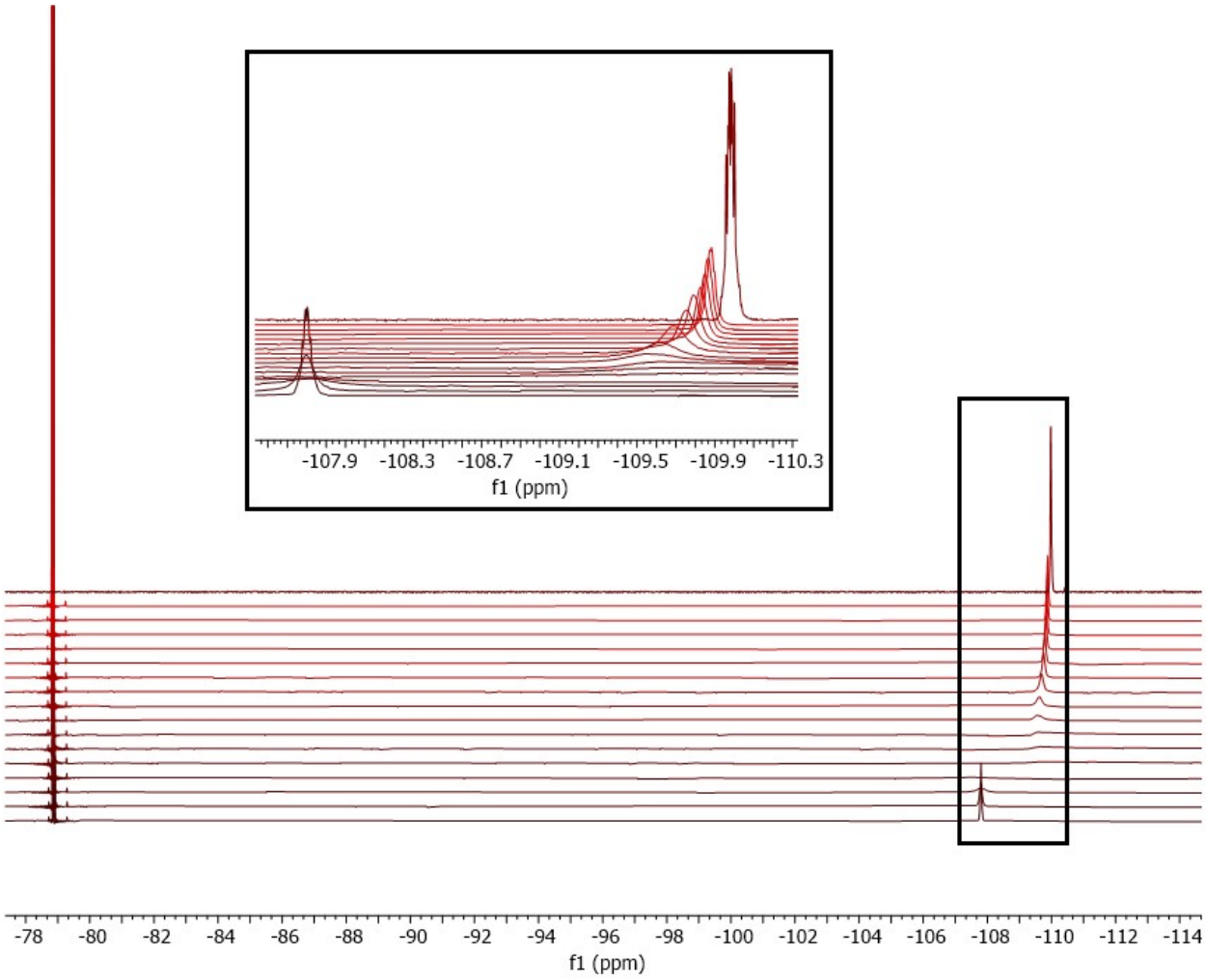

Figure S59. ^{19}F NMR spectra of titration experiments with pyridine and **5-F** (0.0095g, 0.00710 mmol) in CD_2Cl_2. Bottom ^{19}F NMR spectrum is **5-F** in the absence of pyridine. Top ^{19}F NMR spectrum is **4-F** in the absence of pyridine. The second spectrum up from the bottom to the second to last spectrum from the top in ascending order are the titrations of pyridine with 0.19 eq, 0.36 eq, 0.51 eq, 0.74 eq, 1.00 eq, 1.10 eq, 1.42 eq, 1.72 eq, 1.99 eq, 2.45 eq, 2.88 eq, 3.52 eq, 4.15 eq, 4.91 eq, 6.05 eq relative to **5-F**. The box highlights peaks associated with the fluorine substituent on the CNC ligand of complex **5-F** and **4-F**.

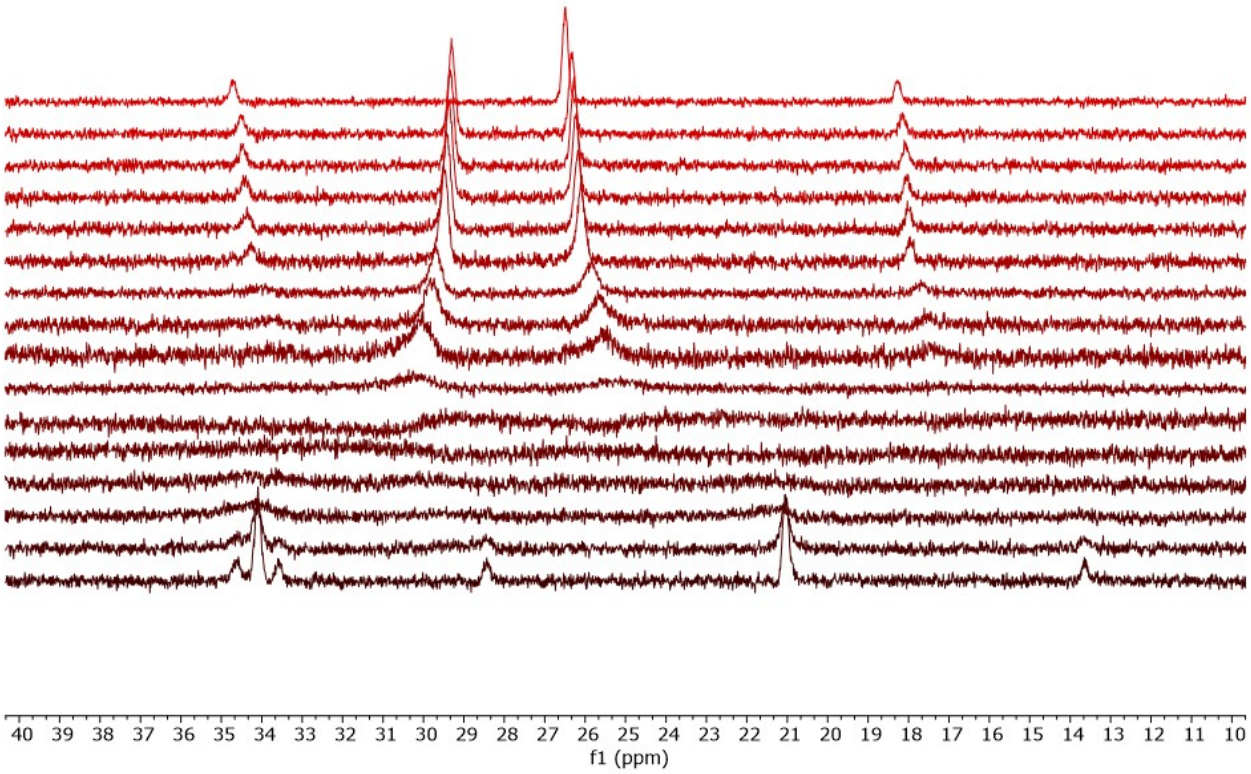

Figure S60. $^{31}P\{^{1}H\}$ NMR spectra of titration experiments with pyridine and **5-F** (0.0095g, 0.00710 mmol) in CD_2Cl_2. Bottom $^{31}P\{^{1}H\}$ NMR spectrum is **5-F** in the absence of pyridine. Top $^{31}P\{^{1}H\}$ NMR spectrum is **4-F** in the absence of pyridine. The second spectrum up from the bottom to the second to last spectrum from the top in ascending order are the titrations of pyridine with 0.19 eq, 0.36 eq, 0.51 eq, 0.74 eq, 1.00 eq, 1.10 eq, 1.42 eq, 1.72 eq, 1.99 eq, 2.45 eq, 2.88 eq, 3.52 eq, 4.15 eq, 4.91 eq, 6.05 eq relative to **5-F**.

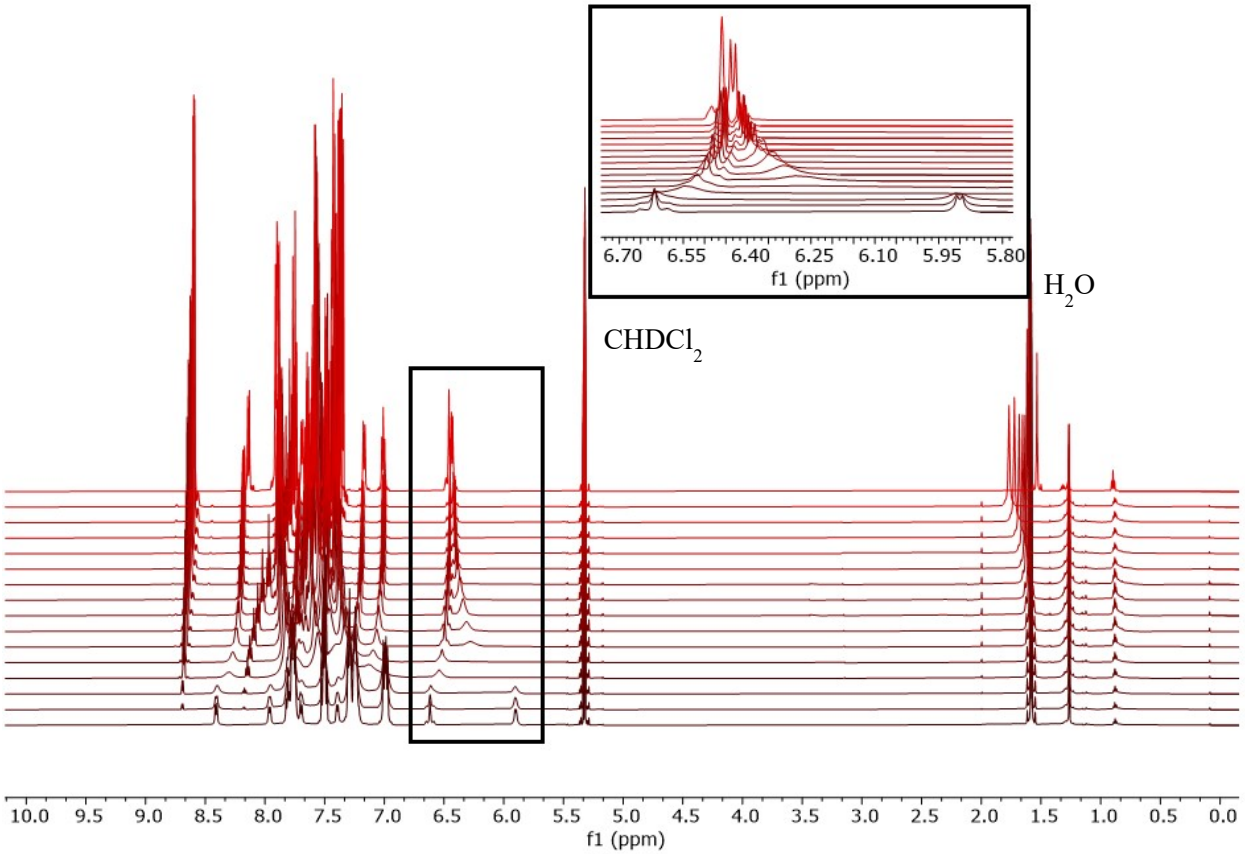

NMR Spectra of Pyridine Titrations with Complex 5-CF_3

Figure S61. ^{1}H NMR spectra of titration experiments with pyridine and **5-CF_3** (0.0104g, 0.00749 mmol) in CD_2Cl_2. Bottom ^{1}H NMR spectrum is **5-CF_3** in the absence of pyridine. Top ^{1}H NMR spectrum is **4-CF_3** in the absence of pyridine. The second spectrum up from the bottom to the second to last spectrum from the top in ascending order are the titrations of pyridine with 0.06 eq, 0.16 eq, 0.55 eq, 0.61 eq, 0.77 eq, 0.94 eq, 1.17 eq, 1.33 eq, 1.87 eq, 2.30 eq, 2.89 eq, 3.61 eq, 4.71 eq, 6.05 eq relative to **5-CF_3**. The box highlights peaks associated with the protons alpha to Pt in complex **5-CF_3** and **4-CF_3**.

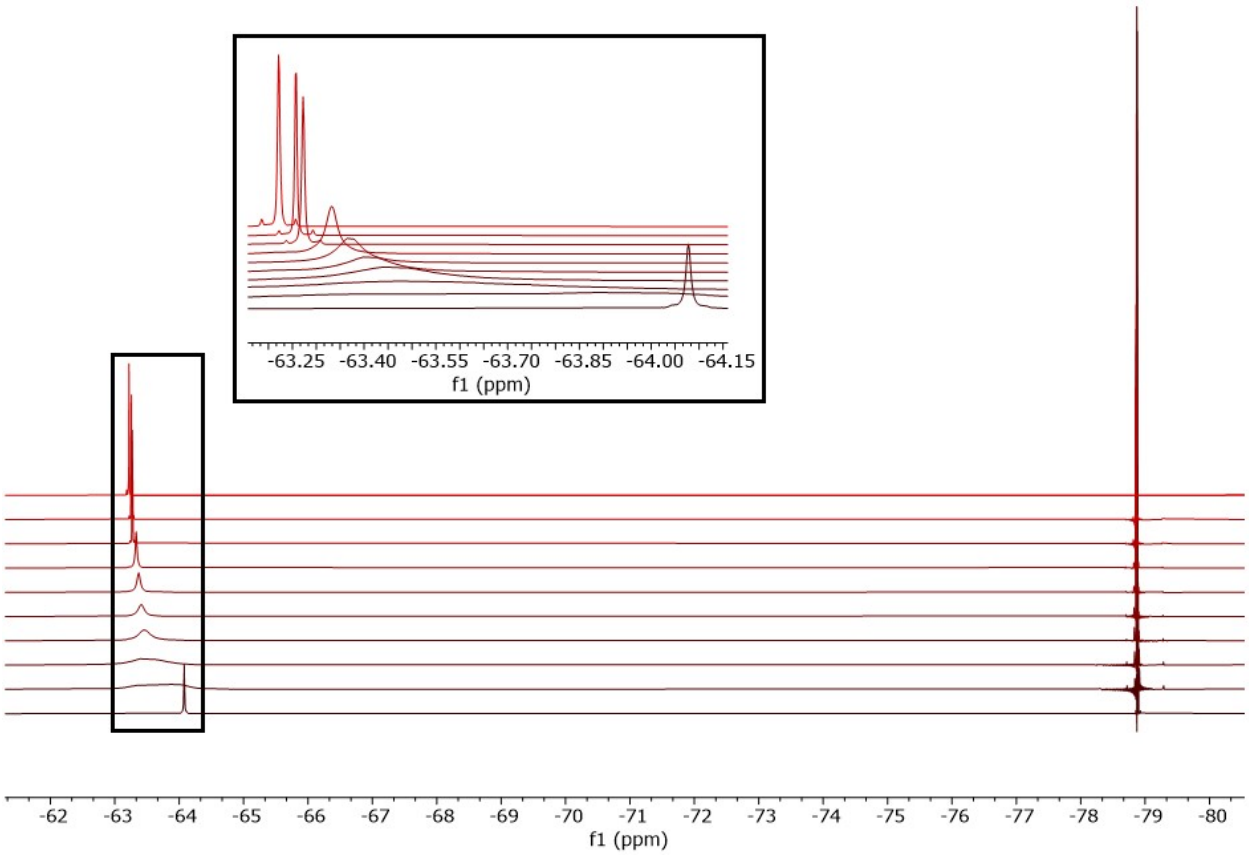

Figure S62. ^{19}F NMR spectra of titration experiments with pyridine and **5-CF_3** (0.0104g, 0.00749 mmol) in CD_2Cl_2. Bottom ^{19}F NMR spectrum is **5-CF_3** in the absence of pyridine. Top ^{19}F NMR spectrum is **4-CF_3** in the absence of pyridine. The second spectrum up from the bottom to the second to last spectrum from the top in ascending order are the titrations of pyridine with 0.55 eq, 0.61 eq, 0.77 eq, 0.94 eq, 1.17 eq, 1.33 eq, 2.89 eq, 4.71 eq relative to **5-CF_3**. The box highlights peaks associated with the trifluoromethyl substituent on the CNC ligand of complex **5-CF_3** and **4-CF_3**.

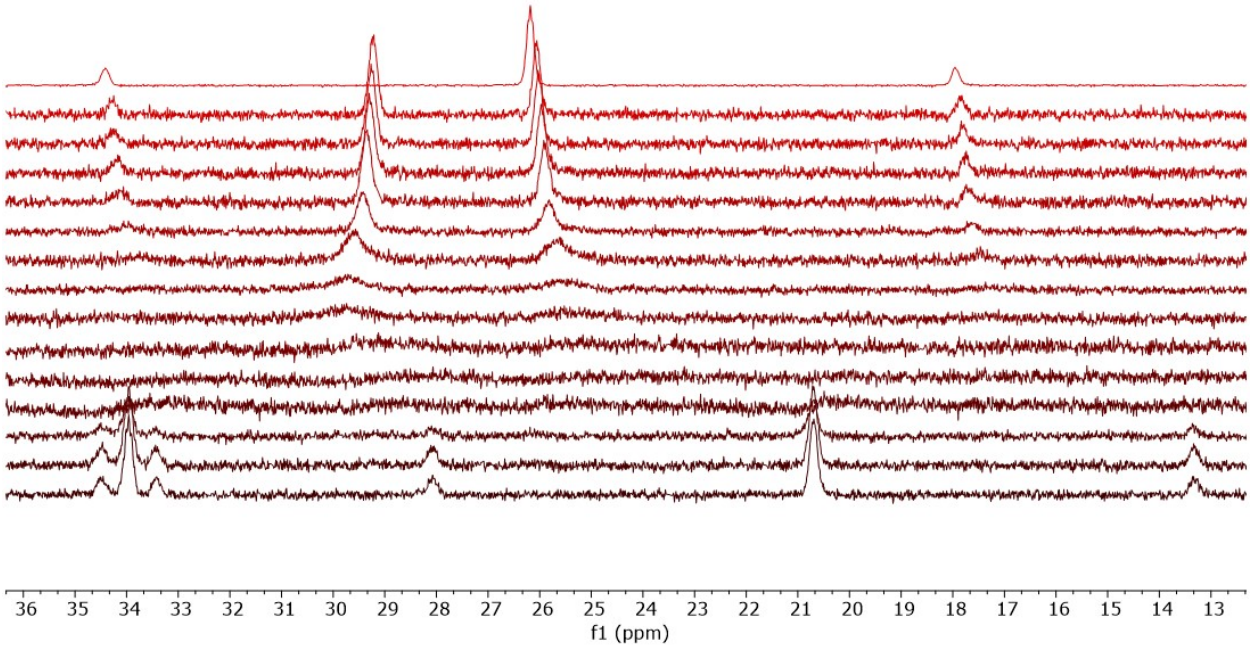

Figure S63. $^{31}P\{^{1}H\}$ NMR spectra of titration experiments with pyridine and **5-CF_3** (0.0104g, 0.00749 mmol) in CD_2Cl_2. Bottom $^{31}P\{^{1}H\}$ NMR spectrum is **5-CF_3** in the absence of pyridine. Top $^{31}P\{^{1}H\}$ NMR spectrum is **4-CF_3** in the absence of pyridine. The second spectrum up from the bottom to the second to last spectrum from the top in ascending order are the titrations of pyridine with 0.06 eq, 0.16 eq, 0.55 eq, 0.61 eq, 0.77 eq, 0.94 eq, 1.17 eq, 1.33 eq, 1.87 eq, 2.30 eq, 2.89 eq, 3.61 eq, 4.71 eq relative to **5-CF_3**.

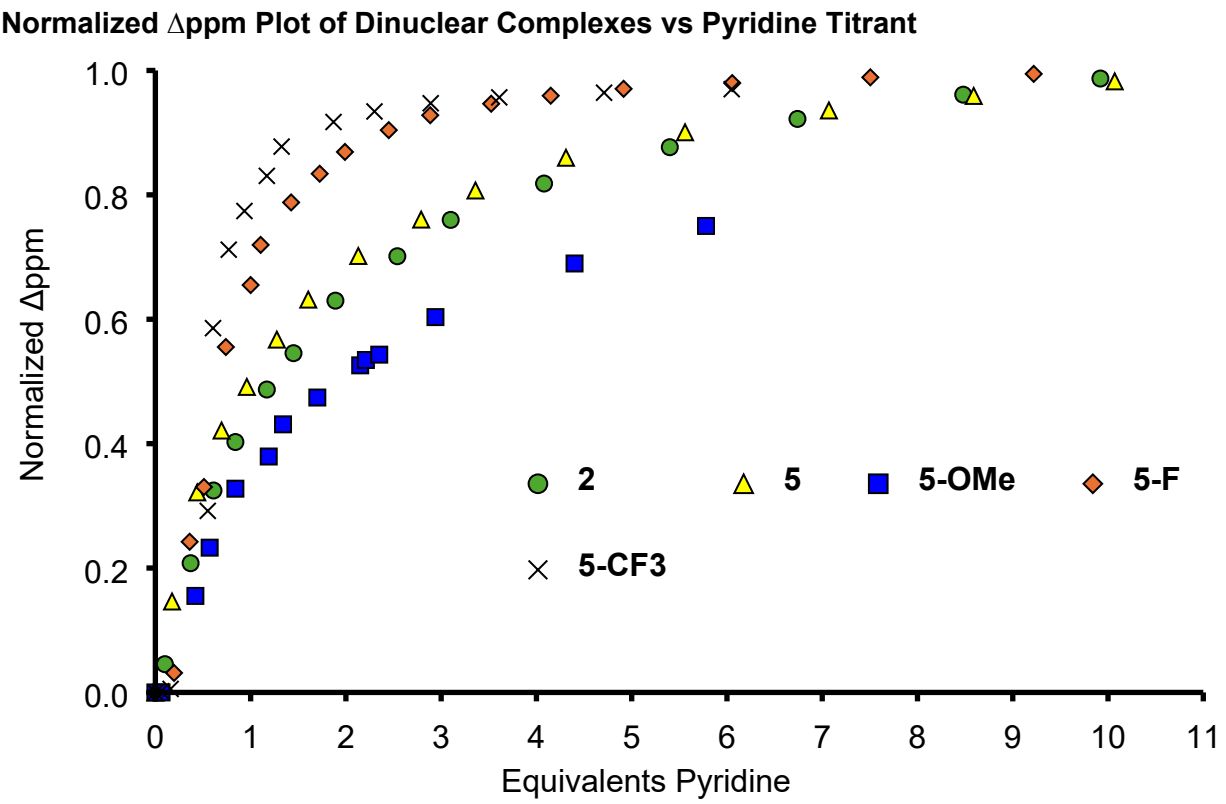

Figure S64. Plot of normalized Δppm vs equivalents of pyridine in the titration of **2**, **5**, **5-OMe**, **5-F**, and **5-CF$_3$** with pyridine. Herein, the value of zero in "normalized Δppm" is the chemical shift of the proton alpha to Pt in the dinuclear complex (**2**, **5**, **5-OMe**, **5-F**, and **5-CF$_3$** respectively). The value of 1 in "normalized Δppm" is the chemical shift of the proton alpha to Pt in the corresponding mononuclear complex (**1**, **4**, **4-OMe**, **4-F**, and **4-CF$_3$** respectively).

Estimating K_{eq} of Pyridine Titrations

This analysis was adapted from a previously reported method.[4,7] In solution, species that rapidly equilibrate on the NMR time scale will exhibit a chemical shift that represents a mole-fraction weighted average of the individual species' chemical shifts.

$$A + X \rightleftharpoons AX$$

For instance, when species A and AX undergo rapid, reversible exchange, the observed chemical shift (∂_{obs}) is an average of the shifts for A (∂_A) and AX (∂_{AX}), based on their respective mole fractions.

$$\partial_{obs} = N_A\,\partial_A + N_{AX}\,\partial_{AX}$$

N_A and N_{AX} represent the mole fractions of A and AX at equilibrium, respectively. Since the total concentration of A and AX equals the initial concentration of A added to the NMR solution, the observed chemical shift can be used to calculate the concentrations of A and AX. By using this averaged shift, along with the known chemical shifts of A and AX, the concentrations can be determined, enabling calculation of the equilibrium constant.

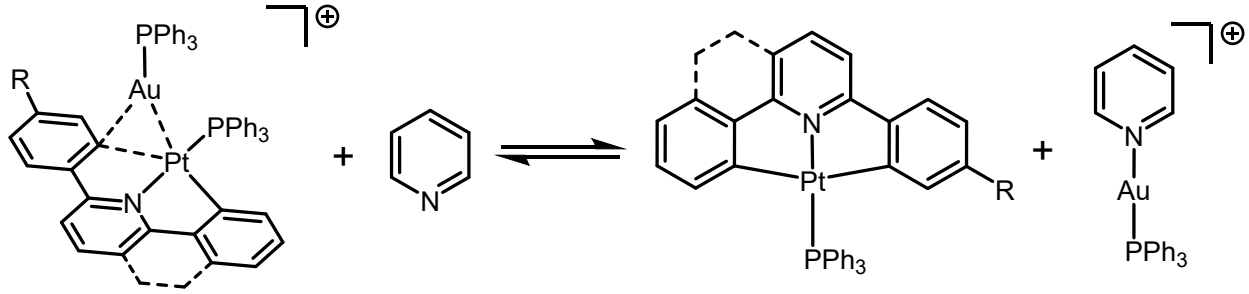

To obtain the actual K_{eq} value, one must consider that the equilibrium reaction is not a simple pyridine binding event. In these pyridine titration reactions however, the concentration of monometallic Pt complex will be equal to the concentration of pyridine ligated cationic gold complex. Thus, we can simply square the calculated mole fraction of AX to obtain K_{eq}.

The dinuclear complex was treated as A, pyridine as X, and the monometallic Pt-species as AX. Using Excel's Solver, the mole fraction of A and AX were calculated from the observed chemical shift during titrations, and K_{eq} was determined for each experiment. The calculated K_{eq} values were then averaged to obtain the K_{eq}.

We note that in these pyridine titration experiments, complexes **5-F** and **5-CF$_3$** exhibit somewhat sigmoidal shape in their titration curves (Figure S64). For **5-CF$_3$** where the sigmoidal shape to the titration curve is substantially pronounced, we have repeated this titration curve (Figure S65) and the duplicate titration experiment exhibits nearly identical behavior. At present, we are unable to draw conclusions regarding the sigmoidal shape except to comment that the substantial broadening in the ^{1}H NMR spectra (Figure S61) make determining the exact chemical shift of various peaks challenging. The same substantial broadening can be observed for 1H NMR spectra of titrations involving **5-F** (Figure S58).

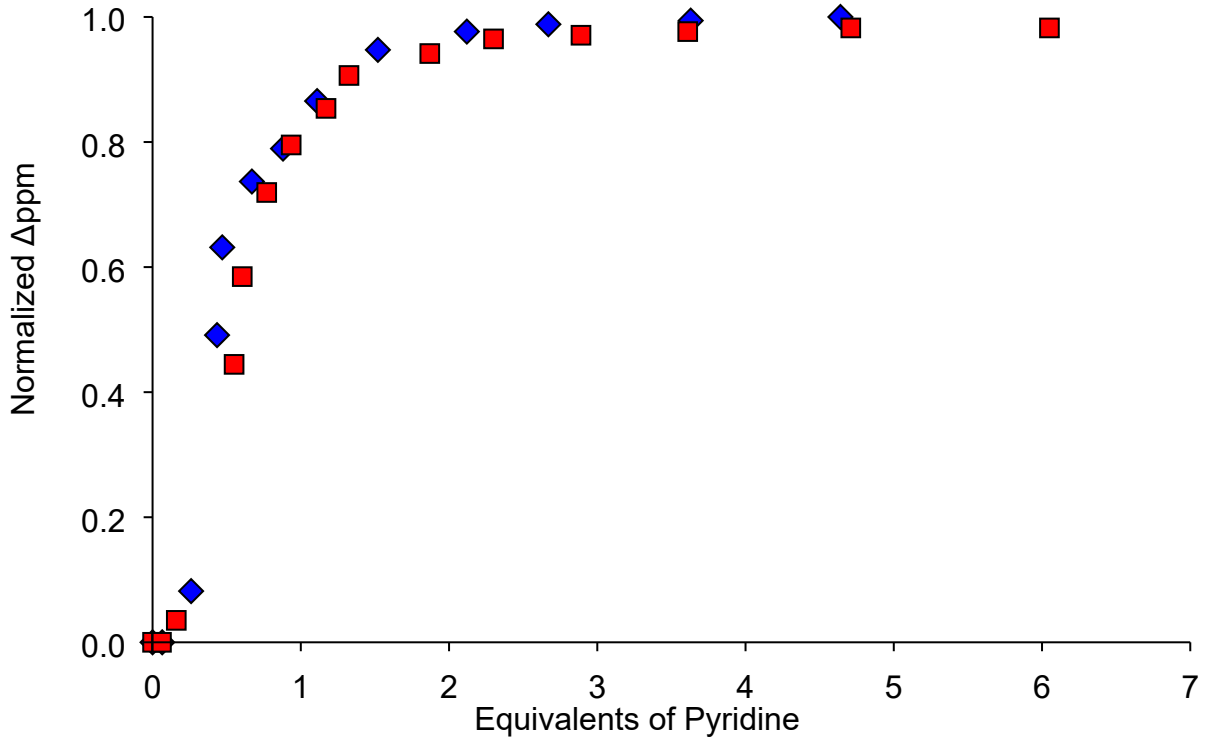

Figure S65. Plot of normalized Δppm vs equivalents of pyridine in the titration of **5-CF$_3$** with pyridine. Two different titration experiments shown, one in red squares and the other in blue diamonds. Herein, the value of zero in "normalized Δppm" is the chemical shift of the proton alpha to Pt in the dinuclear complex (**5-CF$_3$**). The value of 1 in "normalized Δppm" is the chemical shift of the proton alpha to Pt in the corresponding mononuclear complex (**4-CF$_3$**).

K_{eq} Determination for Complexes **5**, **5-OMe**, **5-F**, and **5-CF_3**

Table S1. Data and calculation for the titration of **5** with pyridine. Here, the initial concentrations of X (pyridine) and A (**5**) are known. The ∂A is the chemical shift of **5**, and ∂AX is the chemical shift of **4**. The $[AX]_f$, the concentration of **4** at equilibrium, is determined using Excel's Solver by minimizing the sum of square deviation between the ∂_{obs} and the calculated ∂_{obs}. The $[AX]_f$ can then be used to calculate the K_{eq}; the K_{eq} for each addition of pyridine from 14% to 90% conversion from dinuclear to mononuclear Pt-complex is averaged to give K_{eq} used in the manuscript.

	∂A	**6.009**	**∂AX**	**6.180**					
$[X]_0$	**∂_{obs}**	**$[A]_0$**	**$[A]_f$**	**$[AX]_f$**	**$[X]_f$**	**∂_{obs} (calc)**	**Residual**	**Residual²**	**K_{eq}**
0.18	6.034	1.000	0.854	0.146	2.88E-02	6.034	-7.71E-11	5.95E-21	0.87
0.44	6.064	1.000	0.678	0.321	1.18E-01	6.064	-9.30E-10	8.65E-19	1.29
0.70	6.081	1.000	0.579	0.421	2.74E-01	6.081	-1.53E-09	2.33E-18	1.12
0.96	6.093	1.000	0.509	0.491	4.69E-01	6.093	-3.23E-09	1.04E-17	1.01
1.28	6.106	1.000	0.433	0.567	7.08E-01	6.106	-4.17E-09	1.74E-17	1.05
1.61	6.117	1.000	0.368	0.631	9.73E-01	6.117	-1.19E-09	1.41E-18	1.11
2.13	6.129	1.000	0.298	0.701	1.43E+00	6.129	-2.89E-09	8.36E-18	1.16
2.79	6.139	1.000	0.240	0.760	2.03E+00	6.139	-6.13E-09	3.75E-17	1.19
3.36	6.147	1.000	0.193	0.807	2.55E+00	6.147	0.00E+00	0.00E+00	1.32
4.31	6.156	1.000	0.140	0.859	3.45E+00	6.156	-4.00E-09	1.60E-17	1.53
5.56	6.163	1.000	0.099	0.900	4.66E+00	6.163	-9.53E-09	9.09E-17	1.75
						SSD	**3.51E-16**	**Average K_{eq}**	1.22

Table S2. Data and calculation for the titration of **5-OMe** with pyridine. Here, the initial concentrations of X (pyridine) and A (**5-OMe**) are known. The ∂A is the chemical shift of **5-OMe**, and ∂AX is the chemical shift of **4-OMe**. The $[AX]_f$, the concentration of **4-OMe** at equilibrium, is determined using Excel's Solver by minimizing the sum of square deviation between the ∂_{obs} and the calculated ∂_{obs}. The $[AX]_f$ can then be used to calculate the K_{eq}; the K_{eq} for each addition of pyridine from 15% to 75% conversion from dinuclear to mononuclear Pt-complex is averaged to give K_{eq} used in the manuscript.

	∂A	**5.965**	**∂AX**	**6.081**					
$[X]_0$	**∂_{obs}**	**$[A]_0$**	**$[A]_f$**	**$[AX]_f$**	**$[X]_f$**	**∂_{obs} (calc)**	**Residual**	**Residual²**	**K_{eq}**
0.42	5.983	1.000	0.845	0.155	0.265	5.983	-1.32E-10	1.74E-20	0.108
0.57	5.992	1.000	0.767	0.233	0.337	5.992	-6.15E-10	3.78E-19	0.209
0.84	6.003	1.000	0.672	0.328	0.512	6.003	-4.81E-10	2.31E-19	0.311
1.19	6.009	1.000	0.621	0.379	0.811	6.009	-1.14E-09	1.29E-18	0.286
1.34	6.015	1.000	0.569	0.431	0.909	6.015	-1.79E-09	3.22E-18	0.359
1.70	6.020	1.000	0.526	0.474	1.226	6.020	0.00E+00	0.00E+00	0.349
2.15	6.026	1.000	0.474	0.526	1.624	6.026	-2.66E-09	7.10E-18	0.359
2.21	6.027	1.000	0.466	0.534	1.676	6.027	-3.11E-09	9.66E-18	0.366
2.35	6.028	1.000	0.457	0.543	1.807	6.028	-3.55E-09	1.26E-17	0.357
2.94	6.035	1.000	0.397	0.603	2.337	6.035	-2.65E-09	7.00E-18	0.393
4.40	6.045	1.000	0.310	0.690	3.710	6.045	-3.07E-09	9.43E-18	0.413
5.78	6.052	1.000	0.250	0.750	5.030	6.052	-6.18E-09	3.82E-17	0.447
						SSD	**8.91E-17**	**Average K_{eq}**	**0.330**

Table S3. Data and calculation for the titration of **5-F** with pyridine. Here, the initial concentrations of X (pyridine) and A (**5-F**) are known. The ∂A is the chemical shift of **5-F**, and ∂AX is the chemical shift of **4-F**. The $[AX]_f$, the concentration of **4-F** at equilibrium, is determined using Excel's Solver by minimizing the sum of square deviation between the ∂_{obs} and the calculated ∂_{obs}. The $[AX]_f$ can then be used to calculate the K_{eq}; the K_{eq} for each addition of pyridine from 24% to 95% conversion from dinuclear to mononuclear Pt-complex is averaged to give K_{eq} used in the manuscript.

	∂A	**5.782**	**∂AX**	**6.324**					
$[X]_0$	**∂_{obs}**	**$[A]_0$**	**$[A]_f$**	**$[AX]_f$**	**$[X]_f$**	**∂_{obs} (calc)**	**Residual**	**Residual^2**	**K_{eq}**
0.36	5.913	1.000	0.758	0.2423	0.118	5.913	-1.34E-09	1.80E-18	0.658
0.51	5.961	1.000	0.670	0.3303	0.180	5.961	5.20E-10	2.70E-19	0.906
0.74	6.083	1.000	0.445	0.5554	0.185	6.083	1.28E-09	1.65E-18	3.756
1.00	6.137	1.000	0.345	0.6550	0.345	6.137	1.79E-09	3.22E-18	3.604
1.11	6.172	1.000	0.280	0.7196	0.385	6.172	2.35E-09	5.51E-18	4.790
1.43	6.209	1.000	0.212	0.7878	0.637	6.209	2.71E-09	7.34E-18	4.591
1.73	6.234	1.000	0.166	0.8339	0.891	6.234	2.99E-09	8.94E-18	4.700
1.99	6.253	1.000	0.131	0.8690	1.121	6.253	3.27E-09	1.07E-17	5.143
2.45	6.272	1.000	0.096	0.9041	1.546	6.272	3.46E-09	1.20E-17	5.511
2.89	6.285	1.000	0.072	0.9280	1.957	6.285	3.62E-09	1.31E-17	6.116
3.53	6.295	1.000	0.054	0.9465	2.579	6.295	3.72E-09	1.38E-17	6.493
						SSD	**1.69E-16**	**Average K_{eq}**	**4.206**

Table S4. Data and calculation for the titration of **5-CF$_3$** with pyridine. Here, the initial concentrations of X (pyridine) and A (**5-CF$_3$**) are known. The ∂A is the chemical shift of **5-CF$_3$**, and ∂AX is the chemical shift of **4-CF$_3$**. The $[AX]_f$, the concentration of **4-CF$_3$** at equilibrium, is determined using Excel's Solver by minimizing the sum of square deviation between the ∂_{obs} and the calculated ∂_{obs}. The $[AX]_f$ can then be used to calculate the K_{eq}; the K_{eq} for each addition of pyridine from 30% to 85%* conversion from dinuclear to mononuclear Pt-complex is averaged to give K_{eq} used in the manuscript.

	∂A	**5.900**	**∂AX**	**6.418**					
$[X]_0$	**∂_{obs}**	**$[A]_0$**	**$[A]_f$**	**$[AX]_f$**	**$[X]_f$**	**∂_{obs} (calc)**	**Residual**	**Residual^2**	**K_{eq}**
0.670	6.303	1.000	0.222	0.7780	0.108	6.303	7.11E-15	5.05E-29	25.25
0.880	6.312	1.000	0.205	0.7954	0.085	6.312	0.00E+00	0.00E+00	36.53
1.110	6.339	1.000	0.153	0.8475	0.263	6.339	0.00E+00	0.00E+00	17.94
1.52	6.376	1.000	0.081	0.9189	0.601	6.376	0.00E+00	0.00E+00	17.33
2.120	6.391	1.000	0.052	0.9479	1.172	6.391	0.00E+00	0.00E+00	14.71
2.670	6.398	1.000	0.039	0.9614	1.709	6.398	0.00E+00	0.00E+00	14.01
3.630	6.404	1.000	0.027	0.9730	2.657	6.404	0.00E+00	0.00E+00	13.18
4.640	6.407	1.000	0.021	0.9788	3.661	6.407	0.00E+00	0.00E+00	12.32
6.130	6.410	1.000	0.015	0.9846	5.145	6.410	0.00E+00	0.00E+00	12.20
7.83	6.412	1.000	0.012	0.9884	6.842	6.412	0.00E+00	0.00E+00	12.33
						SSD	**1.00E-06**	**Average K_{eq}**	**17.58**

*We note that for **5-CF$_3$**, the substantial broadening observed at low equivalents of pyridine added (Figure S61) and the sigmoidal shape of the curve of normalized Δppm vs pyridine equivalents (Figure S65) make the K_{eq} determination unreliable at low equivalents of pyridine (< 0.6 eq pyridine) added to **5-CF$_3$**. Thus, those values are excluded in the K_{eq} determination.

Determination of the Degree of Arene Ring Transfer

General Considerations for the Determination of the Degree of Arene Ring Transfer

As noted in the manuscript, the Pt–arene rings are not perfectly aligned. While the complexes deviate slightly from perfect square planar geometries, one also cannot draw a straight line from the C_{para} of one arene ring through the Pt center to the C_{para} of the other arene ring. *Thus, the C_{para}–C_{ipso}–Pt angle is always less than 180º even for complexes that might be perfectly square planar and the CNC ligand remains perfectly planar.* Hence, we have chosen a different method for evaluating the degree of arene group transfer from the C_{para}–C_{ipso}–Pt and C_{para}–C_{ipso}–Au angles used by Martin and coworkers.[5]

Due to strain in the complex, the CNC ligand deviates from planarity in the mononuclear Pt-complexes themselves. This deviation from planarity increases upon $[(PPh_3)Au]^+$ binding to the Pt-complexes. In the solid-state, this deviation is most pronounced for the arene ring that bridges Pt and Au; however, the other Pt–arene ring also further deviates from planarity despite no direct interaction with the Au in the crystal structure. For this reason, we analyze the deviation from planarity of both arene rings with and without binding of $[(PPh_3)Au]^+$.

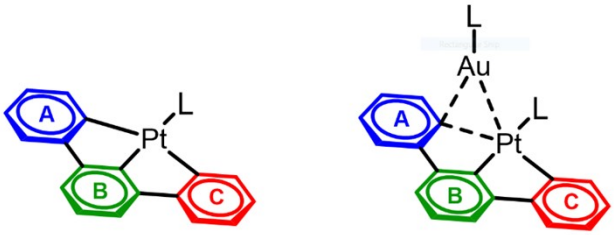

Determination of the degree of arene ring transfer in the dinuclear complexes involves first determining the two different planes formed by arene rings A and C of the mononuclear complex. These planes are generated using the program Mercury. Then, the angle between the A and C rings can be measured, also using Mercury. This measurement reveals the amount of distortion present in the monometallic complex. We use this structural distortion in the monometallic complex as a baseline and compare the angle between the planes of the A and C ring to the angle between the A and C ring upon binding of the $[(PPh_3)Au]^+$.

One could instead determine the angle between the planes formed between rings B (the pyridyl ring) and C (the ring that bridges between Pt and Au). The assignment of ring C in the mononuclear complex is arbitrary. In the solid-state structure, however, the angles formed by the planes between A / B and C / B are slightly different. Thus, the choice of A vs C ring in the monometallic complex would influence the degree of arene group transfer measurement.

We note that in this analysis 0º indicates no arene group transfer. Previously, Martin and coworkers used the C_{para}–C_{ipso}–Au angle as the measure of arene group transfer. Using the C_{para}–C_{ipso}–Au angle method, 90º indicates no arene group transfer and 180º indicates full arene group transfer from Pt to Au.

Determining the Degree of Arene Ring Transfer in Symmetric Complexes

In complex **1**, the angle between the planes formed by the A and C rings is 12.23°, a modest deviation from planarity. We then found a 33.54° angle between planes formed by the A and C rings in **2**. Finally, we use the difference between the angle between the A and C rings upon $[(PPh_3)Au]^+$ binding, 21.31°, as the degree of arene ring transfer. Using the same analysis on complex **2-F**, we find a 7.52º measurement, clearly a smaller degree of arene group transfer with the more electron deficient Pt–arene ring.

Determining the Degree of Arene Ring Transfer in the Benzo[h]quinoline Derivatives

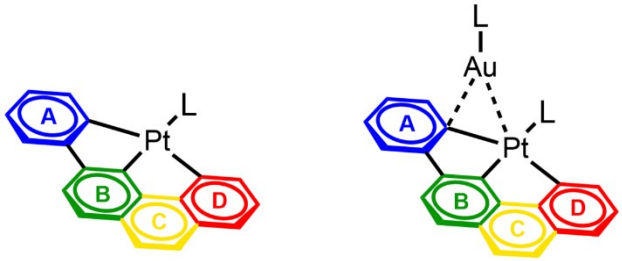

The same structural analysis as above can be conducted on the asymmetric benzoquinoline based ligands. In the benzoquinoline based ligands there are now four arene rings (A – D), but we only consider rings A and D. Unlike in the 2,6-diphenylpyridine ligands, rings A and D are not identical in **4**, so there is no ambiguity. However, we measure the angle between the planes of rings A and D with and without $[(PPh_3)Au]^+$ same as above.

Table S5. Calculated Degree of Arene Transfer Using New Method Described

Complex	***Mononuclear Angle Between Planes***	***Dinuclear Angle Between Planes***	***Degree of Arene Transfer***
2	12.23°	33.54°	**21.31°**
5	11.20°	15.31°	**4.11°**
5-OMe	7.29°	20.10°	**12.81°**
5-F	8.65°	20.99°	**12.34°**
5-CF_3	10.86°	12.43°	**1.57°**
2-F	18.36°	25.88°	**7.52°**

Complex	***C_{para}–C_{ipso}–Pt Mononuclear complex***	***C_{para}–C_{ipso}–Pt Dinuclear complex***	***C_{para}–C_{ipso}–Au***	***Angle Between Planes Method***
2	168.9° 167.3°	**160.4°** 169.0°	120.1°	21.31°
5	166.0° 169.8°	**162.6°** 170.0°	118.5°	4.11°
5-OMe	166.4° 169.3°	166.7° **165.5°**	114.0°	12.81°
5-F	166.8° 168.5°	166.3° **164.0°**	117.4°	12.34°
5-CF_3	166.5° 169.3°	**164.3°** 170.4°	112.0°	1.57°
2-F	168.8° 168.6°	**159.9°** 169.9°	120.9°	7.52°

Table S6. Calculated Degrees of Arene Transfer Method Comparison

For **4**/**5**, **4-OMe**/**5-OMe**, **4-F**/**5-F**, and **4-CF_3**/**5-CF_3**, the C_{para}–C_{ipso}–Pt for the Pt–bhq is shown on top and the Pt–Ph^R on the bottom, the bridging arene ring angle of the dinuclear complexes are denoted in bold. For **1** and **1-F**, both C_{para}–C_{ipso}–Pt are shown. For **2** and **2-F**, the C_{para}–C_{ipso}–Pt of the bridging arene ring is denoted in bold.

X-Ray Crystallography

Data collection: *APEX5* (Bruker, 2016); cell refinement: *SAINT* V8.40A (Bruker, 2019); data reduction: *SAINT* V8.40A (Bruker, 2019); program(s) used to solve structure: SHELXT (Sheldrick, 2015); program(s) used to refine structure: *SHELXL* 2018/3 (Sheldrick, 2015); molecular graphics: Olex2 1.5 (Dolomanov *et al.*, 2009); software used to prepare material for publication: Olex2 1.5 (Dolomanov *et al.*, 2009).

Geometry: All esds (except the esd in the dihedral angle between two l.s. planes) are estimated using the full covariance matrix. The cell esds are taken into account individually in the estimation of esds in distances, angles and torsion angles; correlations between esds in cell parameters are only used when they are defined by crystal symmetry. An approximate (isotropic) treatment of cell esds is used for estimating esds involving l.s. planes.

X-Ray Crystal Structure of 4

Crystals suitable for single crystal X-ray diffraction were obtained by slow diffusion of pentane into a DCM solution of **4**.

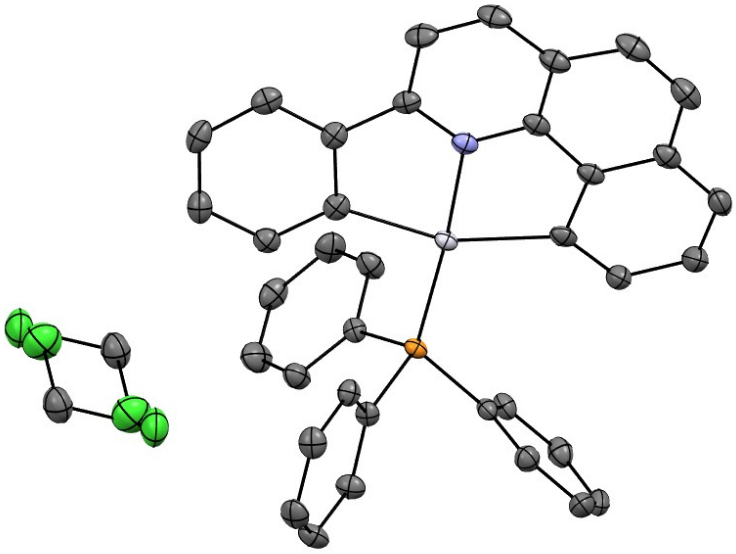

Figure S66. Molecular structure of **4** with one disordered molecule of DCM. Hydrogens are omitted for clarity. Thermal ellipsoids are shown at the 50% probability level.

Table S7. Crystal Data of **4**

$C_{37}H_{26}NPPt \cdot 0.495(CH_2Cl_2)$	$F(000)$ = 1475
M_r = 752.68	D_x = 1.757 Mg m^{-3}
Monoclinic, $P2_1/n$	Cu Ka radiation, l = 1.54178 Å
a = 9.3036 (2) Å	Cell parameters from 9578 reflections
b = 17.0471 (4) Å	θ = 3.6–72.1°
c = 17.9456 (4) Å	μ = 10.83 mm^{-1}
b = 91.1968 (6)°	T = 100 K
V = 2845.54 (11) Å^3	Prism, orange
Z = 4	0.24 × 0.11 × 0.1 mm

Table S8. Data Collection of **4**

Bruker D8 Venture diffractometer	5491 independent reflections
Radiation source: microfocus sealed tube	5448 reflections with $I > 2\sigma(I)$
Helios Cu monochromator	R_{int} = 0.032
ϕ and ω scans	θ_{max} = 72.1°, θ_{min} = 3.6°
Absorption correction: multi-scan *SADABS2016*/2 (Bruker,2016/2) was used for absorption correction. wR2(int) was 0.0946 before and 0.0487 after correction. The Ratio of minimum to maximum transmission is 0.6249. The λ/2 correction factor is Not present.	h = -11→10
T_{min} = 0.471, T_{max} = 0.754	k = -21→21
53614 measured reflections	l = -22→22

Table S9. Refinement of **4**

Refinement on F^2	Primary atom site location: structure-invariant direct methods
Least-squares matrix: full	Hydrogen site location: inferred from neighbouring sites
$R[F^2 > 2\sigma(F^2)] = 0.023$	H-atom parameters constrained
$wR(F^2) = 0.054$	$w = 1/[\sigma^2(F_o^2) + (0.0153P)^2 + 8.0454P]$ where $P = (F_o^2 + 2F_c^2)/3$
$S = 1.17$	$(\Delta/\sigma)_{max} = 0.001$
5491 reflections	$\Delta\rangle_{max} = 0.64$ e Å^{-3}
386 parameters	$\Delta\rangle_{min} = -0.99$ e Å^{-3}
0 restraints	

X-Ray Crystal Structure of 4-OMe

Crystals suitable for single crystal X-ray diffraction were obtained by slow diffusion of pentane into a DCM solution of **4-OMe**.

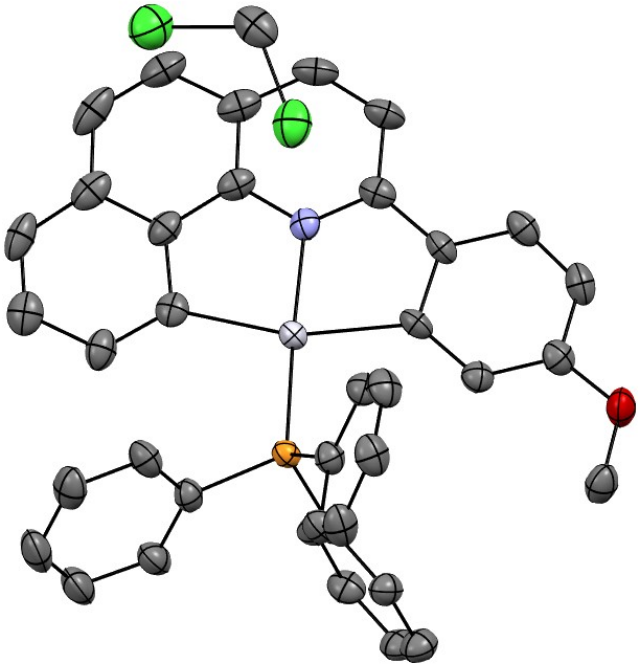

Figure S67. Molecular structure of **4-OMe** with one molecule of DCM. Hydrogens are omitted for clarity. Thermal ellipsoids are shown at the 50% probability level.

Table S10. Crystal Data of **4-OMe**

$C_{38}H_{28}NOPPt \cdot CH_2Cl_2$	D_x = 1.706 Mg m^{-3}
M_r = 825.60	Cu $K\alpha$ radiation, λ = 1.54178 Å
Orthorhombic, $P2_12_12_1$	Cell parameters from 9466 reflections
a = 8.7539 (9) Å	θ = 5.4–72.2°
b = 15.0548 (15) Å	μ = 10.42 mm^{-1}
c = 24.397 (3) Å	T = 100 K
V = 3215.3 (6) Å^3	Irregular, clear light orange
Z = 4	0.17 × 0.12 × 0.12 mm
F(000) = 1624	

Table S11. Data Collection of **4-OMe**

Bruker D8 Venture diffractometer	6240 independent reflections
Radiation source: microfocus sealed tube	6208 reflections with $I > 2\sigma(I)$
Helios Cu monochromator	$R_{int} = 0.064$
ϕ and ω scans	$\theta_{max} = 72.4°$, $\theta_{min} = 3.5°$
Absorption correction: numerical *SADABS2016*/2 (Bruker,2016/2) was used for absorption correction. wR2(int) was 0.1330 before and 0.1112 after correction. The Ratio of minimum to maximum transmission is 0.5507. The λ/2 correction factor is Not present.	$h = -10 \rightarrow 10$
$T_{min} = 0.249$, $T_{max} = 0.453$	$k = -18 \rightarrow 18$
68595 measured reflections	$l = -29 \rightarrow 29$

Table S12. Refinement of **4-OMe**

Refinement on F^2	Hydrogen site location: inferred from neighbouring sites
Least-squares matrix: full	H-atom parameters constrained
$R[F^2 > 2\sigma(F^2)] = 0.027$	$w = 1/[\sigma^2(F_o^2) + (0.0206P)^2 + 6.9375P]$ where $P = (F_o^2 + 2F_c^2)/3$
$wR(F^2) = 0.064$	$(\Delta/\sigma)_{max} = 0.001$
$S = 1.17$	$\Delta\rangle_{max} = 0.83$ e Å^{-3}
6240 reflections	$\Delta\rangle_{min} = -1.29$ e Å^{-3}
408 parameters	Absolute structure: Refined as an inversion twin.
0 restraints	Absolute structure parameter: 0.252 (12)
Primary atom site location: iterative	

X-Ray Crystal Structure of 4-F

Crystals suitable for single crystal X-ray diffraction were obtained by slow diffusion of ether into a THF solution of **4-F**.

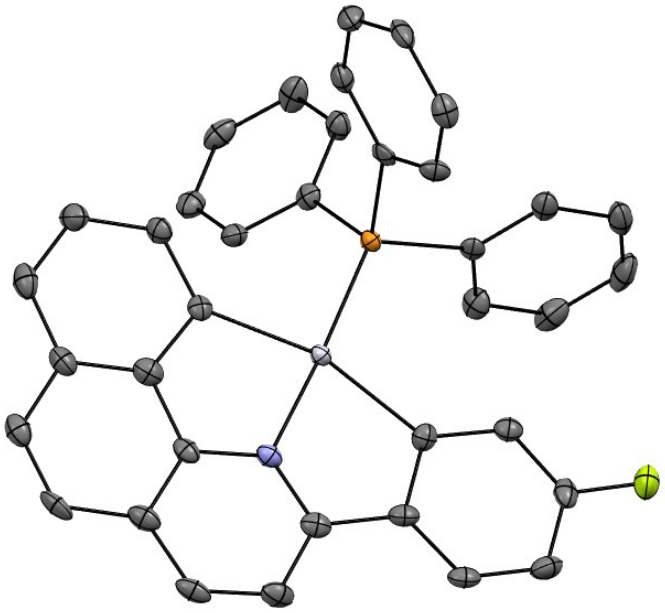

Figure S68. Molecular structure of **4-F**. Hydrogens are omitted for clarity. Thermal ellipsoids are shown at the 50% probability level.

Table S13. Crystal Data of **4-F**

$C_{37}H_{25}FNPPt$	$F(000)$ = 1424
M_r = 728.64	D_x = 1.734 Mg m^{-3}
Monoclinic, $P2_1/c$	Cu $K\alpha$ radiation, λ = 1.54178 Å
a = 18.5974 (10) Å	Cell parameters from 9221 reflections
b = 12.3392 (7) Å	θ = 3.6–72.2°
c = 12.6734 (7) Å	μ = 10.22 mm^{-1}
β = 106.2770 (11)°	T = 100 K
V = 2791.7 (3) Å^3	Block, clear orange
Z = 4	0.20 × 0.14 × 0.10 mm

Table S14. Data Collection of **4-F**

Bruker D8 Venture diffractometer	5316 independent reflections
Radiation source: microfocus sealed tube	5309 reflections with $I > 2\sigma(I)$
Helios Cu monochromator	$R_{int} = 0.045$
ϕ and ω scans	$\theta_{max} = 72.1°$, $\theta_{min} = 4.4°$
Absorption correction: multi-scan *SADABS2016*/2 (Bruker,2016/2) was used for absorption correction. wR2(int) was 0.1575 before and 0.0899 after correction. The Ratio of minimum to maximum transmission is 0.2794. The λ/2 correction factor is Not present.	$h = -22 \rightarrow 21$
$T_{min} = 0.262$, $T_{max} = 0.936$	$k = -15 \rightarrow 15$
34456 measured reflections	$l = -15 \rightarrow 15$

Table S15. Refinement of **4-F**

Refinement on F^2	Primary atom site location: structure-invariant direct methods
Least-squares matrix: full	Hydrogen site location: inferred from neighbouring sites
$R[F^2 > 2\sigma(F^2)] = 0.038$	H-atom parameters constrained
$wR(F^2) = 0.087$	$w = 1/[\sigma^2(F_o^2) + 29.5291P]$ where $P = (F_o^2 + 2F_c^2)/3$
$S = 1.16$	$(\Delta/\sigma)_{max} = 0.001$
5316 reflections	$\Delta\rangle_{max} = 1.30$ e Å^{-3}
370 parameters	$\Delta\rangle_{min} = -1.72$ e Å^{-3}
0 restraints	

X-Ray Crystal Structure of 4-CF_3

Crystals suitable for single crystal X-ray diffraction were obtained by slow diffusion of pentane into a DCM solution of **4-CF_3**.

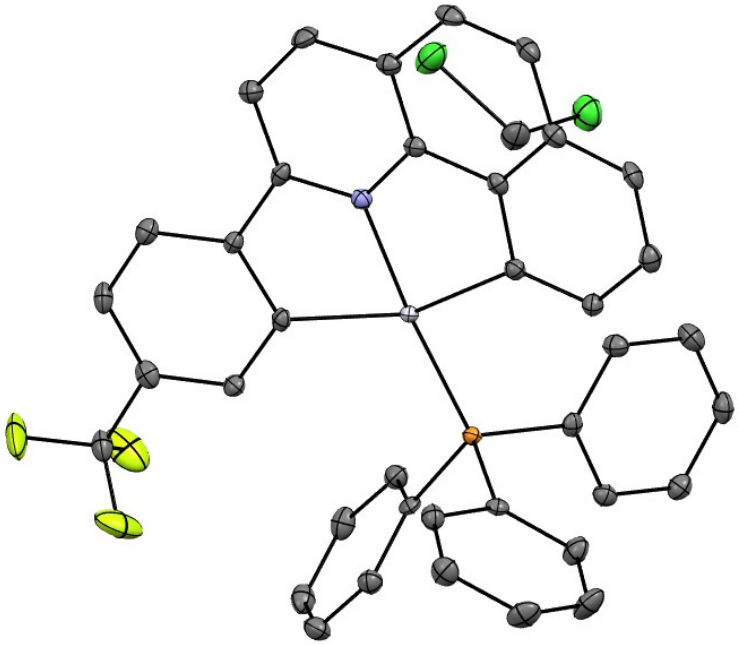

Figure S69. Molecular structure of **4-CF_3** with one molecule of DCM. Hydrogens are omitted for clarity. Thermal ellipsoids are shown at the 50% probability level.

Table S16. Crystal Data of **4-CF_3**

$C_{38}H_{25}F_3NPPt \cdot CH_2Cl_2$	Z = 2
M_r = 863.57	F(000) = 844
Triclinic, $P\bar{1}$	D_x = 1.804 Mg m^{-3}
a = 9.2829 (5) Å	Cu $K\alpha$ radiation, λ = 1.54178 Å
b = 13.3536 (7) Å	Cell parameters from 9925 reflections
c = 13.8469 (7) Å	θ = 3.2–72.1°
α = 81.094 (1)°	μ = 10.69 mm^{-1}
β = 89.205 (1)°	T = 100 K
γ = 69.801 (1)°	Prism, clear orange
V = 1590.03 (14) Å^3	0.24 × 0.20 × 0.13 mm

Table S17. Data Collection of **4-CF_3**

Bruker D8 Venture diffractometer	6202 independent reflections
Radiation source: microfocus sealed tube	6202 reflections with $I > 2\sigma(I)$
HELIOS Cu monochromator	$R_{int} = 0.034$
ω and ϕ scans	$\theta_{max} = 72.1°$, $\theta_{min} = 3.2°$
Absorption correction: numerical *SADABS2016*/2 (Bruker,2016/2) was used for absorption correction. wR2(int) was 0.1348 before and 0.0988 after correction. The Ratio of minimum to maximum transmission is 0.0338. The λ/2 correction factor is Not present.	$h = -11 \rightarrow 11$
$T_{min} = 0.002$, $T_{max} = 0.068$	$k = -16 \rightarrow 16$
85436 measured reflections	$l = -17 \rightarrow 17$

Table S18. Refinement of **4-CF_3**

Refinement on F^2	0 restraints
Least-squares matrix: full	Hydrogen site location: inferred from neighbouring sites
$R[F^2 > 2\sigma(F^2)] = 0.021$	H-atom parameters constrained
$wR(F^2) = 0.052$	$w = 1/[\sigma^2(F_o^2) + (0.0221P)^2 + 3.7962P]$ where $P = (F_o^2 + 2F_c^2)/3$
$S = 1.15$	$(\Delta/\sigma)_{max} = 0.001$
6202 reflections	$\Delta\rangle_{max} = 0.98$ e Å^{-3}
424 parameters	$\Delta\rangle_{min} = -1.45$ e Å^{-3}

X-Ray Crystal Structure of 5

Crystals suitable for single crystal X-ray diffraction were obtained by slow diffusion of pentane into a DCM solution of **5**.

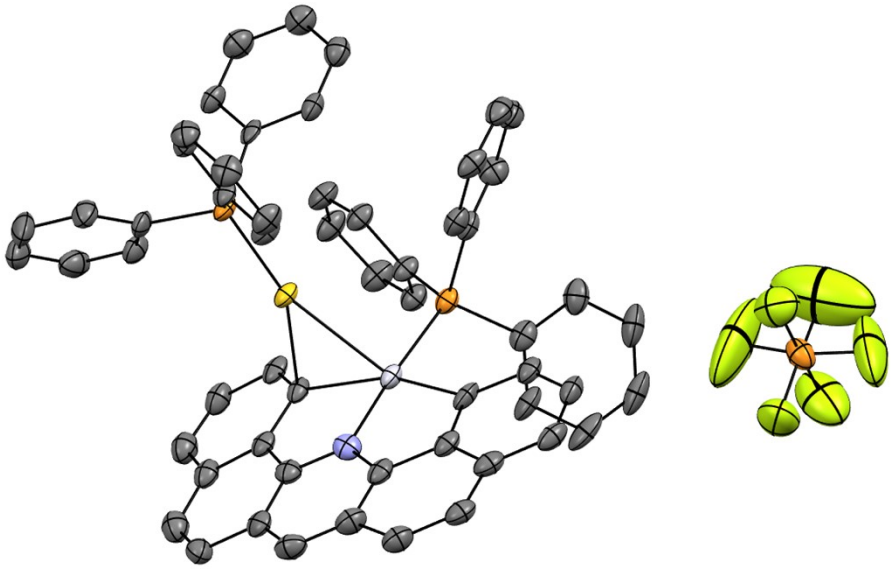

Figure S70. Molecular structure of **5** with [PF_6] as the counteranion. Image contains fully mapped disorder. Hydrogens are omitted for clarity. Thermal ellipsoids are shown at the 50% probability level.

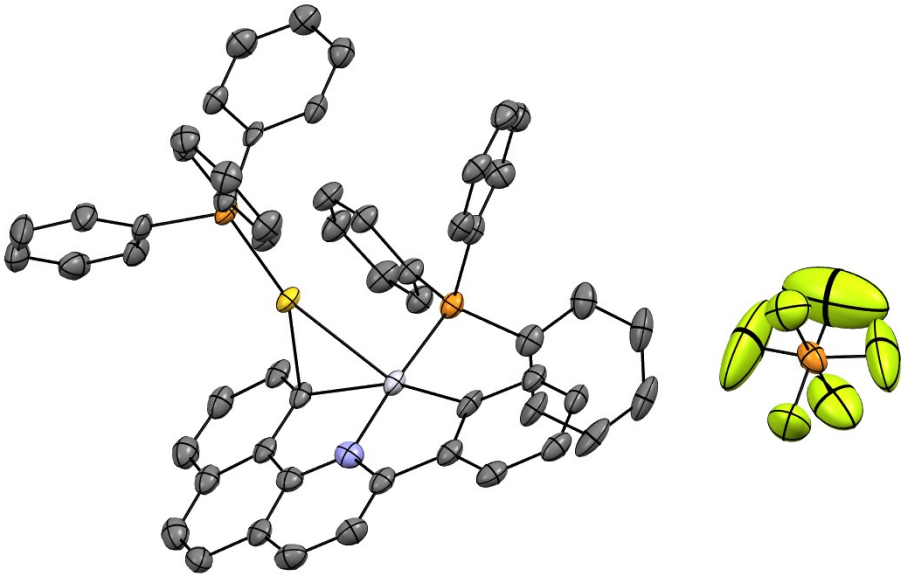

Figure S71. Molecular structure of **5** with [PF_6] as the counteranion. Image contains partially mapped disorder (~ 90%) with [$Au(PPh_3)$]$^+$ coordinated to the benzo[*h*]quinoline fragment of the CNC ligand. Hydrogens are omitted for clarity. Thermal ellipsoids are shown at the 50% probability level.

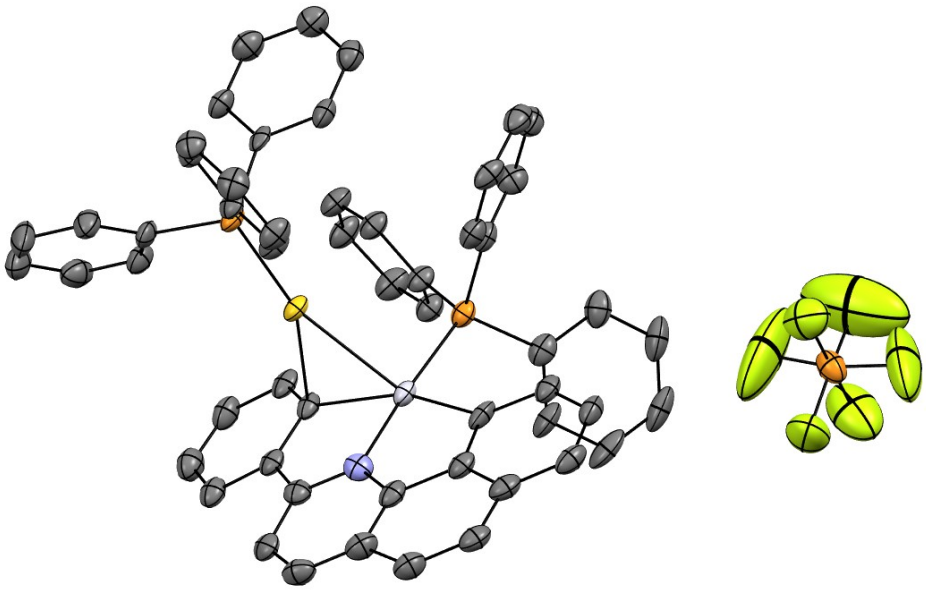

Figure S72. Molecular structure of **5** with [PF_6] as the counteranion. Image contains partially mapped disorder (~ 10%) with [$Au(PPh_3)$]$^+$ coordinated to the phenyl fragment of the CNC ligand. Hydrogens are omitted for clarity. Thermal ellipsoids are shown at the 50% probability level.

Table S19. Crystal Data of **5**

$C_{55}H_{41}AuNP_2Pt{\cdot}F_6P$	Z = 2
M_r = 1314.85	F(000) = 1268
Triclinic, $P\bar{1}$	D_x = 1.647 Mg m^{-3}
a = 13.2038 (6) Å	Cu $K\alpha$ radiation, λ = 1.54178 Å
b = 15.1044 (7) Å	Cell parameters from 9833 reflections
c = 15.2786 (7) Å	θ = 3.2–70.2°
α = 68.185 (2)°	μ = 11.32 mm^{-1}
β = 73.142 (2)°	T = 100 K
γ = 73.330 (2)°	Prism, clear orange
V = 2651.8 (2) Å^3	0.31 × 0.22 × 0.12 mm

Table S20. Data Collection of **5**

Bruker D8 Venture diffractometer	10041 independent reflections
Radiation source: microfocus sealed tube	9778 reflections with $I > 2\sigma(I)$
HELIOS Cu monochromator	$R_{int} = 0.053$
ω and ϕ scans	$\theta_{max} = 70.2°$, $\theta_{min} = 3.2°$
Absorption correction: numerical *SADABS2016*/2 (Bruker,2016/2) was used for absorption correction. wR2(int) was 0.1600 before and 0.0976 after correction. The Ratio of minimum to maximum transmission is 0.1988. The λ/2 correction factor is Not present.	$h = -14 \rightarrow 16$
$T_{min} = 0.134$, $T_{max} = 0.672$	$k = -18 \rightarrow 18$
154341 measured reflections	$l = -18 \rightarrow 18$

Table S21. Refinement of **5**

Refinement on F^2	109 restraints
Least-squares matrix: full	Hydrogen site location: inferred from neighbouring sites
$R[F^2 > 2\sigma(F^2)] = 0.041$	H-atom parameters constrained
$wR(F^2) = 0.107$	$w = 1/[\sigma^2(F_o^2) + (0.0521P)^2 + 18.9718P]$ where $P = (F_o^2 + 2F_c^2)/3$
$S = 1.08$	$(\Delta/\sigma)_{max} = 0.001$
10041 reflections	$\Delta\rangle_{max} = 1.69$ e Å^{-3}
611 parameters	$\Delta\rangle_{min} = -1.71$ e Å^{-3}

X-Ray Crystal Structure of 5-OMe

Crystals suitable for single crystal X-ray diffraction were obtained by slow diffusion of diethyl ether into a DCM:MeOH solution of **5-OMe.**

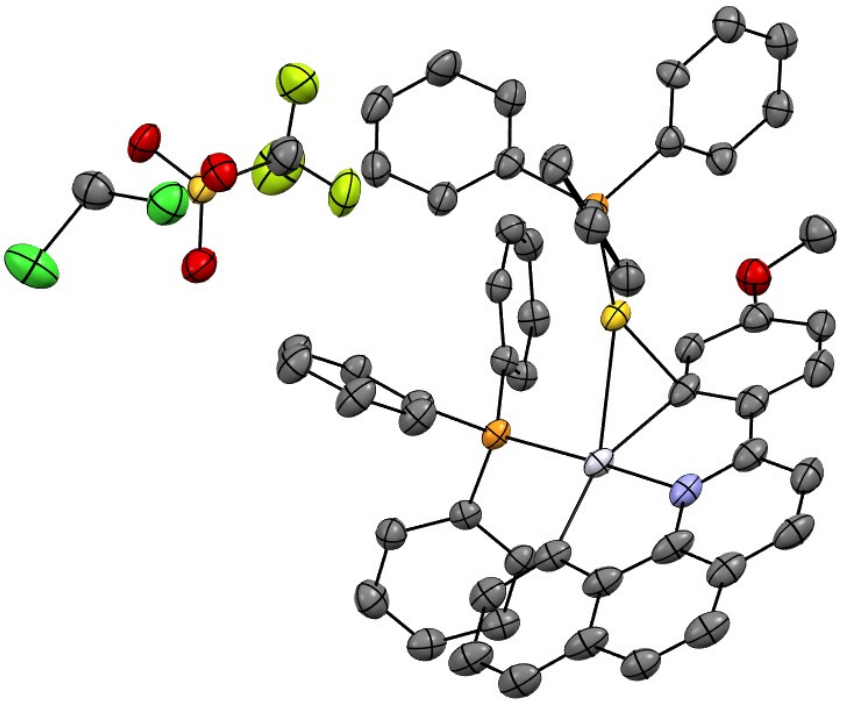

Figure S73. Molecular structure of **5-OMe** with one molecule of DCM and [OTf] as the counteranion. Hydrogens are omitted for clarity. Thermal ellipsoids are shown at the 50% probability level.

Table S22. Crystal Data of **5-OMe**

$C_{56}H_{43}AuNOP_2Pt \cdot CF_3O_3S \cdot CH_2Cl_2$	$F(000)$ = 2784
M_r = 1433.90	D_x = 1.828 Mg m^{-3}
Monoclinic, $P2_1/c$	Cu $K\alpha$ radiation, λ = 1.54178 Å
a = 14.3136 (8) Å	Cell parameters from 9605 reflections
b = 9.5807 (5) Å	θ = 2.3–72.0°
c = 38.117 (2) Å	μ = 12.56 mm^{-1}
β = 94.663 (3)°	T = 100 K
V = 5209.9 (5) Å^3	Plate, clear orange
Z = 4	0.14 × 0.08 × 0.03 mm

Table S23. Data Collection of **5-OMe**

Bruker D8 Venture diffractometer	10260 independent reflections
Radiation source: Microfocus Sealed Tube	9152 reflections with $I > 2\sigma(I)$
Helios Cu monochromator	$R_{int} = 0.080$
ϕ and ω scans	$\theta_{max} = 72.4°$, $\theta_{min} = 2.3°$
Absorption correction: numerical *SADABS2016*/2 (Bruker,2016/2) was used for absorption correction. wR2(int) was 0.1349 before and 0.0881 after correction. The Ratio of minimum to maximum transmission is 0.5847. The λ/2 correction factor is Not present.	$h = -17 \rightarrow 17$
$T_{min} = 0.437$, $T_{max} = 0.747$	$k = -11 \rightarrow 11$
141036 measured reflections	$l = -47 \rightarrow 47$

Table S24. Refinement of **5-OMe**

Refinement on F^2	Primary atom site location: dual
Least-squares matrix: full	Secondary atom site location: difference Fourier map
$R[F^2 > 2\sigma(F^2)] = 0.045$	Hydrogen site location: inferred from neighbouring sites
$wR(F^2) = 0.112$	H-atom parameters constrained
$S = 1.08$	$w = 1/[\sigma^2(F_o^2) + (0.0431P)^2 + 42.763P]$ where $P = (F_o^2 + 2F_c^2)/3$
10260 reflections	$(\Delta/\sigma)_{max} = 0.004$
659 parameters	$\Delta\rangle_{max} = 2.77$ e Å^{-3}
0 restraints	$\Delta\rangle_{min} = -3.17$ e Å^{-3}

X-Ray Crystal Structure of 5-F

Crystals suitable for single crystal X-ray diffraction were obtained by slow diffusion of pentane into a DCM solution of **5-F.**

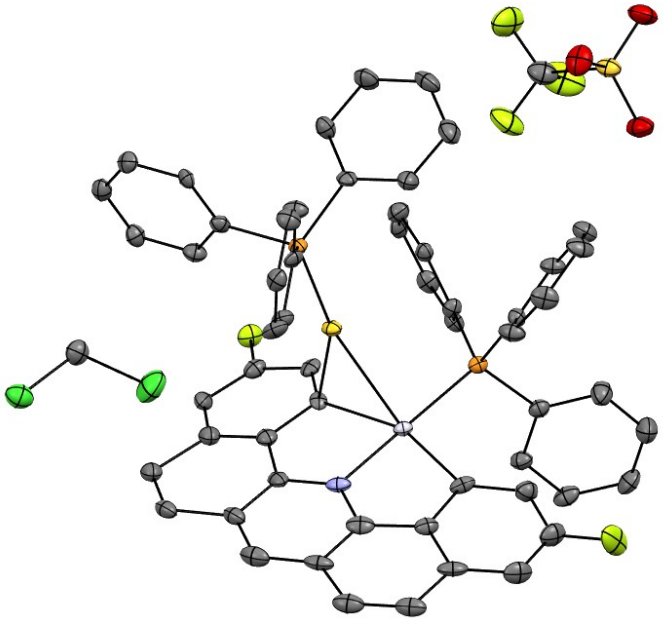

Figure S74. Molecular structure of **5-F** with one molecule of DCM and [OTf] as the counteranion. Image contains fully mapped disorder. Hydrogens are omitted for clarity. Thermal ellipsoids are shown at the 50% probability level.

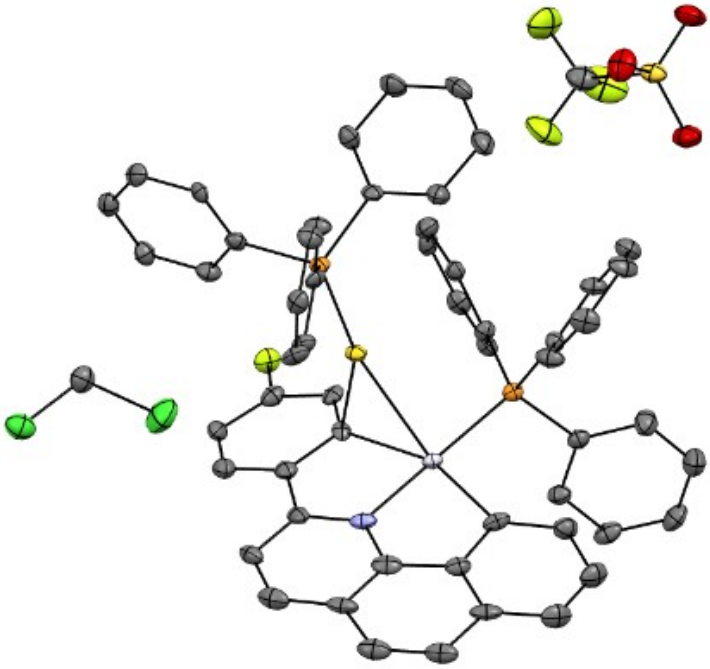

Figure S75. Molecular structure of **5-F** with one molecule of DCM and [OTf] as the counteranion. Image contains partially mapped disorder (~ 89%) with $[Au(PPh_3)]^+$ coordinated to the phenyl fragment of the CNC ligand. Hydrogens are omitted for clarity. Thermal ellipsoids are shown at the 50% probability level.

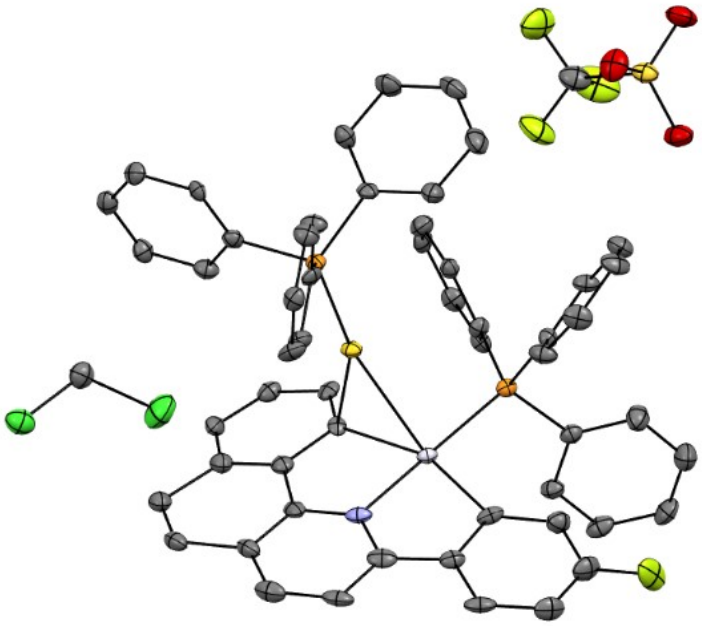

Figure S76. Molecular structure of **5-F** with one molecule of DCM and [OTf] as the counteranion. Image contains partially mapped disorder (~ 11%) with $[Au(PPh_3)]^+$ coordinated to the benzo[*h*]quinoline fragment of the CNC ligand. Hydrogens are omitted for clarity. Thermal ellipsoids are shown at the 50% probability level.

Table S25. Crystal Data of **5-F**

$C_{55}H_{40}AuFNP_2Pt \cdot CF_3O_3S \cdot CH_2Cl_2$	$F(000)$ = 2752
M_r = 1421.87	D_x = 1.841 Mg m^{-3}
Monoclinic, $P2_1/c$	Cu $K\alpha$ radiation, λ = 1.54178 Å
a = 14.2188 (13) Å	Cell parameters from 9880 reflections
b = 9.5432 (9) Å	θ = 3.1–72.2°
c = 37.948 (3) Å	μ = 12.77 mm^{-1}
β = 94.984 (2)°	T = 100 K
V = 5129.8 (8) Å^3	Prism, clear dark orange
Z = 4	0.25 × 0.11 × 0.10 mm

Table S26. Data Collection of **5-F**

Bruker D8 Venture diffractometer	10046 independent reflections
Radiation source: microfocus sealed tube	10006 reflections with $I > 2\sigma(I)$
HELIOS Cu monochromator	$R_{int} = 0.050$
ω and ϕ scans	$\theta_{max} = 72.3°$, $\theta_{min} = 2.3°$
Absorption correction: numerical *SADABS2016*/2 (Bruker,2016/2) was used for absorption correction. wR2(int) was 0.1394 before and 0.0982 after correction. The Ratio of minimum to maximum transmission is 0.1906. The λ/2 correction factor is Not present.	$h = -17 \rightarrow 17$
$T_{min} = 0.184$, $T_{max} = 0.967$	$k = -11 \rightarrow 11$
76488 measured reflections	$l = -46 \rightarrow 46$

Table S27. Refinement of **5-F**

Refinement on F^2	Secondary atom site location: difference Fourier map
Least-squares matrix: full	Hydrogen site location: inferred from neighbouring sites
$R[F^2 > 2\sigma(F^2)] = 0.050$	H-atom parameters constrained
$wR(F^2) = 0.112$	$w = 1/[\sigma^2(F_o^2) + 126.6999P]$ where $P = (F_o^2 + 2F_c^2)/3$
$S = 1.09$	$(\Delta/\sigma)_{max} = 0.001$
10046 reflections	$\Delta\rangle_{max} = 3.03$ e Å^{-3}
665 parameters	$\Delta\rangle_{min} = -3.60$ e Å^{-3}
701 restraints	

X-Ray Crystal Structure of **5-CF_3**

Crystals suitable for single crystal X-ray diffraction were obtained by slow diffusion of pentane into a DCM solution of **5-CF_3**.

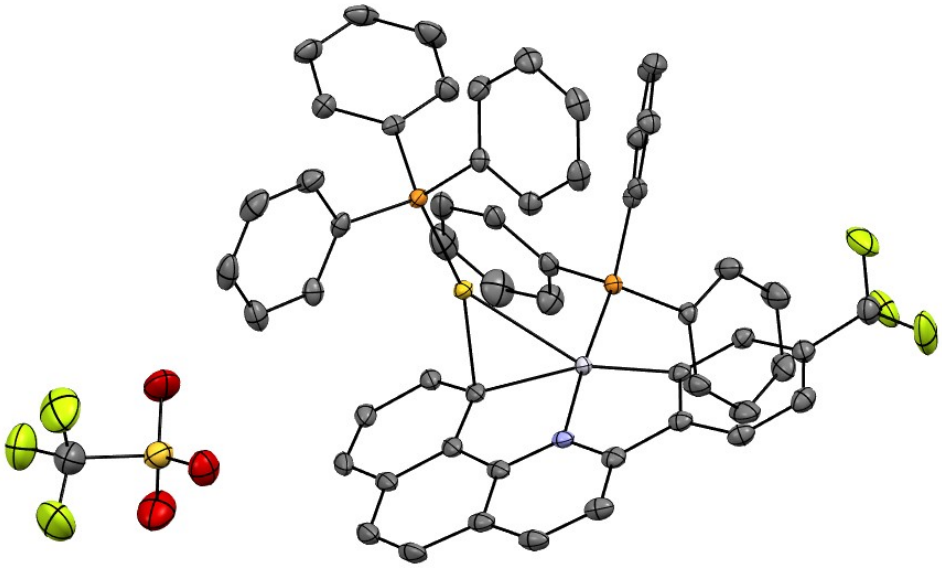

Figure S77. Molecular structure of **5-CF_3** with [OTf] as the counteranion. Hydrogens are omitted for clarity. Thermal ellipsoids are shown at the 50% probability level.

Table S28. Crystal Data of **5-CF_3**

$C_{56}H_{40}AuF_3NP_2Pt \cdot CF_3O_3S \cdot H_2O$	Z = 2
M_r = 1404.97	F(000) = 1360
Triclinic, $P\bar{1}$	D_x = 1.842 Mg m^{-3}
a = 13.1086 (4) Å	Cu $K\alpha$ radiation, λ = 1.54178 Å
b = 14.1393 (4) Å	Cell parameters from 9904 reflections
c = 14.9467 (5) Å	θ = 3.2–72.0°
α = 68.526 (1)°	μ = 12.05 mm^{-1}
β = 89.457 (1)°	T = 100 K
γ = 79.859 (1)°	Plate, clear orange
V = 2533.16 (14) Å^3	0.18 × 0.17 × 0.04 mm

Table S29. Data Collection of **5-CF_3**

Bruker D8 Venture diffractometer	9428 independent reflections
Radiation source: microfocus sealed tube	9035 reflections with $I > 2\sigma(I)$
HELIOS Cu monochromator	$R_{int} = 0.042$
ω and ϕ scans	$\theta_{max} = 72.1°$, $\theta_{min} = 3.2°$
Absorption correction: multi-scan *SADABS2016*/2 (Bruker,2016/2) was used for absorption correction. wR2(int) was 0.1031 before and 0.0609 after correction. The Ratio of minimum to maximum transmission is 0.6948. The λ/2 correction factor is Not present.	$h = -16 \rightarrow 15$
$T_{min} = 0.524$, $T_{max} = 0.754$	$k = -17 \rightarrow 17$
97582 measured reflections	$l = -18 \rightarrow 17$

Table S30. Refinement of **5-CF_3**

Refinement on F^2	4 restraints
Least-squares matrix: full	Hydrogen site location: mixed
$R[F^2 > 2\sigma(F^2)] = 0.019$	H atoms treated by a mixture of independent and constrained refinement
$wR(F^2) = 0.047$	$w = 1/[\sigma^2(F_o^2) + (0.0194P)^2 + 5.1811P]$ where $P = (F_o^2 + 2F_c^2)/3$
$S = 1.02$	$(\Delta/\sigma)_{max} = 0.004$
9428 reflections	$\Delta\rangle_{max} = 0.86$ e Å^{-3}
666 parameters	$\Delta\rangle_{min} = -1.19$ e Å^{-3}

Computation details

The Density Functional Theory (DFT) studies carried out in this manuscript were performed using the Gaussian 16 program.[8] For the geometry optimization of **4-OMe**, the calculation was performed in the gas phase with the B3LYP functional and a split basis set, LANL2DZ for Pt atom with a pseudo potential used for the core electrons of the Pt atom and 6-31G(d) for all other atoms. The geometry of the X-ray crystal structure of **4-OMe** was used as a starting point for the geometry optimization calculation. The coordinates for the optimized structures of **4-OMe** are included with this submission as a .xyz file. The optimized geometry for **4-OMe** was used for the molecular orbital calculation also using the Gaussian 16 program. For the molecular orbital calculations, the M06 functional was used with a split basis set, LANL2DZ for Pt atoms with a pseudo potential used for the core electrons of the Pt atom and 6-311+G(2d,p) for all other atoms. The highest occupied molecular orbital was visualized using the Gaussian 16 program and images for the HOMO of **4-OMe** are shown in Figure S78.

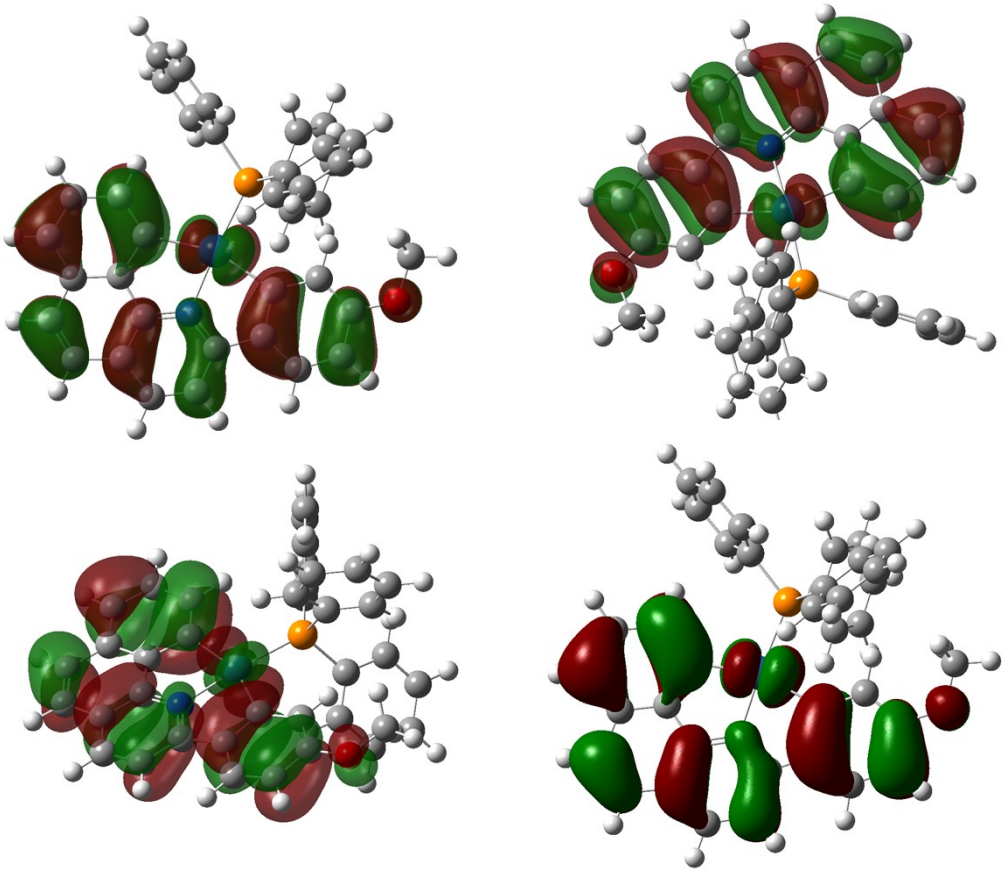

Figure S78. Images, produced in Gaussian, of the HOMO of **4-OMe** at various angles.

References

1. Lu, W.; Chan, M. C. W.; Cheung, K.-K.; Che, C.-M., π−π Interactions in Organometallic Systems. Crystal Structures and Spectroscopic Properties of Luminescent Mono-, Bi-, and Trinuclear Trans-cyclometalated Platinum(II) Complexes Derived from 2,6-Diphenylpyridine. *Organometallics* **2001,** *20*, 2477-2486
2. Baya, M.; Belio, U.; Fernandez, I.; Fuertes, S.; Martin, A., Unusual Metal-Metal Bonding in a Dinuclear Pt-Au Complex: Snapshot of a Transmetalation Process. *Angew Chem Int Ed Engl* **2016,** *55*, 6978-6982
3. Shaw, P. A.; Phillips, J. M.; Clarkson, G. J.; Rourke, J. P., Trapping five-coordinate platinum(iv) intermediates. *Dalton Trans* **2016,** *45*, 11397-11406
4. Marghalani, R.; Cueny, E. S., Stability of metal–metal interactions in transmetallation intermediates based on electronics of bridging arene ligands determined through pyridine titrations. *Dalton Transactions* **2024,** *53*, 18839-18844
5. Sangu, K.; Fuchibe, K.; Akiyama, T., A Novel Approach to 2-Arylated Quinolines: Electrocyclization of Alkynyl Imines via Vinylidene Complexes. *Organic Letters* **2004,** *6*, 353-355
6. Zheng, Z.; Deng, G.; Liang, Y., Synthesis of quinolines through copper-catalyzed intermolecular cyclization reaction from anilines and terminal acetylene esters. *RSC Advances* **2016,** *6*, 103478-103481
7. R. S. Drago, *Physical Methods for Chemists*, Surfside Scientific Publishers, Gainesville, FL, 2nd edn, 1992, pp. 290–291
8. Gaussian 16 M. J. Frisch, G. W. Trucks, H. B. Schlegel, G. E. Scuseria, M. A. Robb, J. R. Cheeseman, G. Scalmani, V. Barone, G. A. Petersson, H. Nakatsuji, X. Li, M. Caricato, A. V. Marenich, J. Bloino, B. G. Janesko, R. Gomperts, B. Mennucci, H. P. Hratchian, J. V. Ortiz, A. F. Izmaylov, J. L. Sonnenberg, Williams, F. Ding, F. Lipparini, F. Egidi, J. Goings, B. Peng, A. Petrone, T. Henderson, D. Ranasinghe, V. G. Zakrzewski, J. Gao, N. Rega, G. Zheng, W. Liang, M. Hada, M. Ehara, K. Toyota, R. Fukuda, J. Hasegawa, M. Ishida, T. Nakajima, Y. Honda, O. Kitao, H. Nakai, T. Vreven, K. Throssell, J. A. Montgomery Jr., J. E. Peralta, F. Ogliaro, M. J. Bearpark, J. J. Heyd, E. N. Brothers, K. N. Kudin, V. N. Staroverov, T. A. Keith, R. Kobayashi, J. Normand, K. Raghavachari, A. P. Rendell, J. C. Burant, S. S. Iyengar, J. Tomasi, M. Cossi, J. M. Millam, M. Klene, C. Adamo, R. Cammi, J. W. Ochterski, R. L. Martin, K. Morokuma, O. Farkas, J. B. Foresman, D. J. Fox, Gaussian, Inc., Wallingford CT, **2016**